Investigation of the Reliability of Satellite Imagery for Generating Shallow Water Depth Information for Navigational Purposes
Red Sea
Saudi Arabia

By

Ahmed Saleh Alzahrani

A thesis Submitted for the degree of Doctor of Philosophy

Supervised by

Prof. Richard Birmingham

Newcastle University

Sep 2007

The work is dedicated to:

- My country (Saudi Arabia).

- My parents, wife and children.

- Those people who faithfully supported and helped me in performing this research.

ACKNOWLEDGEMENTS

I deeply grateful to my supervisors Professor Richard Birmingham and Dr William Meredith for their advice, helpful, suggestions, guidance, continual encouragement and for pertinently reading the initial draft of this thesis. I am also grateful and thankful to Lt. General Talal Bi Mohsen Al Angawi, the General Directorate of Saudi Border Guard for the unlimited support during all stages of this study, deep thanks to Rear-Admiral Misfer Alghamdi and Rear-Admiral Abdulhameed Almwaree for their support and help. I am also grateful and thankful to my colleagues in Border guard training Institute and other departments.

Spatial thank to the president of Saudi Geological Survey Dr Mohammed Asaad and his staff for their help during field work.

I am very grateful and indebted to my wife and our children who gave me all their time, understanding, and patience during my busy time of preparing this thesis.

My mother, brother and sister are all thanked for their considerable help.

TABLE OF CONTENTS

CHAPTER ONE

INTRODUCTION

CHAPTER TWO

CHARACTERISTICS OF THE STUDY AREA

CHAPTER THREE

METHODS OF STUDY

CHAPTER FOUR

FIELDWORK METHODOLOGY

CHAPTER FIVE
IMAGE PROCESSING

CHAPTER SIX
DATA ANALYSIS

CHAPTER SEVEN

APPLYING THE FIELD MEASUREMENTS TO IMAGES ACQUIRED UNDER THE MOST UNFAVORABLE CONDITIONS

(JULY 2006)

CHAPTER EIGHT

APPLICATION OF STUDY RESULTS FOR NAVIGATIONAL PURPOSES USING GIS TECHNIQUES

CHAPTER NINE

CONCLUSION AND RECOMMENDATIONS

LIST OF FIGURES

LIST OF TABLES

NOMENCLATURE

EMR		Electro Magnetic Radiation.
GPS		Global Positioning System.
DN		Digital Number.
µm		Microns (Wave Length)
ECDIS		Electronic Chart Display Information System.
DGPS		Deferential Global Positioning System.
UTM		Universal Transverse Macerator.
ERTS		Earth Resources Technology Satellite.
m		Meter.
IMO		International Maritime Organization
IR		Infrared.
Lat		Latitude.
Long		Longitude.
LAT		Lowest Astronomical Tide.
MEPA		Meteorology and Environment Protection Administration.
PC		Personal Computer.
RGB		Red, Green and Blue Colour.
RO		Central Meridian.
Vo		The radius of Curvature at Right Angles.
ϕ		The latitude of 0.
GIS		Geographic Information System.
MSS		Multi-Spectral Scanner.
NASA		National Aeronautics and Space Administration.

NOAA		**National Oceanic and Atmospheric Administration.**
PERSGA		**Regional Organization for The Conservation of The Environment of The Red Sea And Gulf of Aden.**
TM		**Thematic Mapper.**
WGS		**World Geodetic System.**
WRS		**Worldwide Reference System.**
ASD		**Analytical Spectral Device**
RTK		**Real-Time Kinematic**
GCPs		**Ground control points**
KACST		**King Abdulaziz City for science and technology**
RMS		**Root Mean Square**
km		**Kilometer**
IDW		**Inverse Distance weighted**
TIN		**Triangulated Irregular Network**
ETM		**Enhanced Thematic Mapper**
MTF		**Modulation Transfer Function**
IRS		**Indian Remote sensing Satellite**
m		**Meter**
GMT		**Greenwich Mean Time**
P		**p-value**
T		**the value of t-test (calculated t)**
SE coef		**Standard Error of the Coefficient**
Coef		**Coefficient of the regression**
F		**the value of F-test (calculated f)**

MS		**Mean Squares**
SS		**Sum Squares**
DF		**Degree of Freedoms**
r2		**r squared (coefficient of corrlation)**
MSE		**Mean Square Error**
s^2		**standard deviation**
n		**sample size**
α		**confidence level**
$\bar{X}$		**sample mean**

ABSTRACT

The Red Sea is considered to be one of the most dangerous seas for navigation. The Saudi territorial waters along the Red Sea are characterised by coral reefs, which cause difficulties for local navigation, especially for coast guard vessels. The responsibilities of the Saudi Border guard necessitate safe navigation through out the entire area including the area of coral reefs; in this thesis a new approach and methods of study have been developed to generate navigational charts from photographic images.

Two study areas investigated: Rabigh 150km north of Jeddah and Kishran 200 km south of Jeddah. IKONOS multispectral satellite images acquired specifically for this study with a spatial resolution of 4 meters. The images were processed and georeferenced against control points taken during field measurements. The field work was carried out during the period of acquisition with *d*GPS being the positioning system (with an accuracy of ±5cm), and depths being measured using HT100 portable digital echo sounder, purchased specifically for this purpose.

After calibration of the satellite images and converting the images from digital numbers to radiance and then finally to reflectance, and after collecting the field depths for both study areas linear regression technique have been employed to build suitable models for extracting the estimated depths, this methodology and process led to successful results with an accuracy reached 97%. The same process employed under the most unfavourable conditions, where the humidity and temperature and water vapour reach the maximum, produced results with an accuracy of 65% are not recommended. Application of the study results were carried out for navigational purposes, by converting the images from raster format to a map containing all the necessary information which is normally available in navigational charts such as depths, contour lines (labeled with depth figures), compasses, scales…etc. This process was carried out

using Geographical Information System (GIS) techniques. As a conclusion the results achieved in this study prove that satellite imagery could play an important part in updating navigational charts by deriving the bathymetry of shallow water areas, especially in areas where the traditional survey could not be undertaken due to the spread of coral reefs, islands and underwater obstacles.

- Blue band was found to be the best for penetration and extracting depth data
- Timing of acquisition was found to be very important factor for achiving the best accuracy (97.3%)

CHAPTER ONE

INTRODUCTION

1. INTRODUCTION

1.1. Background

Hydrographic surveying actually plays an important role in many different aspects of the marine environment, such as in mineral resource management (including oil and gas), fishery management, submarine cable routes, marine archaeology, search and recovery efforts, environmental monitoring, oceanographic research and safe navigation. The West Coast of the Red Sea along the Saudi Arabian territorial waters is characterized by coral reefs. These reefs are identical to the vulnerable Australian barrier reef in some ways and their situation is even more serious, since the hydrographic surveys are less extensive as compared to the barrier reef. The coral reefs on the West Coast of Saudi Arabia extend seaward up to 50 miles or more. Their existence with little, doubtful or inconsistent hydrographic data endangers shipping. The Saudi Coast Guard vessels and local shipping are facing this problem day in and day out. The navigational charts produced by the Saudi Port Authority in 1982 were established after carrying out hydrographic surveying of the western coast of Saudi Arabia. This surveying had inherent inaccuracies regarding the details near the shore because of the humble facilities and abilities of the hydrographic surveying devices and technology available at that time. Positioning and depth finding in such surveys were carried out using normal boats equipped with an echo sounder and position fixing depended on a distance-finding device to calculate the distance from the survey boat to designated points on the shore.

Accurate surveying was difficult to achieve using these traditional methods to cover such places because of the wide spread of the coral reefs. It is also clear that the areas near the coast have not been surveyed using perfect methods, because of the defects of the hydrographic surveying devices. Of course, that is an indication that such data have been transferred from very old charts. Such surveying processes were also carried out a long time ago and since that period great technological developments have taken place, especially in the field of satellite remote sensing technology.

As a result of such developments, Global positioning systems GPS, especially differential *d*GPS, have now covered the world with an acceptable standard of output regarding the hydrographic surveying processes. These devices provide location in successive periods having a time difference of a fraction of a second. In addition, satellite systems have been developed especially for remote sensing techniques.

Very high resolution satellite (VHR) sensors were available by the end of the 1990s. IKONOS has high spatial resolution (4 m), with spectral bands closely matching the first four bands of the ETM+ sensor (Thome, 2001), and with the ability to penetrate water and discriminate different features such as land, water and vegetation. Because these services provide complete and accurate coverage, as well as time and effort saving in contrast to the traditional field methods that required much time, great effort and high financial expenditure, the researcher recognised an opportunity to attempt to update the nautical charts and to determine the locations of navigational hazard using remote sensing techniques. These techniques can be used to follow the process of topographic and depth changes resulting from the sedimentation process, and the growing of coral reefs. This helps in making the navigational process safer and allows the coast guard forces to cover the region safely.

1.2. Research Questions

- Are the high spatial resolution sensors able to detect the submerged coral reefs and other navigational obstacles and be part of the solution by deriving bathymetry? And what is the calculated accuracy?
- Can we rely upon high spatial resolution images as a method or data resource for updating the nautical charts?
- Can local shipping and navigators rely upon bathymetry derived by satellite images to navigate safely?

1.3. Aims of the research:

1. The aim of the study is to demonstrate the suitability of VHR multispectral satellite imagery for the creation of bathymetric maps appropriate to conditions in the Red Sea coastal area and the updating of these nautical charts.

2. The successful completion of this project will enable dangerous changes in coastal reefs to be identified from satellite images.

1.4. Specific objectives:

1- Assess the suitability of high spatial resolution sensors for estimating the water depth.

2-convert the images from raster format to maps could be used for navigational purposes

3-Update the navigational charts according to the results of this study

1.5. Research plan

- Collect hydrographic data from previous studies, both inside the Kingdom and abroad.
- Acquire of the synchronised digital images of the area under study.
- Conduct field measurement using the most accurate means to achieve the study aims.
- Study the navigational aspects of the area. Process and analyse the digital images.
- Applying the study result for navigational purposes
- Suggest methods for the updating of navigational charts.

1.6. The methodology of the Research

The methodology of the research is based on several stages:

- Analytical methods, which depend on collecting data and information concerning the duties and tasks of the Saudi Coast Guard. It also relies on collecting the information related to territorial waters of the study area, problems and difficulties that confront navigation, in addition to suggesting scientific and practical solutions to ensure navigational safety.
- Conducting a hydrographic survey of a selected area within the area under study and comparing its results with the remote sensing data and nautical charts.
- Conducting a remote sensing survey of the area under study through analysing data of digital images, and comparing field survey results to the data shown on available nautical charts.
- Collecting oceanographic and hydrographic data of the study area.
- Data processing (image and field data).
- Building suitable models for deriving bathymetry.
- Comparing the predicted depth derived from the image and establishing a safety factor.
- Using GIS techniques convert the satellite images from raster format into maps to be used by navigators
- Update the navigational charts accordingly

CHAPTER TWO

CHARACTERISTICS OF STUDY AREA

2. CHARACTERISTICS OF THE STUDY AREA

2.1 Introduction

For many years, the Red Sea has been a subject of great interest to scientists because of its unique character and the information it contributes to such subjects as rifting, continental drift and sea-floor spreading. The Red Sea offers exceptional research potential as it is regarded as the best modern example of a young expanding ocean (Purser and Bosence, 1998).

The Red Sea contains some of the world's most important coastal and marine environments and resources. There is a great variety of coral reef types in the Red Sea, with a structural complexity unmatched on the available charts. The diversity of coral is greater than anywhere else in the Indian Ocean (Bersga, 1998). The Red Sea is one of the most important repositories of marine biodiversity on a global scale.

In this chapter, an environmental and a hydrographic study of the Red Sea are presented. Such studies show that this area has so many features that are very distinct and clear. The Red Sea is considered the only marine route having unique importance in terms of both economic and military affairs. It contains 379 islands, the largest being Farasan Island. The climate of the Red Sea is largely controlled by the distribution of atmospheric pressure and it changes over a very wide area (north of 20°N, south of 20°N, and the intermediate area). The areas under study are located in Allith (22 45 00N 038 53.6E) and Rabigh (20 16.8N 040 00 E). It is difficult to navigate through these areas, because they are embedded with shoals and reefs.

The air temperature is normally lowest in the northern part of the Red Sea throughout the year. In the area south of 20°N, temperature increases rapidly. The rainfall over the Red

Sea is extremely low. It is mostly in the form of showers of short duration with dust storms. Surface water currents in the Red Sea are driven partly by the wind and partly by density gradient, which is established by the heating and evaporation that cause salinity to rise.

Navigation in the Red Sea is facing many difficulties due to the spread of coral reefs and lack of updated navigational charts. Furthermore, the limited navigational markers present more problems to the shipping in this area. There are also high risk zones for ship navigation within the Red Sea, especially near the ports (Gladstone, 1999). The inaccuracy of the available charts and the difficulty of surveying the area by traditional means directed our attention to space technology as a means of updating navigational charts.

The importance of the Red Sea increased after the opening of the Suez Canal in 1869. Table 2.1 shows the Suez Canal route as the shortest link between the east and the west (El Sayed, 1985).

Table 2.1. The distance between UK and eastern countries.

Distance from UK to	**Via Suez Canal**	**Via Cape of Good Hope**
India	6,200 km	10,500 km
Iran	6,500 km	11,300 km
Singapore	8,100 km	11,400 km
Hong Kong	9,500 km	12,800 km

Source : El Sayed (1985).

The importance of the Red Sea as an international navigational route lies in its role of creating a short and fast route for trade. That means that it has unique importance in terms of both economy and commerce. Another point is that the length of its coast is about 1,190 nautical miles, with an average width of about 180 nautical miles; this allows a better control of the area and reliable defence against any threat. As there are many ports on both the western and eastern banks that can be used as naval bases for defence purposes.

2.2 Location

The Red Sea is a long narrow basin separating the continents of Africa and Asia. It is oriented from northwest to southeast. The sea forms an elongated depression over 2,000 km in length between latitude 30° N in the tip of the Sinai Peninsula, where it bifurcates into the Gulfs of Suez and Aqaba, and where it becomes narrow at the strait of Bab El Mandab in the south at latitude 12° 30'N (Edwards et al., 1987). In the northern part of the Red Sea, the Sinai Peninsula divides the northern extremity into the shallow water (<100 m) of the Gulf of Suez and the deeper (>1,000 m) Gulf of Aqaba. The Gulf of Aqaba extends for about 150 km and on average it is only 16 km wide, whereas the Gulf of Suez is longer and wider (Bantan, 1999). The Red Sea is a large marginal sea, connected to the NW Indian Ocean via the Gulf of Aden at 11° north (Fig. 2. 1). The long (2,000 km) and narrow (230 km) basin extends as far as 28° north, where it bifurcates to form the Gulf of Suez and the Gulf of Aqaba. At the southern end, the shallow Bab el Mandab strait, just 137 m deep at Hanish Sill, connects the Red Sea to the Gulf of Aden (Siddall et al., 2004).

The Red Sea occupies an elongated depression. At the south end, the flat lying, coral topped Farasan and Dahlak Archipelagos rise above sea level and are part of a shallow shelf extending nearly to the centre of the Red Sea. The southern part of the Red Sea narrows at the strait of Bab El Mandab (see Fig. 2.1).

Figure 2.1 The location of the Study area (Red Sea) in Saudi Arabia map

2-3 Coral Reefs

The Red Sea is fringed by coral reefs of varying abundance (Cochran, 1983). Due to the rift-related origin of the Red Sea, the gross reef physiography seems to have been primarily controlled by tectonics rather than by sea level change. However, in relation to this major control, salt diapirism and siliciclastic input are additional factors that may influence the present day morphology and setting of reefs (Dullo, 1998). The system of identifying the position of reefs includes: capital English letters are used horizontally instead of longitude and numbers are used vertically instead of latitude; this is done to facilitate the interpretation of positions.

Coral reefs in the northern part of Red Sea, the Gulf of Suez and Gulf of Aqaba are mainly of a fringing nature (Bantan, 1999). Due to the shallow depths in the Gulf of Suez, reefs are transitional from fringing reefs towards barrier reefs, especially along the south-eastern coast near the entrance to the Red Sea (Dullo, 1998)

2.4 Costal Zone

The Red Sea coastal plain in Sudan and Egypt is narrow and is traversed by numerous large wadis (valleys) (Clay et al., 1998). On the Arabian side, the coastal plains broaden south of latitude (21° N) into the Tehama plain, reaching a width greater than 50 km in Yemen. North of latitude 21° N, the coastal plains are narrower and contain raised terraces that represent older shorelines (Behairy et al., 1992).

The coastal plain within Yemen and Saudi Arabia is mainly an actively alluviating surface that covers most of the earlier tertiary structural trends (Coleman, 1993). The only significant relief on the plain is provided by salt domes rising about 70 m above sea level at Jizan city, and by small extinct volcanoes 100 to 150 m high, southeast of Jizan city (Blank et al., 1986).

2.5 Islands

The Red Sea contains 379 islands (El Sayed, 1985). The largest are "Breem, Moleeh, Komran, Teran, Sanafeer, Farsan, Aldoyma, Zaquox, Hanesh Alkobra and Al Soghro, Dahlak, Fatma and Al tair"

Three distinct kinds of island are present in the Red Sea, excluding the many smaller isolated islands related to coral reef formation. At the southern end of the Red Sea, the flat-lying, coral limestone-topped Farasan Bank and Dahlak Archipelagos rise slightly more than 50 m above the sea level. The second type is the volcanic islands located in the southern part of the Red Sea such as Jabal Tair, Zubayr, Zukur and Hanish Islands. Zebargad Island represents the third kind of island. It consists of both mantle and lower crustal metamorphic and igneous rocks. This small island is located on the western shelf of the Red Sea (23° 37'N-36° 12'E). It is triangular in shape, rising about 235 m above sea level (Bonatti et al., 1983).

2.6 Hydrographic description of the study area:

The research has been applied to two study areas 400 km apart. The reason for conducting this study in two areas rather than one is to find out how much information can be obtained from each because they are far from each other and moreover to investigate the extent to which the algorithm model used to derive the bathymetry of each area is transferable to regions with differing conditions. The two areas were carefully selected to represent all the common environments that can be found in the whole Red Sea, such as coral reefs, sand, mud and sea grass. In addition, these two areas represented clear and turbid water. The first site (Rabigh) is located in the middle part of the Red Sea (Fig. 2.2), while the second one (Kishran) is located in the southern part of the Red Sea (Fig. 2.3).

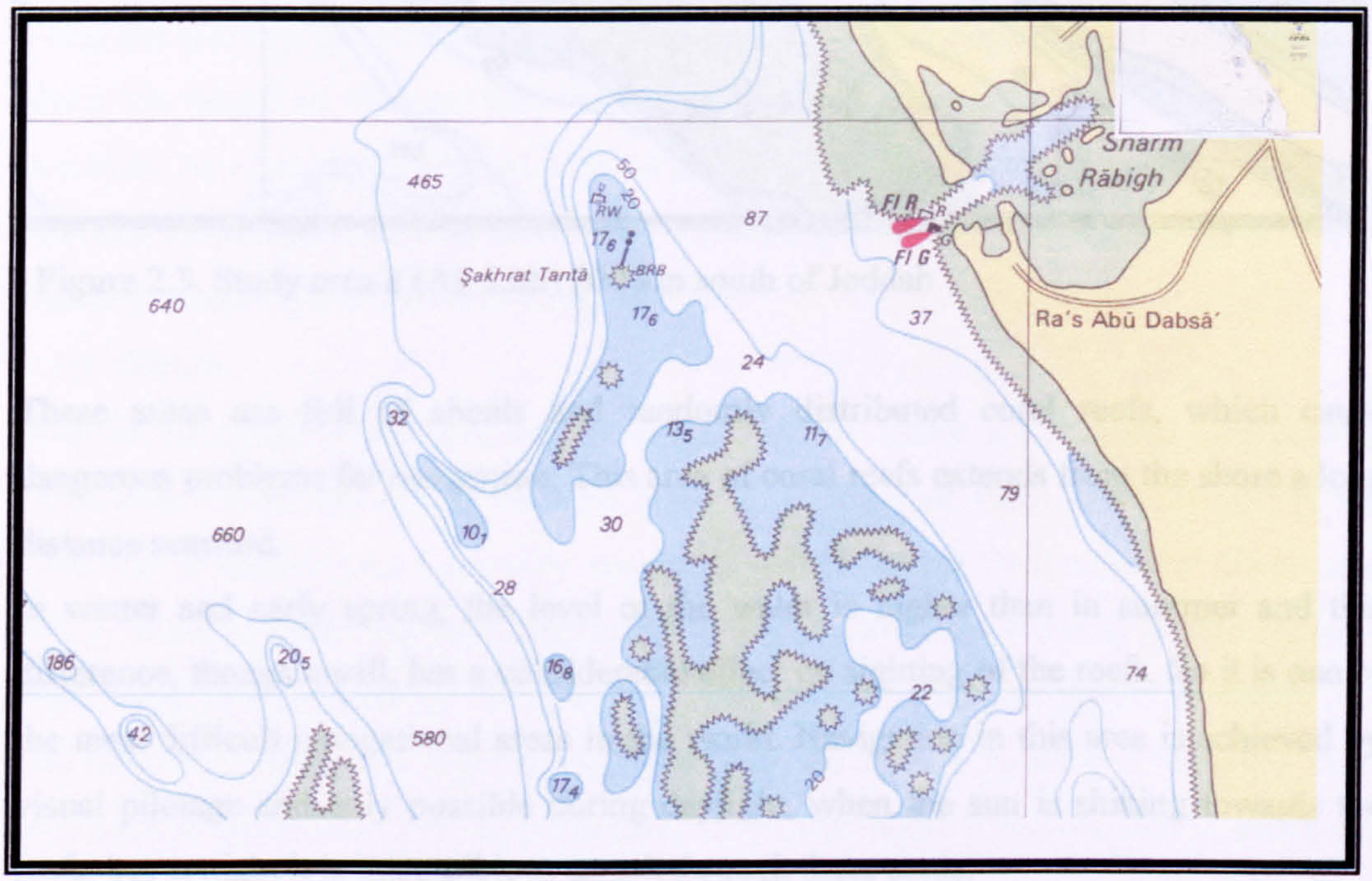

Figure 2.2. Study area 1 (Rabigh area) 150 km north of Jeddah.

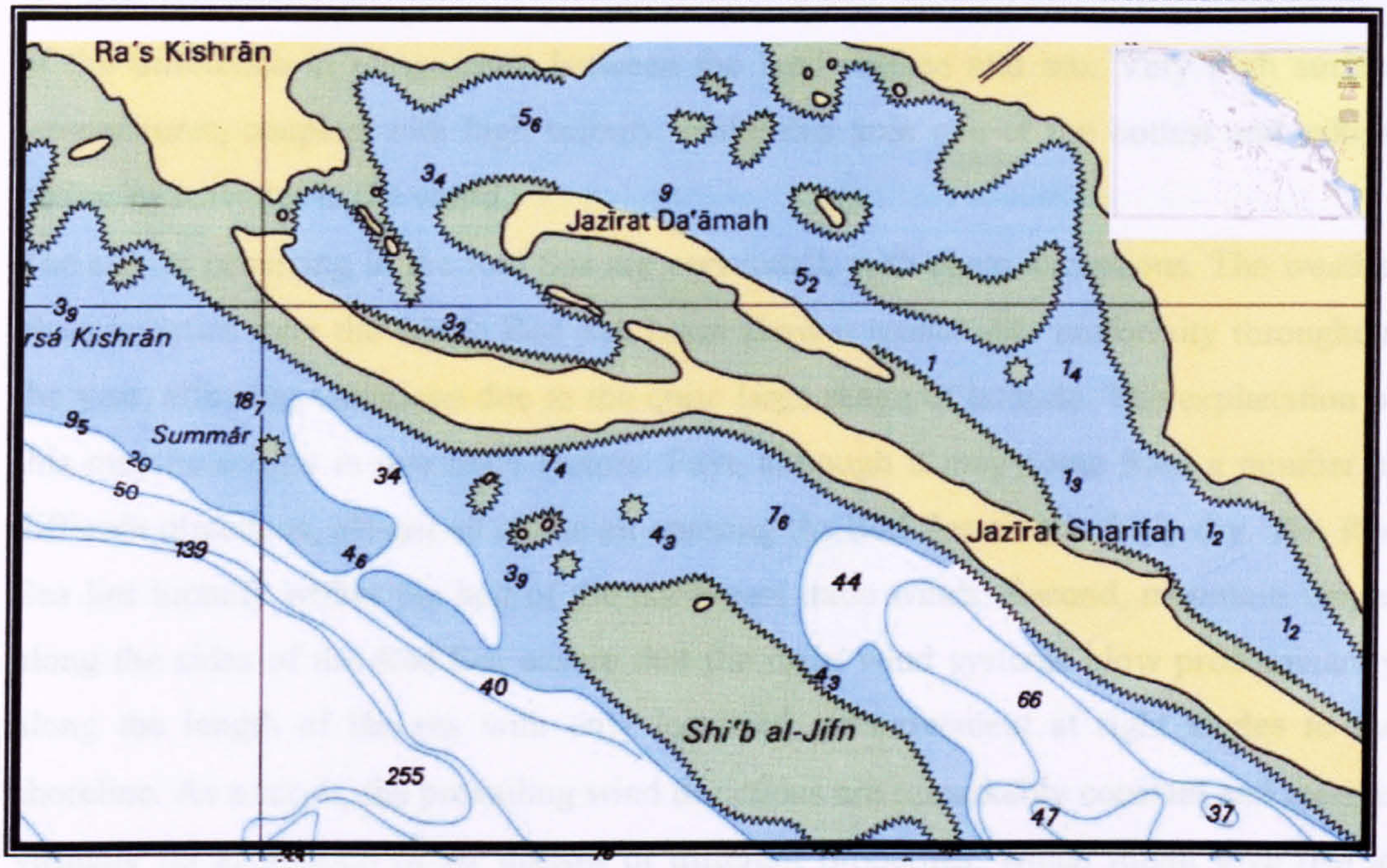

Figure 2.3. Study area 2 (Al- Lith) 200 km south of Jeddah.

These areas are full of shoals and randomly distributed coral reefs, which cause dangerous problems for navigation. This area of coral reefs extends from the shore a long distance seaward.

In winter and early spring, the level of the water is higher than in summer and this difference, though small, has a considerable effect on sighting of the reefs. So it is one of the most difficult navigational areas in the world. Navigation in this area is achieved by visual pilotage and only possible during daylight, when the sun is shining towards the reefs, but at night it is impossible to transit through these areas.

2.7 Climate and Oceanography

The climate of the Red Sea is largely controlled by the distribution of atmospheric pressure and its changes over a wide area. The pressure centres involved are generally distant from the Red Sea and they undergo variations in the course of the year, which result in widespread and sometimes dramatic seasonal changes over extensive areas. The climate of the Red Sea is the result of two distinct monsoon seasons, a north-easterly monsoon and a south-westerly monsoon (Morcos, 1970). Monsoon winds occur because of the difference in temperature between the land surface and sea. Very high surface temperatures, coupled with high salinity, make this area one of the hottest and saltiest bodies of seawater in the world.

The effects occurring in the Red Sea are very small, with some exceptions. The weather characteristics over the whole Red Sea basin show a remarkable uniformity throughout the year, allowing variations due to the quite large range of latitude. The explanation of this may be sought in two main factors. First, although it may come from a number of different directions, almost all of the air entering the Red Sea area is fairly dry. The Red Sea lies broadly within the belt of the north-east trade winds. Second, mountain ranges along the sides of the Red Sea ensure that the main wind systems blow predominantly along the length of the sea with only localized air movement at right angles to the shoreline. As a result, the prevailing wind directions are remarkably constant and there is virtually no alternation of air masses of different properties, which might give rise to changeable conditions (Edwards et al., 1987).

2.7.1 Winds

With the exception of the northern part of the Red Sea, which is dominated by persistent north-west winds, the rest of the Red Sea and the Gulf of Aden are subjected to the influence of regular and seasonally reversible winds (Naval Oceanography Command, 1982). In the Arabian Sea, the north-east monsoon prevails from November until March – April when it is replaced by the summer south-west monsoon, as shown in Figure 2.4. The north-east monsoon is mild and dry, the winds are light to moderate and there is little precipitation since they blow from the land, in contrast to the monsoon that is moist and also much stronger.

The occurrence of the monsoon is related to the great change in pressure that takes place between summer and winter over central Asia (Fig. 2.4). During the winter monsoon and due to continental cooling, a strong atmosphere develops over Asia; the air in the lowest atmospheric layer flows outwards. In January, the high pressure extends from Mongolia to central Europe, and passes over Turkey to Arabia. The atmospheric circulation is reversed as the monsoon blows from the north-east across the Arabian Sea and Gulf of Aden towards central Africa. On the basis of its climate, the Red Sea may be subdivided into three regions (Morcos, 1970).

– Northern Red Sea. The prevailing wind is mainly north/north-west all the year round.

– Southern Red Sea. From May to September, the winds blow from north/north-west in the same direction as in the northern Red Sea. In October, the winds start changing to south/south-east and retain this direction until April. Table 2.2 gives the climatologic normals of extreme wind in the study area recorded over 30 years.

– Intermediate area. This develops only in the winter months between the north/north-west winds of the northern half and the south/south-east winds of the southern half. The wind speed over the study area throughout the 30 years from 1962–1992 never exceeded 25 m/sec (MEPA, 1992) (see Table 1). Applying linear regression between Usea and Uland, an expression is obtained giving

Usea = 2.73 + 1.07 Uland (Abdulrahman 1995)

Where:

Uland= is the measured wind speed over land in the study area (m/sec), and

Usea= is the corrected wind speed over water in the study area (m/sec).

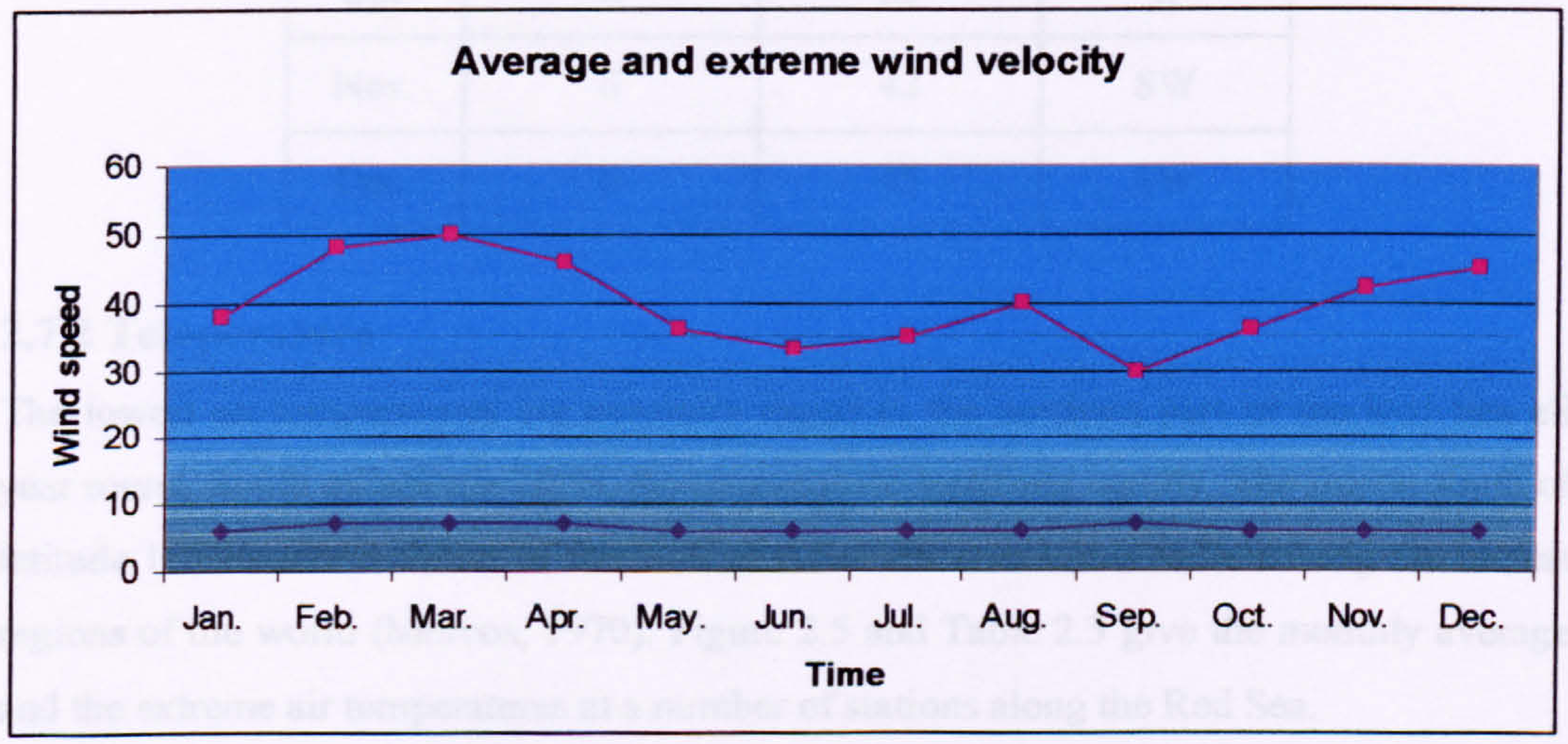

Figure 2.4. Wind speed over 30 years.

Table 2.2. Wind recorded during 30 years in. the study area.

Month	Average velocity (Knots)	Maximum velocity (Knots)	Direction
Jan.	6	38	SW
Feb.	7	48	W
Mar.	7	50	SW
Apr.	7	46	SW
May.	6	36	W
Jun.	6	33	W
Jul.	6	35	W
Aug.	6	40	W
Sep.	7	30	W
Oct.	6	36	W
Nov.	6	42	SW
Dec.	6	45	SW

2.7.2 Temperature

The lowest air temperatures are normally found in the northern part of the Red Sea all year round. South of latitude 26°N, the temperature increases rapidly. The region south of latitude 18°N and the shores of the Gulf of Aden are considered to be among the hottest regions of the world (Morcos, 1970). Figure 2.5 and Table 2.3 give the monthly average and the extreme air temperatures at a number of stations along the Red Sea.

The Red Sea demonstrates an exceptional condition, namely that south of latitude 20°N, the surface water is cooler throughout the year than the overlying air, which blows off the neighbouring hot deserts. The same condition prevails from March to September in the northern half of the Red Sea proper and from May to August in the Gulf of Suez (Morcos, 1970).

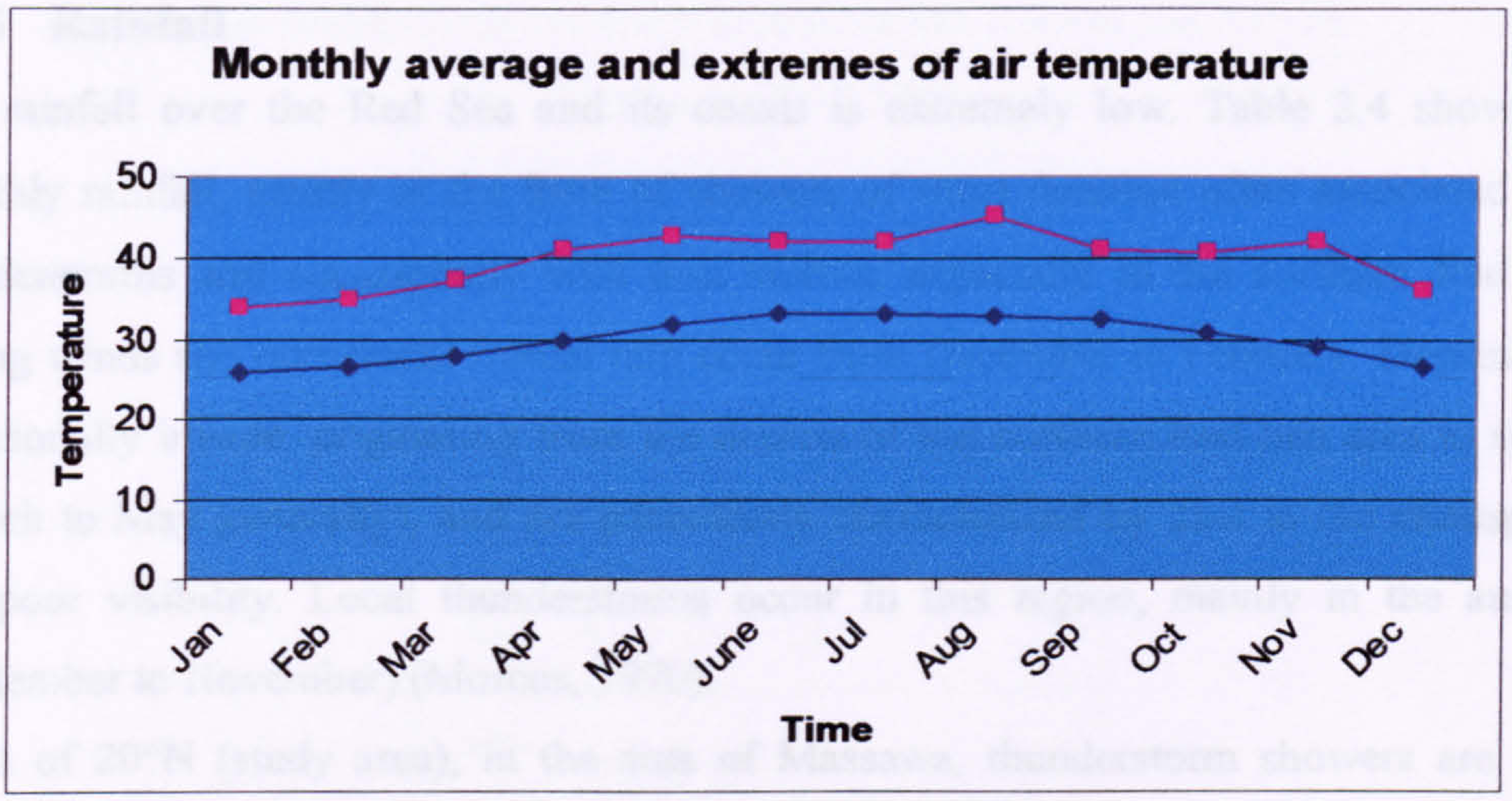

Figure 2.5. Monthly average air temperatures.

Table 2.3. Monthly average and the extremes of air temperature Jan 1988 to Dec 1998

Source: MEPA 2005

Month	Average (C°)	Maximum (C°)
Jan	26	34
Feb	26.4	34.9
Mar	27.9	37.5
Apr	30.1	41.1
May	32.1	43
June	33.3	42.3
Jul	33.4	42.3
Aug	32.9	45.3
Sep	32.7	41.3
Oct	31.1	40.9
Nov	29.1	42.3
Dec	26.7	35.9

2.7.3 Rainfall

The rainfall over the Red Sea and its coasts is extremely low. Table 2.4 shows the monthly rainfall, mostly in the form of showers of short duration often associated with thunderstorms and occasionally with dust storms, especially in the northern Red Sea. Strong winds and occasional frontal rain occur from December to February. Depressions occasionally invade, originating from the deserts of the northern Red Sea area in spring (March to May generally), and are particularly characterized by dust in the atmosphere and poor visibility. Local thunderstorms occur in this region, mainly in the autumn (September to November) (Morcos, 1970).

South of 20°N (study area), in the area of Massawa, thunderstorm showers are most frequent in winter and from October to May.

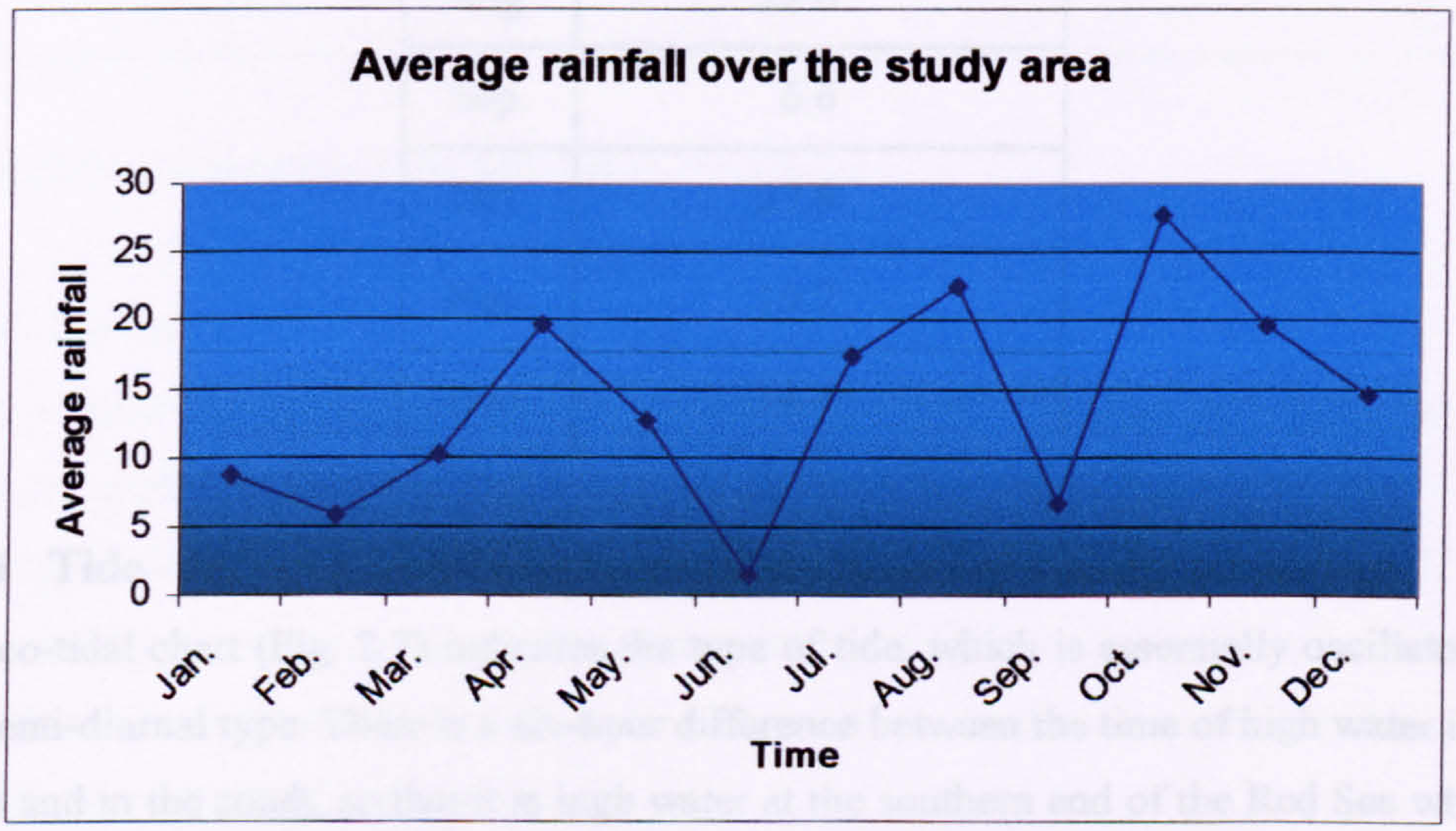

Figure 2.6. Monthly average rainfall.

Table 2.4. Average rainfall over the study area from Jan 1989 to Dece 1998

Source : MEPA 2005

Month	Rainfall average (mm)
Jan.	8.7
Feb.	5.7
Mar.	10.2
Apr.	19.7
May.	12.6
Jun.	1.4
Jul.	17.4
Aug.	22.6
Sep.	6.6
Oct.	27.8
Nov.	19.7
Dec.	14.4

2.7.4 Tide

The co-tidal chart (Fig. 2.7) indicates the type of tide, which is essentially oscillatory of the semi-diurnal type. There is a six-hour difference between the time of high water in the north and in the south, so that it is high water at the southern end of the Red Sea when it is low water at the northern end and vice versa (Robinson, 1979). The average spring range is 0.5 m in both the north and south, but it decreases from both ends towards the central area.

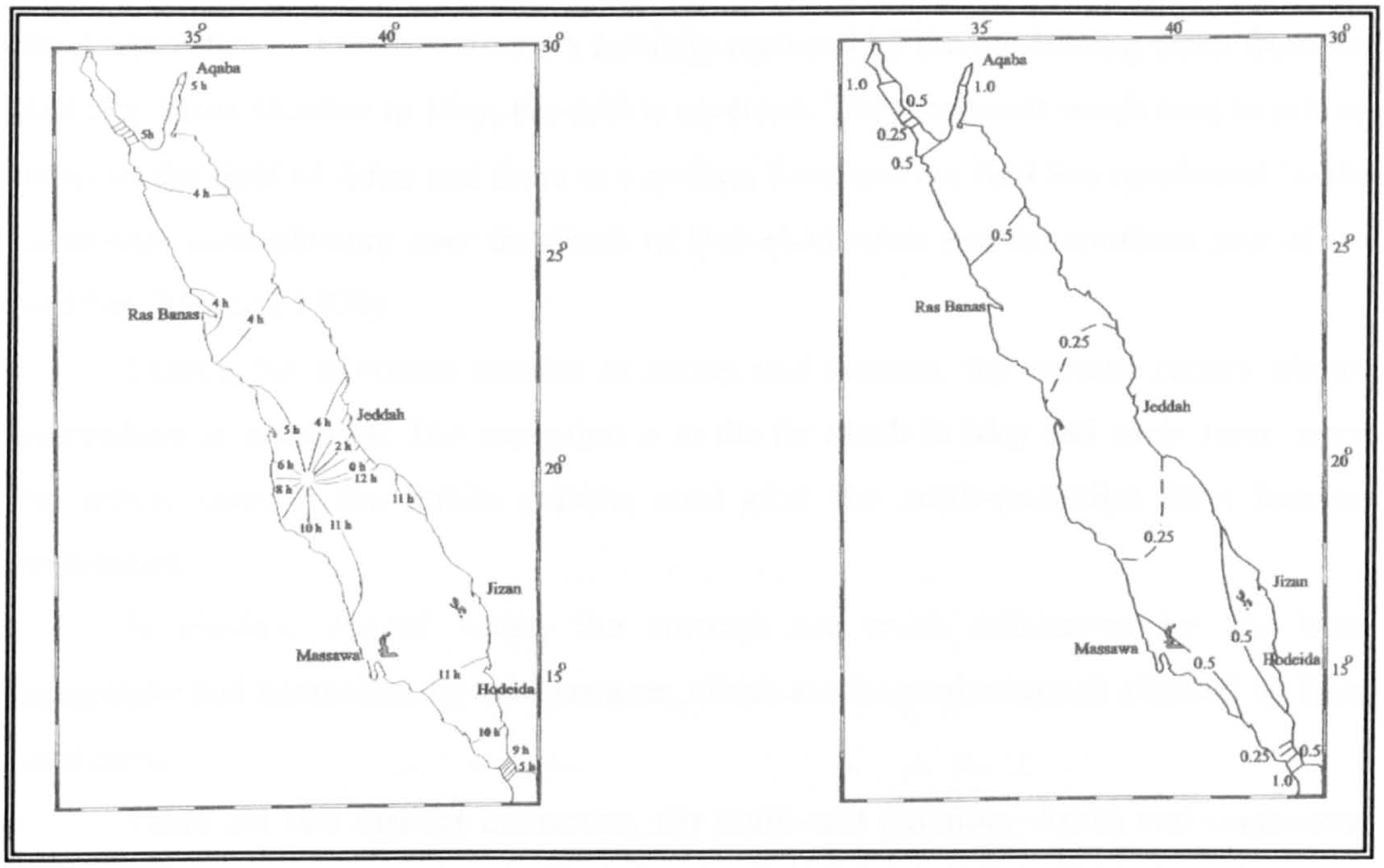

Figure 2.7 cotidal chart of the Red Sea

2.7.5 Currents

Surface water currents in the Red Sea are driven partly by wind and by density gradient, which is established by heating and evaporation (Morcos, 1970). In summer, water entering the Red Sea through Bab-el-Mandeb drifts northwards on the eastern side. The winds and high temperatures result in evaporation, and this causes salinity to rise from about 38–39% to about 42% at the Gulf of Suez. However, the increasing salinity causes a small increase in water density.

The main features of the surface current circulation, at least as far the deep waters along the main axis of the sea are concerned, are as follows:

- During the summer months, the north/north-west winds over the entire basin cause a movement of surface water in the south/south-east direction and down the western coast. This average flow is about a quarter of a knot (12 cm/sec) over the northern two thirds of the Red Sea, but south of latitude 16°N it is about twice as strong and reaches a maximum of about 1.25 knots in the Bab-el-Mandeb. At this time of the year, the south-west monsoon moves the surface water of the Gulf of Aden eastwards to the Arabian Sea and these waters are partially replaced by the outflowing water from the Red Sea. From October to May, the drift is reversed. The south-east winds tend to pile up water in the Gulf of Aden and there is a surface flow into the Red Sea reinforced by the south-east wind blowing over the Strait of Bab-el-Mandeb and the southern part of the Red Sea (Morcos, 1970).

- During the transition months in spring and autumn, the current pattern almost everywhere is indefinite. The exception is in the far south in May and early June, when the inflow through the Straits persists until after the north-westerlies have become established.
- In shallow coastal water, the currents are much influenced by the local topography and sometimes by tidal streams, which are themselves much affected by local conditions.
- There are two distinct monsoons, the north-east (October–April) and south-west monsoon (May–September), controlling the weather in the southern half of the Red Sea. In the northern half, the wind blows north-northwest all year. The water surface currents in the northern half are driven partly by these winds and partly by a density gradient. In the northern part of the Red Sea, north of about 19°N, the increase in temperature with decreasing latitude is both well marked and fairly regular. Temperatures are higher on the Arabian than on the African coast. South of about 19°N in the vicinity of the temperature maximum, there is no marked difference in temperature across the sea.
- Tidal streams are present at the two extremities of the Red Sea, the Gulf of Suez and the Strait of Bab-el-Mandeb; but moving away from these two zones the intensity of the currents decreases rapidly (Bantan, 1999).

2.8 Conclusion

In this chapter, environmental and hydrographic studies of the Red Sea have been presented. Such studies show that this area has many features that are very distinct.

The Red Sea is considered to be the only marine route that has a unique importance in terms of both economic and military affairs, it contains 379 islands, the largest being Farasan Island. The climate of the Red Sea is largely controlled by the distribution of atmospheric pressure and it changes over a very wide area (north of 20°N, south of 20°N, and an intermediate area).

The air temperature normally has its lowest values in the northern part of the Red Sea all year round. South of 20°N, the temperature increases rapidly. The rainfall over the Red Sea is extremely low. It is mostly in the form of showers of short duration with dust storms. Surface water currents in the Red Sea are driven partly by the wind and partly by density gradient, which is established by the heating and evaporation causing salinity to rise

CHAPTER THREE

METHODS OF STUDY

3. METHODS OF STUDY

3.1 Introduction

Method of study can be defined as the process of carrying out work in order to make it more effective and efficient. One of the goals of the method of study is to provide effective and sufficient data, which then leads to the achievement of the aim of the project in both qualitative and quantitative terms. In this project, four methods have been employed to achieve the main aim of the study: fieldwork, image processing, and data analyses, and finally Geographical Information System techniques GIS have been used to apply the results of the study to navigation. This chapter gives brief overviews of the methods followed in this research; more detailed explanations can be found in the following chapters.

3.2 Fieldwork

Fieldwork was undertaken between 20 December 2004 and 10 January 2005, coincident with the time of satellite image acquisition. The field programmes were concentrated on two study areas, the Rabigh (port and approach) and Kishran areas (400 km apart). These two areas contain many types of environment found in the Red Sea, such as turbid and clear water, coral reefs, sand, mud, rocks, sea grass, and small merged and submerged Islands. The field data collected came from three data sources:

- Spectral measurements – carried out using the Analytical Spectral Device (ASD) FieldSpec field spectroradiometer – to measure the reflectance spectra on the ground.
- Horizontal coordinates – from a Real-time Kinematic (RTK) Differential GPS (*d*GPS) positioning system – with an accuracy of ±5 cm. The reason for employing such accuracy is to obtain precise position for depth measurements and for accurate mapping of the coastline.

- Horizontal coordinates – from a Real-time Kinematic (RTK) Differential GPS (*d*GPS) positioning system – with an accuracy of ±5 cm. The reason for employing such accuracy is to obtain precise position for depth measurements and for accurate mapping of the coastline.
- Hydrographic surveying or depth measurement – carried out from a 12 m boat, with a 500 hp engine, 0.5 m draft, which was equipped with a Leica System 500 RTK GPS. Bathymetry lines were obtained over the entire study area using 50 and 200 kHz signals provided by an Odom hydrographic system (HT100) echo sounder.

3.3 Image processing

A main part of this study involved the use of remotely sensed satellite data for deriving bathymetry and mapping the sea bottom. The main goal was to map the areas dangerous for navigation; most threats come from coral reefs and submerged islands. IKONOS imagery was selected to solve parts of the navigational issues. IKONOS acquires images in four bands, including one NIR (Near Infra Red) and three visible bands (1, 2 and 3); the NIR can be used to map the coastline and merged islands, and it also can be useful for studying the surface features, whereas the visible bands provide the best water penetration (for more details, see Chapter 4).

The issues considered in selecting this type of imagery are: IKONOS has high spatial resolution of 4 m or better; secondly, the blue wavelength can penetrate water and map sea bottom types; and finally the ability of NIR to discriminate land from water. Coral reefs in coastal water (shallow water) can be mapped and characterized using active or passive optical sensors (Brock et al., 2001, 2002, 2004; Hochberg & Atkinson, 2003; Holden & LeDrew, 2002; Purkis et al., 2002). In particular, the sensor on the IKONOS satellite with 4 m multispectral resolution in the blue (445–520 nm), green (520–595 nm) and red (632–698 nm) bands (Dial et al., 2003) has been demonstrated to provide enhanced thematic accuracy (Andre'foue˜t et al., 2003; Maeder et al., 2002; Mumby & Edwards, 2002).

The image base underlying this research consisted of IKONOS 11-bit multispectral satellite imagery of 4 m spatial resolution in the red, green and blue bands and 1 m resolution in the panchromatic band. The imagery was acquired on 17 December 2004 at 08:08 GMT (10.08 local time). It was an 11-bit raw image, without Modulation Transfer Function (MTF) which will be explained in detail in chapter 5 or geometric corrections applied. The importance of acquiring a non-georeferenced image was to allow the conduct of precision geometric corrections, which should be better than 4 m to make the map useful, as the automatic georeferencing applied by the ground station would be inadequate. Water clarity was high outside the Rabigh port area and turbid inside the port area, and the surface was calm. Atmospheric conditions were optimal, with low levels of water vapour, and there was no cloud cover.

The geometric correction was undertaken against ground control points (GCPs) selected from the field and consisted of jetty corners, road junctions or intersections, fixed navigational buoys and other easily identified objects, acquired with (*d*GPS).

Radiometric correction was taken into consideration; spectroradiometer readings from the field were used in this study but due to some errors occurring during the fieldwork and which will be explained in detail in the data processing chapter, the manufacturer's published calibration constants were used to convert at-satellite reflectance (Methodology of Markham & Barker, 1985,1987) using ERDAS Imagine to carry out the process

3.4 Data analyses

More than 60,000 observations were collected from the two study areas; these data consist of spectral measurements, hydrographic survey and horizontal coordinates of coastlines and mapping of the jetties of the port. The data were then evaluated and filtered for unessential readings, with the useful data then used for further analyses.

3.4.1 Depth prediction

MINITAB software was used to predict water depth using image reflectance versus actual depth measured by echo sounder during field trips. The final algorithm or equation ($D_i = \beta_0 + \beta_1 R_i$) has been used with the original image to build a new model by ERDAS software, converting the image from reflectance to estimated depth. Another method of analysis was to predict new depths using the actual depth versus the estimated depth, the aim of this step being to calculate the navigational safety factor.

3.4.2 Using the Rabigh algorithm model to predict Kishran depths

The aim of this step was to use one algorithm model to predict water depth for different locations, which if successful would mean that this technology could be used for the entire area of the Rea Sea coastal water.

3.5 Application of study results for navigational purposes using GIS techniques

The application of the study results for navigational purposes will be the final part of the project. GIS will be the main tool for converting the raster image to a navigational map. It is clear that the raster image could be used by highly skilled decision maker such as the analysts, but not as a map or chart to be used by navigators (for more details, see Chapter 8).

CHAPTER FOUR

FIELDWORK

4. FIELDWORK METHODOLOGY

4.1 Introduction to methodology

As a result of previous reading and experience of the study area, it was essential to carry out fieldwork (hydrographic surveying), using the most modern and accurate equipment in order to obtain useful information on the water depth and sea bottom type, as the area had not been properly surveyed and charted. Fieldwork was undertaken between 10/12/2004 and 15/01/2005 (simultaneously with the acquisition of the IKONOS satellite imagery of the area) as the first step of a hydrographic survey integrated with navigational charts and satellite images of selected areas within the area under study. The reason for conducting this survey at the same time as image acquisition was to obtain more accuracy in the study methodology.

However, the main goal of the fieldwork is to obtain comparative data from remote sensing (satellite images) and field measurements such as depth measurement and photographic recording of the area, and to obtain accurate horizontal coordinates over the entire area under study to use for geometric and radiometric correction of the satellite images, in addition to spotlighting the dangerous changes in coastal reefs and updating the nautical charts accordingly.

4.2 Fieldwork plan

The planning of the fieldwork was commenced six months before the planned starting date of the field measurements and ground truthing in order to acquire the most important tools for this study. The Saudi Border Guard had offered the survey boat and the operational team. DGPS, current meter and echo sounder were supplied by the Saudi Geological Survey, while KACST offered the Spectroradiometer and satellite images. This preparation could be explained as follows.

- **Satellite images:**

The satellite images were selected according to the needs of the study. It is known that the growth and changes of the coral reefs can only be detected by using a very high resolution sensor with multispectral bands (visible and IR bands) that allow water penetration and location of the coastline and merged islands. IKONOS was the sensor selected due to its resolution and availability of multispectral bands.

The request to purchase these images was made to KACST with some conditional requirements such as:

1- 4 metre multispectral (all 4 bands)
2- No georeferencing applied
3- Full 11-bit radiance imaging
4- Viewing angle 72-90°
5- Single-date image (no mosaicing)
6- The date required was to coincide with the fieldwork.

The survey zone was covered by the satellite images, as shown by the location coordinates given in Table 4.1 and the images shown in figures 4.1 and 4.2. The Al-lieth area represents the middle south; this area is characterized by coral reefs, small islands, patches, sediments and mangrove, and is one of hundreds of dangerous areas for navigation in the Red Sea, and having no details available near the coast. Another issue or reason for selecting this area is the environment; all classes of environment in the Red Sea are available in this area, as mentioned previously.

Table 4.1. The location of study areas.

Study Area	**Location**	**Comments**	**Image data set**
Rabigh	Upper left 20 16.8N 040 00 E Upper right 20 16.8 N 040 06.6 E Lower left 20 11.0N 040 00 E Lower right 20 11.0 N 040 06.6 E	Rabigh city. Located 150 km north of Jeddah, this area consists of Rabigh port and approach (study area). The port is used by oil tankers and some other shipping that cause turbidity in the water (inside the port). The other part of this area is clear water characterized by coral reefs.	The first study area image of Rabigh covers an area of ca. 11 × 10 km.
Kishran (Shab Aljefen)	Upper left 22 45 00N 038 53.6E Upper right 22 45 00N 039 00 00E Lower left 22 39 00N 038 53.6 Lower right 22 39 00N 039 00 E	This area is located 200 km south of Jeddah and 30 km south-west of Al-lith Town. This area consists of several small islands surrounded by coral reefs and is not far from the coastline of Sharifah Island (the biggest island in the area).	The second study area image (Kishran area) is about 400 km south of the first stud yarea (Rabigh).

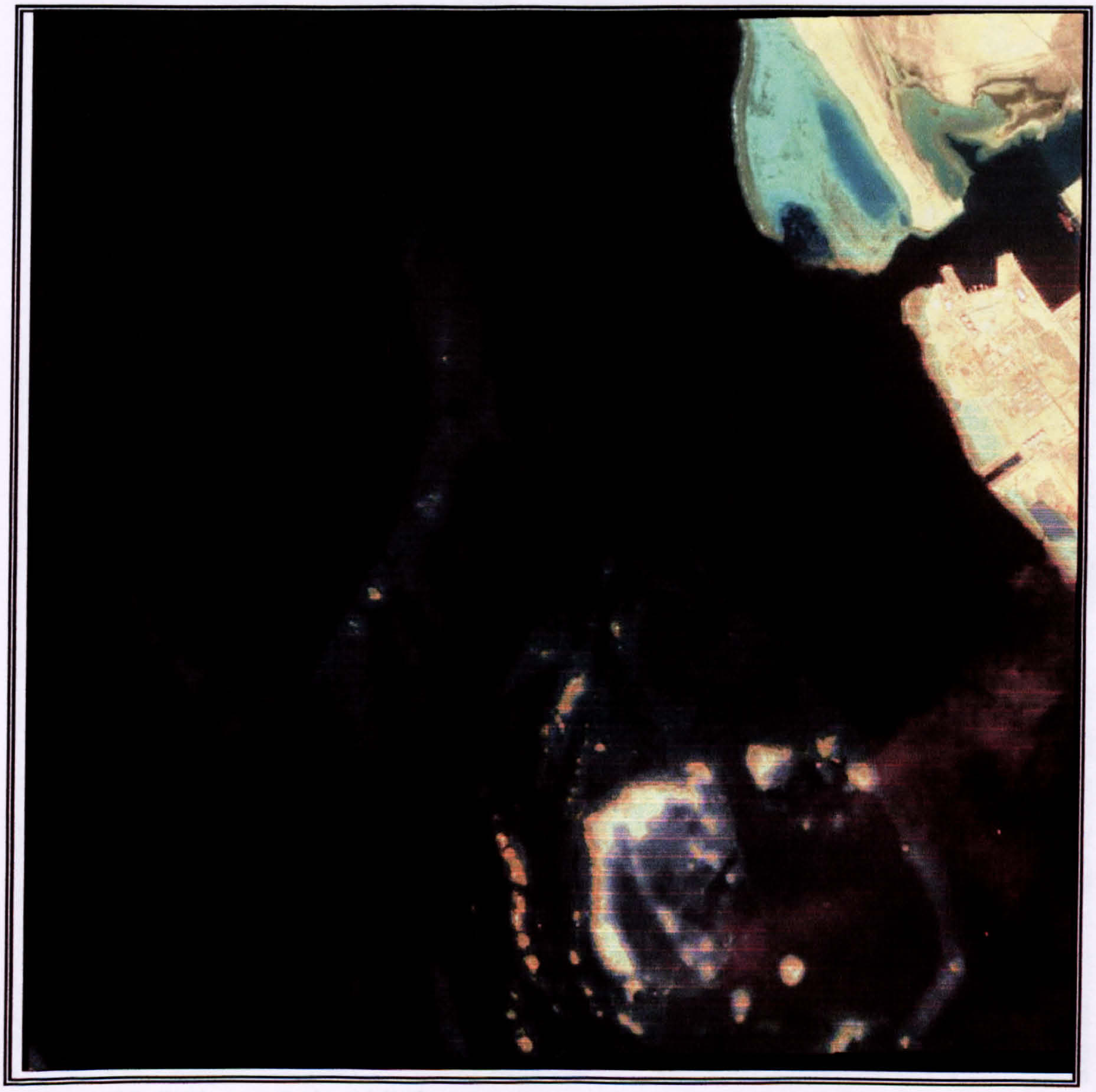

Figure 4.1. Study area 1, the Rabigh area.

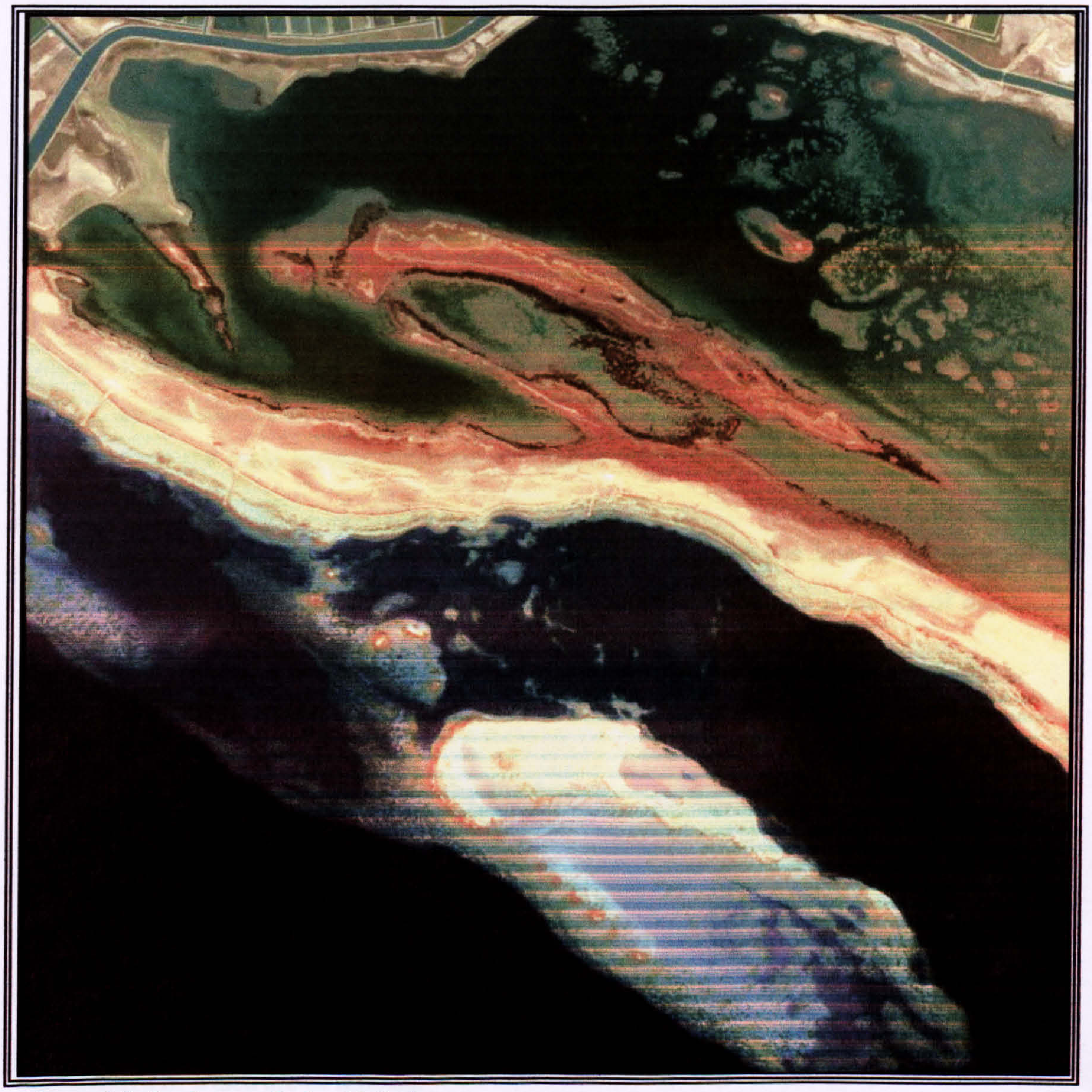

Figure 4.2. Study area 2, the Al-lieth area.

4.3 Hydrographic surveying plan:

- Locating and establishing the land coordinates, which are clearly located within the area under study.
- Preparing the survey boats and fixing the equipment ready for the actual survey.
- Carrying out the bar check calibration for the echo sounder.
- Carrying out the first survey trial with the use of all equipment interfaced with each other and examining the performance and result.
- Carrying out a trial survey in an area of known depth to ensure that the measurements are correct.
- Start the main survey, with survey lines at intervals of 50 metres (the standard interval).
- After completing the survey work, carrying out a reference line survey (check lines) perpendicular to the original survey lines to ensure the accuracy of depth measurement and positioning.
- Locating the coral reefs and navigational hazards within the area.

4.3.1 Preparing the equipment for fieldwork

4.3.1.1 Horizontal coordinates

All GPS positioning of the field measurements were recorded in the world geodetic latitude/longitude system, and the datum used was the WGS 1984 ellipsoid (WGS 1984). The navigational charts of the study area, such as admiralty charts, were also in the form of WGS84. The projection used is the Universal Transverse Mercator (UTM), the parameters of which are as follows:

• Zone	37
• Central longitude	39E
• Primary latitude	00 Equator

High accuracy was required for the field measurement of locations, especially for the horizontal control, which was used for geometric corrections and also for the comparison of field depths and bathymetry derived from satellite images. Due to the huge offset resulting from S/A with most civilian GPS receivers, reaching up to 75 metres, the RTK dGPS (± 5 cm) Leica GPS system 500 was used (Fig. 4.3).

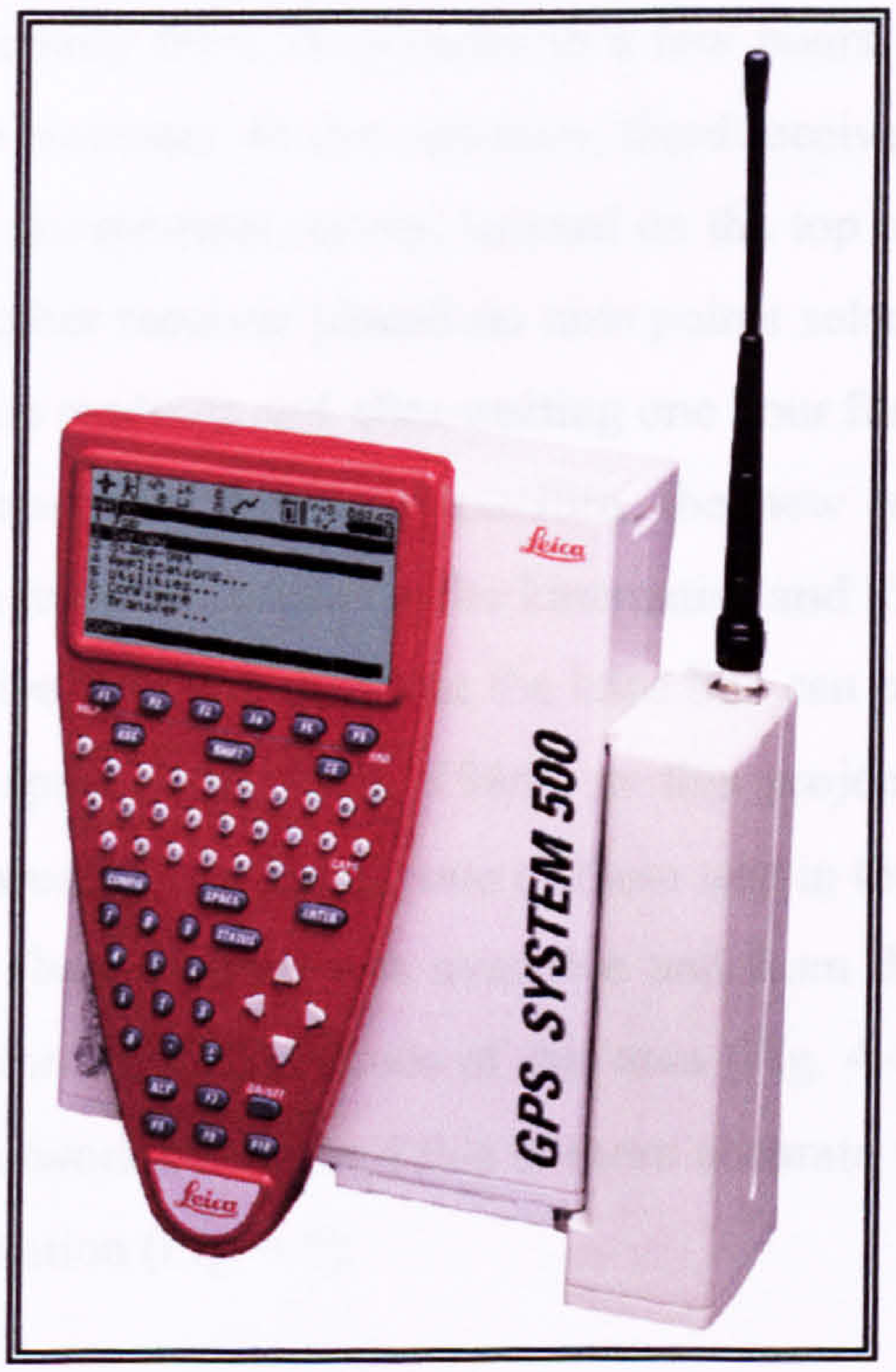

Figure 4.3 The GPS system used in this study.

It was necessary to use the following post-processing differential correction operations on the positional data.

DGPS processing methods

1- Static control

Static GPS surveying is a relative positioning technique that depends on carrier phase measurements (El-rabbany, 2002 & 2006). Therefore, the method of achieving position with high accuracy involves two stationary receivers, one of them set up over a point with precisely known coordinates and the other receiver, which is the remote receiver, set up over a point within the area under study. Both receivers simultaneously track the same satellites as shown in Figure 4.6. However, before carrying out any measurements, the parameters of the software are corrected for important factors, such as the setup error, and the datum and projection must be selected. In addition, the coordinates of the reference station and the height of the antenna must be entered. This method is based on collecting data at the same time from the same satellite for a certain period of time, usually from 20 minutes to a few hours, depending upon the distance between the two receivers. In this situation, fixed receiver placed on a known point identified from the government survey, located on the top of a water tower near the study area, with the other receiver placed on new points selected within the study area. After getting accurate readings and after waiting one hour for the two receivers to collect and track simultaneously the same satellite, the new receiver reading was corrected, to be used as a reference point for the kinematics and RTK GPS. One of the advantages of static relative positioning is that the base line can be measured between points many kilometres apart (Krakiwsky, 1986). In this project, the base line and static control processing were in two forms: one of them was in the Al-lith area, where only one reference point (base station) was available and from this point new points have been established according to the needs of this area (Fig. 4.4); the other form of static processing was a network survey and this is more accurate with the presence of more than one reference station (Fig. 4.5).

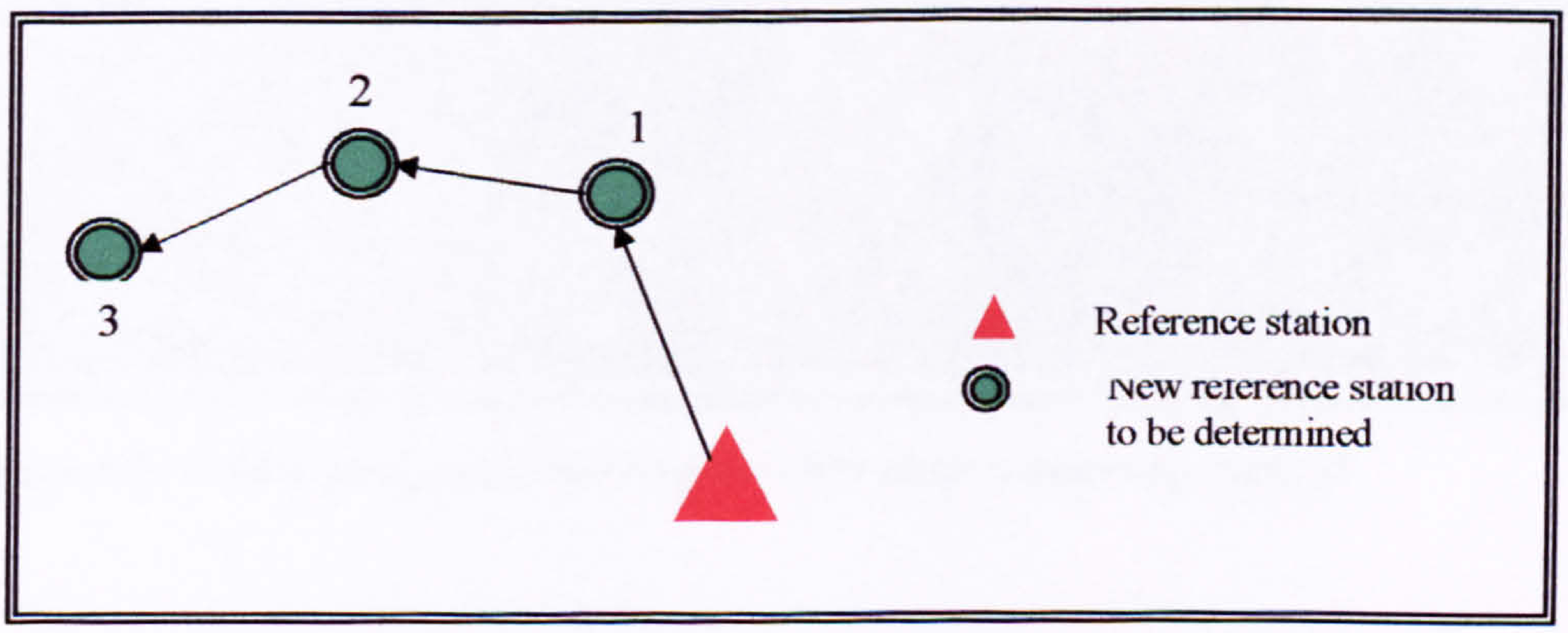

Figure 4.4. Static control based on one reference point.

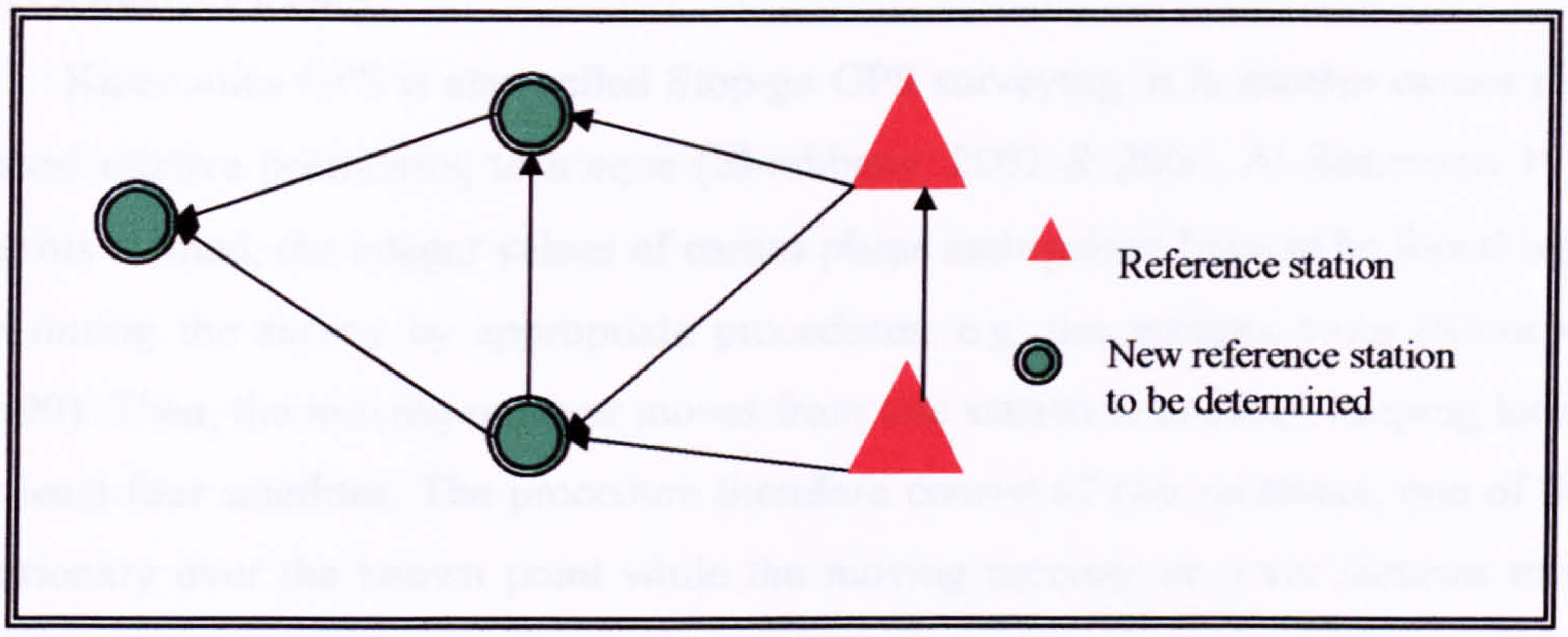

Figure 4.5. Static control based on more than one reference point (network survey).

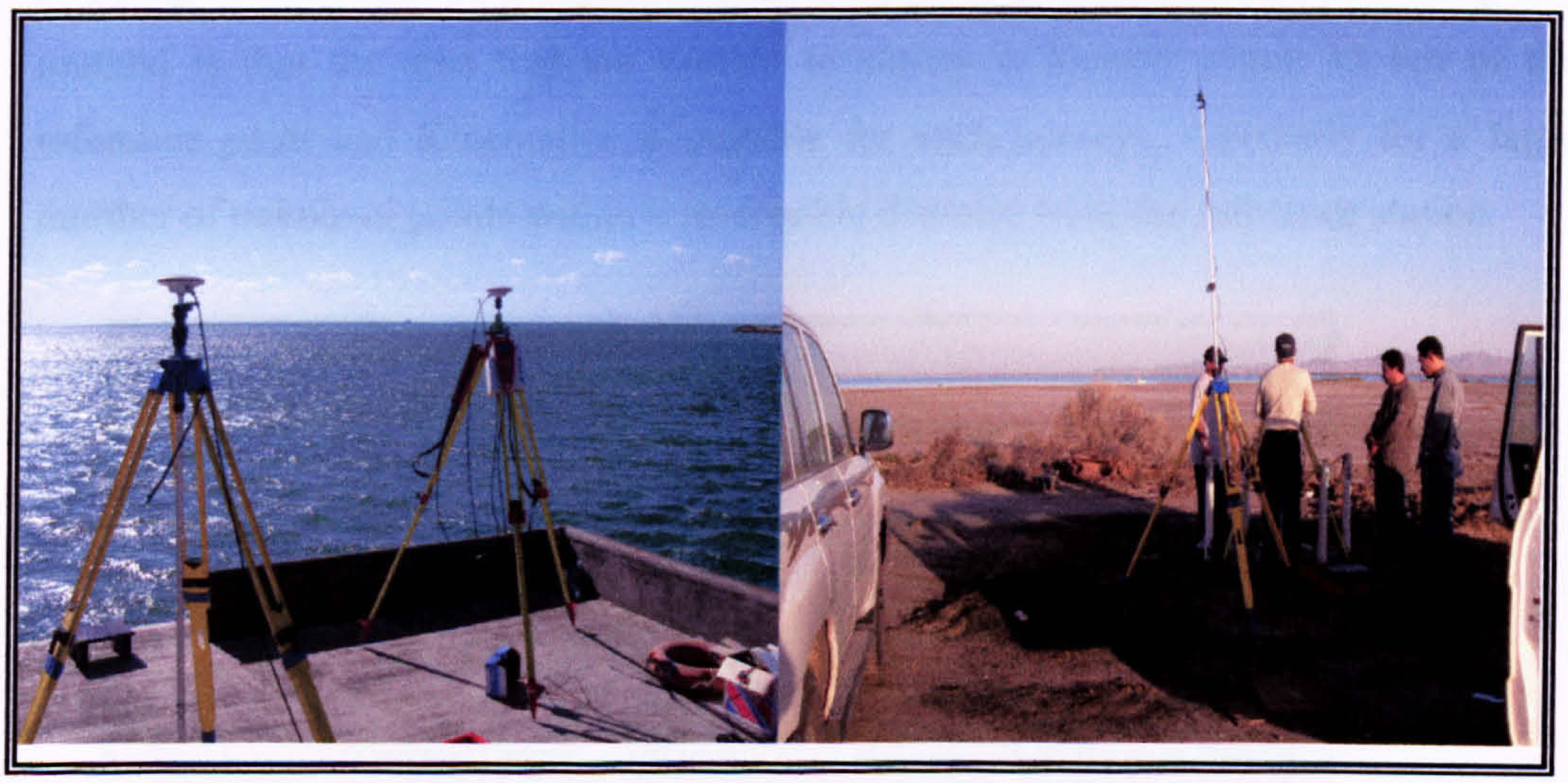

Figure 4.6. Field photographs showing the GPS static processing method

2- Kinematics GPS

Kinematics GPS is also called Stop-go GPS surveying; it is another carrier phase based relative positioning technique (El-rabbany, 2002 & 2006, Al-Shammari 1996). In this method, the integer values of carrier phase ambiguities have to be found before or during the survey by appropriate procedures, e.g. the antenna swap (Kleusberg, 1990). Then, the moving receiver moves from one station to another, keeping lock on at least four satellites. The procedure therefore consist of two receivers, one of them stationary over the known point while the moving receiver or rover receiver travels within the area under study to collect GPS data. The recording interval for the collection of data is normally between 1 and 2 seconds for a period of 30 seconds at each stop (El-rabbany, 2002 & 2006, Celik, R. (1996), King, M. (2003), Leick, A. (2004), Parkinson, B., J, Spilker (1996), MISRA, P. & ENGE, P. (2001), BORRE, G. S. A. K. (1997), CHEN, G. (1998)). This method has been used during the survey and mapping of the coastline and jetty corners (Figure 4.7). The reason for choosing this method is that the area that we wanted to survey is located within 15 km of the reference point and Kinematics is suitable for such surveys, especially for a large number of unknown points within a reasonable distance from the reference station.

Figure 4.7. The kinematics GPS mapping of the coastline.

3- RTK GPS is the method of positioning used in hydrographic surveying. It is one of the *d*GPS methods and consists of a GPS base station, which is placed over a known point within the study area, and the second GPS receiver (Rover) is in the survey boat. The GPS system on the survey vessel receives differential correction signals from the base station via the radio modems and automatically corrects the GPS signals to display centimetre level accuracy. The rover GPS remains in radio contact with the base station, giving positional updates every few seconds. The accuracy usually depends upon the distance from the base station to the rover; as the distance increases the accuracy decreases, and vice versa. In this study, three reference or base stations were used to get maximum accuracy. The GPS output data are in the form of WGS84 and are connected to the parallel output of the echo sounder data (see Figure 4.8).

Figure 4.8 The RTK GPS equipment used during the hydrographic survey.

4.3.1.2 Preparing the boat with survey equipment

The survey boat used in this study is 12 m long, has a 500 hp engine and a 0.5 m draught. It was equipped with the necessary instruments for hydrographic survey. However, after completion of the DGPS processing procedure, such as the base line surveys (static GPS survey) and placing the reference stations in suitable locations within the study area, the survey boat was equipped with an HT100 portable digital echo sounder and GPS, with the GPS antenna located on the top of the echo sounder transducer to give precise positioning (see Figure 4.9). These instruments were connected to the laptop computer to allow the recording of measured depth and precise position.

Figure 4.9. GPS antenna on the top of the Echo sounder transducer.

4.3.1.3 Vertical co-ordinates

Due to the importance of depth to navigators, it is essential to maintain a zero level for use as a reference point for correcting all depths. This can be defined as the level of water from which charted depths displayed on nautical charts are measured. Chart datum is the height of water at the lowest spring tide. This is known as the lowest astronomical tide.

Echo Sounder used in this Study

- The HT100 portable digital echo sounder (Figure 4.10) was used in this study. It is an "all-in-one" Digitizer/Transceiver. Data output is automatically saved in a PC, simultaneously with the DGPS data as shown in Figure 4.11.

The specifications of the HT 100 echo sounder are as follows:

- Tx/Rx Frequency:	High: 100 kHz – 750 kHz, Low: 12 kHz – 50 kHz
(The HT100 is frequency agile in two bands)	
Resolution	0.01 metre, 0.1 feet
Accuracy (Corrected for sound Velocity)	200 kHz - 0.01 metre ± 0.1% depth, 33 kHz - 0.10 metre ±0.1% depth
Depth Range	From 20 cms (0.8 ft.) to 600 metres (2000 ft.)

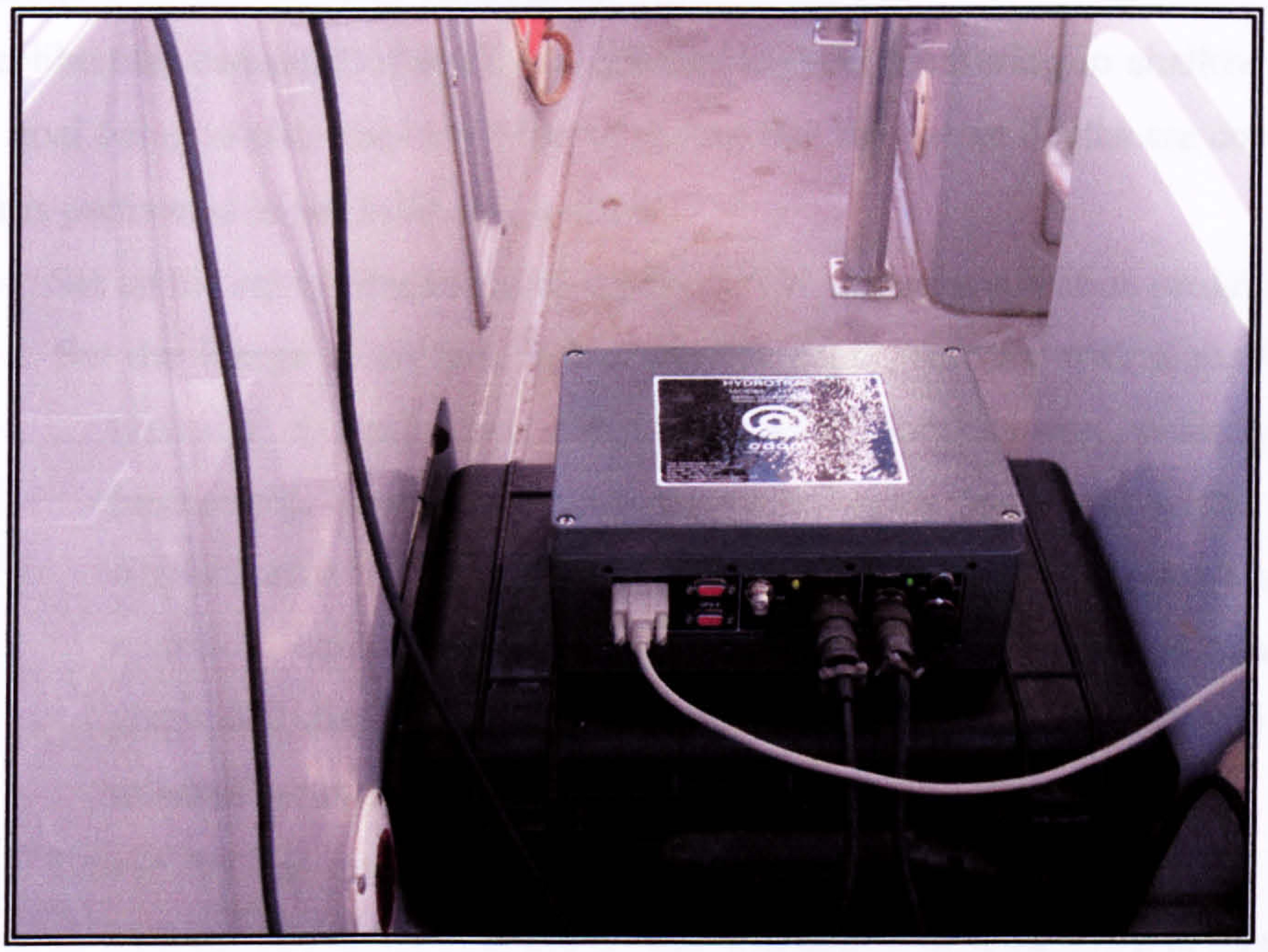

Figure 4.10. HT100 echo sounder used in this study.

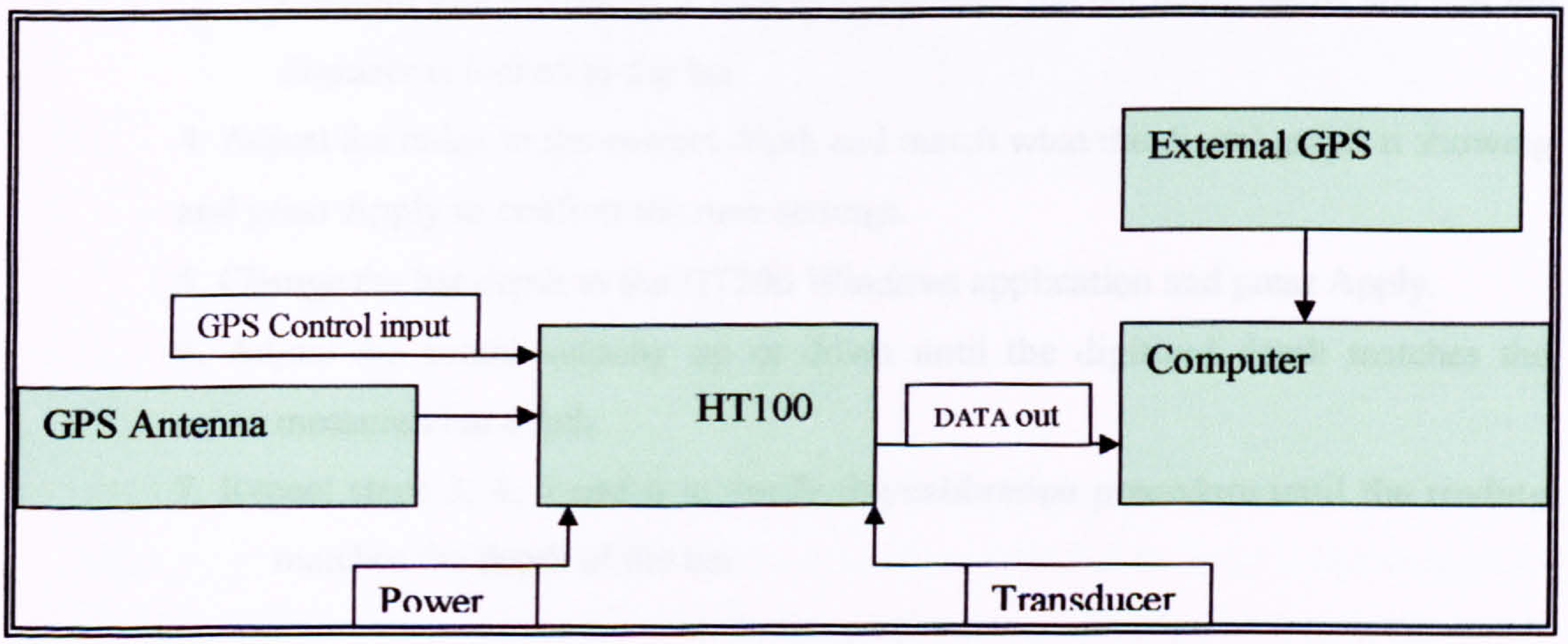

Figure 4.11. Interconnection block diagram of project equipment.

4.3.1.4 Calibration of echo sounder

The calibration consisted of the bar check and manual measuring in shallow water, the main goal being to eliminate any error to ensure that the output depths are correct. A bar check is performed in the following manner.

1. Set up the equipment and start the HT100 Windows application program.
2. Set the Range at 60 feet. Select the bar depth (starting with a shallow depth, typically 5 feet), bar width (typically1 foot), sound velocity, draught (measured), Index (start with 0), end-of-scale and scale width. Press the Apply button to confirm the new settings. The HT100 Windows application is now in calibration mode because the bar depth is greater than "0". The graph will display the tracking gate at the selected width, centred about the selected bar depth.
3. Lower the bar into the water column and place it at 5 feet below the water surface. The digitizer in the HT100 will expect to see a target at that 5.00 foot depth, while rejecting all other returns (including those from the bottom). Confirm that the return is displayed between the bar width limits and that the digitizer is locked to the bar.
4. Adjust the index to the correct depth and match what the digital graph is showing and press Apply to confirm the new settings.
5. Change the bar depth in the HT100 Windows application and press Apply.
6. Adjust the sound velocity up or down until the digitized depth matches the measured bar depth.
7. Repeat steps 3, 4, 5 and 6 to verify the calibration procedure until the reading matches the depth of the bar.

4.3.1.5 Preparing survey lines and reference line

After conducting the bar check and getting the output reading with GPS data, the echo sounder automatically takes the depth reading and displays it in the computer. These readings are collected simultaneously with the GPS readings, also delivered to the field computer through special software (Figure 4.12). Survey lines were mapped with 50 m interval and the survey was carried out at a scale of 1:5,000 according to IHO procedures point 1.A.1.3 (IHO 1987), which states that the survey scale of port approaches that are used continually by ships should not be less than 1: 25,000.

Figure 4.12. Integrating data from GPS and echo sounder.

4.3.1.6 Collecting tide prediction

Tide prediction has been used to correct all depths according to chart datum. 30-minute intervals are used for tide prediction corrections. It is noted that the tidal range in the Red Sea is relatively small during this study, the maximum tide reaches 1.12 m at 08:00 hrs and the minimum is 0.86 m at 01:30hrs.

Table 4.2. The tide prediction during the time of survey.

01/01/2005			
Time	(m)Tide	Time	(m)Tide
00:00	0.90	12:00	0.99
00:30	0.88	12:30	0.97
01:00	0.87	13:00	0.95
01:30	0.86	13:30	0.93
02:00	0.86	14:00	0.92
02:30	0.87	14:30	0.91
03:00	0.88	15:00	0.92
03:30	0.91	15:30	0.92
04:00	0.93	16:00	0.93
04:30	0.96	16:30	0.95
05:00	0.99	17:00	0.97
05:30	1.02	17:30	0.99
06:00	1.05	18:00	1.01
06:30	1.08	18:30	1.03
07:00	1.10	19:00	1.04
07:30	1.11	19:30	1.06
08:00	1.12	20:00	1.06
08:30	1.12	20:30	1.06
09:00	1.12	21:00	1.06
09:30	1.11	21:30	1.05
10:00	1.09	22:00	1.03
10:30	1.07	22:30	1.01
11:00	1.04	23:00	0.99
11:30	1.02	23:30	0.95

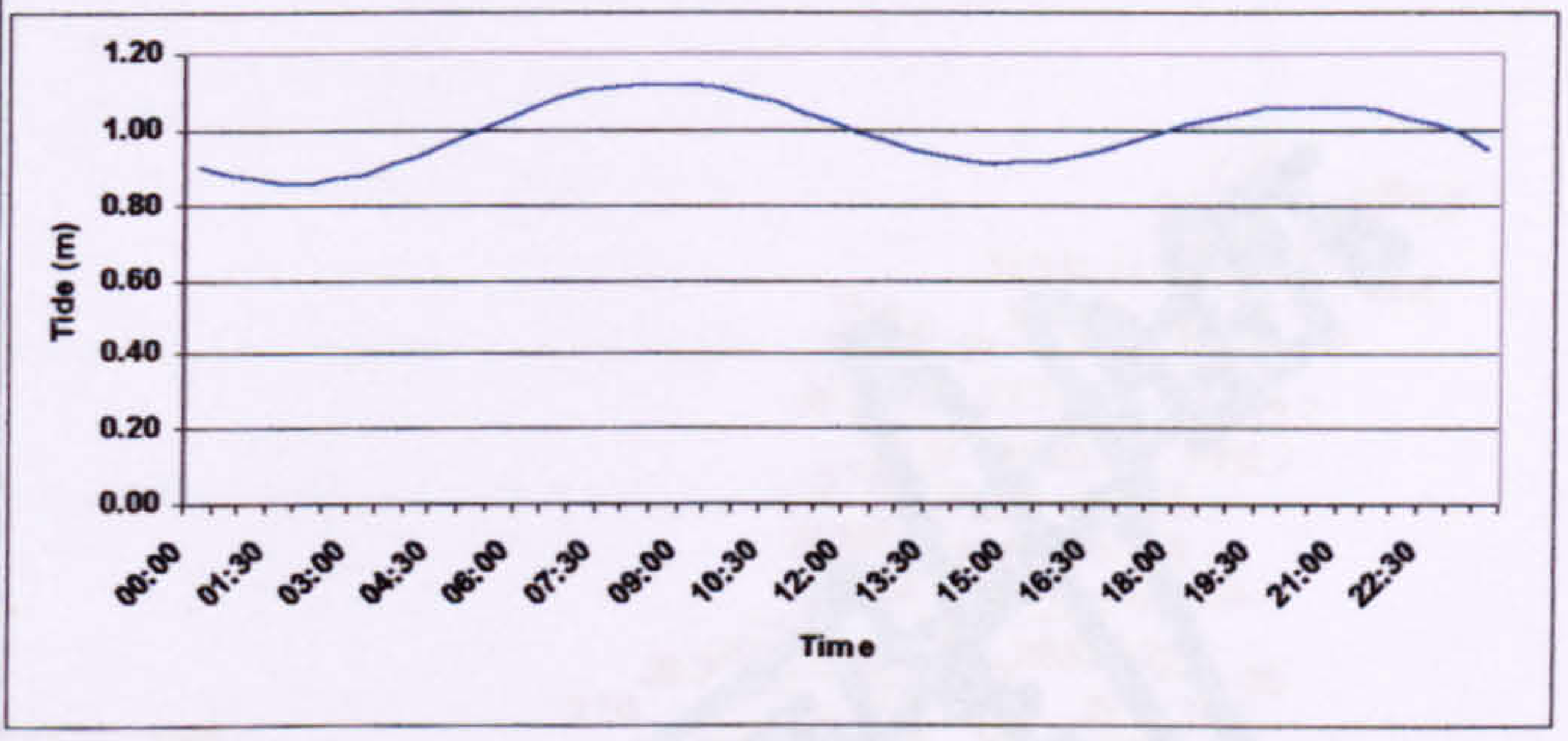

4.3.1.7 Starting the field measurement

The field survey started after the completion of all preparations, such as setting up the positioning system, calibration of echo sounder and conducting a survey trial to add tide information to the software that receives the GPS information and depth data.

The actual survey was according to survey lines planned before, namely 50 m apart, followed by reference lines or check lines.

Final data collection

The final data collection in this project was as follows:

- Mapping the coastline and port jetties with DGPS
- Conducting hydrographic surveys using very accurate equipment and procedures
- The final bathymetric map containing the depth data and the coastline is shown in Figure 4.13 & 4.14.

Figure 4.13. water bathymetric chart for the area under study.

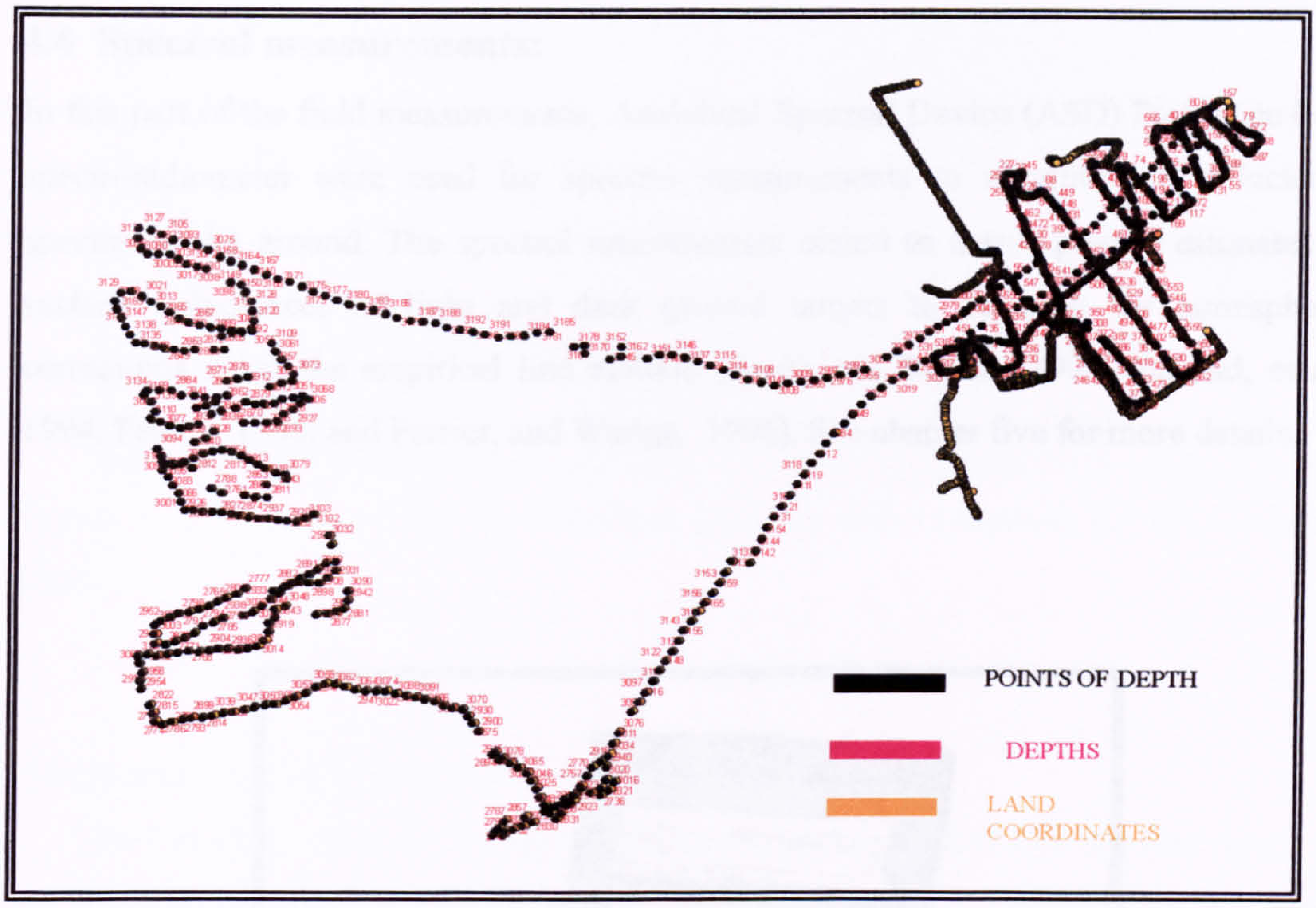

Figure 4.14 The final bathymetric chart for the area under study including Jetties and coast lines survey.

4.4 Spectral measurements:

In this part of the field measurements, Analytical Spectral Device (ASD) FieldSpec field spectroradiometer were used for spectral measurements to measure the reflectance spectra on the ground. The spectral measurement aimed to derive precise estimates of surface reflectances of light and dark ground targets to be used for atmospheric corrections using the empirical line method (Smith and Milton, 1999, Farrand, et al., 1994, Ferrier, 1995, and Ferrier, and Wadge, 1996). See chapter five for more details.

Figure 4.15. The Analytical Spectral Device (ASD) (spectroradiometer).

Figure 4.16. Practical spectral measurement. (A) Dark object (Asphalt). (B) Bright object (Sand).

4.5 Summary and conclusion

The two study areas are located in the east coast of the Red Sea (coastal waters of Saudi Arabia); they are about 400 km apart; the Rabigh Area (study area 1) is about 150 km north of Jeddah, while the second study area (Kishran area) is located 200 km south of Jeddah. The selection of these areas as case studies was due to several factors. Firstly, they contain all habitats related to our study, such as coral reefs, shallow waters, deep waters, vegetation, islands, clear and turbid waters. Secondly, all facilities needed for surveying, such as survey vessels and their crew, were available there. Finally, the two areas are located near to the Saudi national geodetic network

The field measurements began by establishing new reference stations using *d*GPS within the study areas. The known stations, to be used as reference stations for the positioning system, were equipped with radios to send the correction to the GPS rover on board the survey vessel. With *d*GPS, the positioning error was found to be ±5 cm, which is less than the pixel size of 4 m x 4 m.

The survey boat used for this work was 12 m in length, with a 500 hp engine and a 0.5 draught, equipped with a HT100 portable digital echo sounder with a resolution of 0.01 m. The dGPS and echo sounder were interfaced to the laptop computer to record the depth readings and the positions. A bar check was carried out to calibrate the echo sounder before starting the real survey. The distance between the survey lines was 50 m, with a scale of 1:5,000 according to International Hydrographic Organization IHO procedures. The tide prediction was taken into consideration to correct the depth measured by the echo sounder. The depth measurement was not the only work done in this study. The coastline and port jetties were mapped using dGPS, to be used for image georeferencing.

Finally, spectral measurements were performed using the Analytical Spectral Device (ASD), to measure the reflectance spectra on the ground. The main goal of this measurement is radiometric correction of the images.

The field measurements (position and depth) were made according to high accuracy methodologies; the work was carried out during the acquisition of satellite images, with the images being acquired especially for this study, which gave the opportunity to carry out the fieldwork at the time of image acquisition.

CHAPTER FIVE

IMAGE PROCESSING

5. IMAGE PROCESSING

5.1 Introduction

Many researchers have supported the utilization of remote sensing technology for monitoring environment habitats. Remote sensing techniques provide an effective way to observe and monitor shallow coral reefs worldwide, to detect inter-reef structural differences, and to map intra-reef habitat diversity and zonations, assess bathymetric variations, design survey protocols, conduct biogeochemical budgets, and map beta-diversity (Andre'foue"t and Payri, 2000; Andre'foue"t et al., 2001; Capolsini et al., 2003; Hochberg et al., 2000; Jupp et al., 1988; Liceaga-Correa et al., 2002; Mumby, 2001; Mumby et al., 2002; Mumby et al., 1998; Palandro et al., 2003; Purkis et al., 2002; Roelfsma et al., 2002). The use of satellite images became common from the middle of the 1980s for observing and mapping coral reefs, although the spatial resolution was medium (10–30 m) in sensors such as the Indian Remote Sensing C (IRS-C), SPOT, Landsat 5 TM and ETM+. Green et al. (1996) in their review presenting the use of remote sensing for coastal tropical assessment pointed out the difficulty of comparing different reef assessments due to the lack of consistency in classification schemes, in situ data collection and image processing methods, and in accuracy assessment protocols, but for geomorphology and habitat-scale applications, SPOT and Landsat data have spectral resolutions that are adequate for simple complexity mapping (3–6 classes), but for more complex targets (7–13 classes) they are limited by their spatial resolution and also often by their radiometric resolution (8 bits) (Capolsini et al., 2003; Hochberg and Atkinson, 2003; Mumby et al., 1998; Mumby and Edwards, 2002). The limitations of Landsat and SPOT imageries have two principal causes. Firstly, pixel sizes (20–30 m) are of a similar magnitude to the size of habitat patches (Mumby et al., 1997). Secondly, many seagrass and reef habitats are dominated by photosynthetic organisms (coral zooxanthellae, macroalgae, seagrasses) and the spectral differences between organisms are subtle, often requiring high-order spectral derivative analysis for segregation (Clark et al., 2000; Hochberg and Atkinson, 2000; Holden and LeDrew, 1998b, 1999; Lubin et al., 2001; Myers et al., 1999).

The bathymetry of coastal waters, such as in the Red Sea, is of fundamental importance for shipping safety, due to the presence of navigational hazards. The conventional hydrographic surveying or measuring of water depth is accurate for point measurement (Li-Guang et al., 2005). On the other hand, it is characterised by a list of difficulties or disadvantages. Firstly, it is a time consuming, labour-intensive task requiring a huge budget. Secondly, the traditional survey has poor geographical coverage, particularly in coral reef areas, due to the survey vessel draught limitations. An alternative solution was found to be the remote sensing method. Since the mid 1980s, medium spatial resolution (10–30 m) optical satellite data have been used to study and monitor coral reefs (Andrefouet et al., 2001). This includes data delivered by the Indian Remote Sensing Satellite C (IRS-C), Satellite pour l'Observation de la Terre (SPOT), Landsat 5 Thematic Mapper (TM), and more recently by SPOT 4–5, Landsat 7 Enhanced Thematic Mapper Plus (ETM+), and the Advanced Spaceborne Thermal Emission and Reflection Radiometer (ASTER) sensors. In contrast, high spatial resolution images, i.e. those with higher spatial resolution than 10 m, such as those provided by IKONOS or Quickbird (1–4 m), have not been widely utilized (Andrefouet et al., 2003).

Active and passive optical sensors can map and characterize coral reefs in shallow water (Brock et al., 2001, 2002, 2004; Hochberg and Atkinson, 2003; Holden and LeDrew, 2002; Purkis et al., 2002). In IKONOS, the multispectral resolution of the blue, green and red bands has been verified to afford enhanced thematic accuracy (Andre'foue"t et al., 2003; Maeder et al., 2002; Mumby and Edwards, 2002). Palandro et al. (2003) mentioned that IKONOS had become an ideal tool for mapping coral reefs, or any other framework type, as it is possible to discriminate between coral reef community characteristics due to the resolution of the image and its large scale.

For the purpose of mapping coral reef environments, high spatial resolution is obligatory due to the relatively small horizontal spatial scales and the ecological importance of vertical structures in those environments in the form of patch reefs, spur and groove, mini-atolls, and so on. Mapping the fine-scale variability will improve characterization of habitats, both for corals and for various species living in the reefs (Stumpf and Holderied, 2003).

Until recently, only two options existed for such information: airborne measurements (photo and hyperspectral) and multispectral satellite imagery (typically Landsat). Landsat, particularly the Landsat-7 Enhanced Thematic Mapper Plus (ETM+), offers global coverage of coral reefs, but only with a 30-m instantaneous field of view. With the launch of the high-resolution sensors in IKONOS in 1999 and QuickBird in 2002, 4-m (or finer) multispectral imagery became available from space, providing a new resource for the development of mapping and monitoring programmes for coral reefs in remote locations. These satellites provide multispectral data with three visible bands (blue, green, red), which can simulate aerial photography, and one near-infrared (near-IR) band (Stumpf et al., 2003). The high spatial resolution (IKONOS) calibrated data in four wide spectral bands are potentially useful for coral reef studies. The spectral bands closely match the first four bands of the ETM+ sensor (Table 5.1).

Table 5.1 Spectral bands (nm).

Spectral region	IKONOS	Landsat-7
Blue	445–515	450–520
Green	510–595	530–610
Red	630–700	630–690
Near-infrared	760–850	780–900

In a review of remote sensing bathymetric applications, Lyzenga (1978) noted that the previous studies, using aerial photography, had determined that bottom reflectance patterns, even in shallow water, were modified by the attenuation of light in the overlying water column. Early studies, using multispectral methods, established that several factors control the accuracy of deriving bathymetry, including water characteristics, sea bottom type (bottom reflectance) and atmospheric conditions (El-Raey, M. 1988, El-Raey, M. et al., 2000, El-Raey, M. et al., 2004). Under such conditions, depth as well as the effective attenuation coefficient could be derived from multispectral imagery (Mishra and Narumalani, 2004). The theory was explained and developed by Lyzenga (1978, 1981) and then extended by Philpot (1989). Maritorena et al. (1996) confirmed the validity and problems involved with using remote sensing for the determination of water depth. Changing water characteristics and atmospheric conditions will affect the reliability with which absolute bathymetry can be determined, and spectral data can only be used to establish depths if accompanied by contemporaneous in-situ measurements. Mapping and deriving water depths using satellite images have several limiting factors, especially those related to the variable effects of the water column on the optical reflectance properties as measured remotely and in situ (Holden and LeDrew, 2001). Although passive optical systems are limited in depth penetration and constrained by water turbidity, the use of such satellite data might be the only possible way to reliably map water depth in some situations. (Stumpf and Holderied, 2003). in particular, the use of satellite data is the safest way to map coral reef areas due to the difficulty of obtaining water depth by traditional hydrographic depth measurement. In order to measure water depth in regions where coral reefs present a major hazard to navigation, and when their horizontal extent can be as little as 10 m or less, the optical satellite imagery required to provide a reliable tool for mapping such reefs must have a spatial resolution of 4 m or better. Landsat and SPOT imagery offer global coverage of coral reefs, but they have limitations, these limitations caused by the pixel sizes of 30 and 20 m, respectively.

Aircraft can provide sufficiently high spatial resolution for coral reef mapping, but with high costs. Stumpf et al. (2003) stated that the information about bathymetry related to globally extensive coral reefs is fragmented and incomplete due to difficulties of obtaining echo sounding data for oceanic regions. They suggested that the development of new strategies to enhance depth estimation techniques could be possible with high spatial resolution imagery such as IKONOS and Quick Bird.

5.2 Satellite IKONOS

The IKONOS satellite was lunched by Space Imaging as the first high resolution commercial space sensor on 24 September 1999. It has a spatial resolution of 4 m in the multispectral mode, and 1 m in the panchromatic mode and a radiometric resolution of 11 bits per pixel (2,048 radiance levels) compared to 256 levels in the Landsat and SPOT systems. The bands of IKONOS closely match the first four bands of Landsat Thematic Mapper (TM) and (ETM+). The characteristic of the IKONOS sensor are briefly described in Table 5.2.

Table 5.2. Characteristic of the IKONOS sensor (Karpouzli, 2003).

Lunch date	24 September 1999
Altitude	681 kilometres
Orbit	98.1 degree, sun-synchronous
Revisit frequency	3 days
Bits per pixel	11 (2048 brightness level)
Sun angle Azimuth	146.6127°
Sun angle elevation	46.20799°
Multispectral data spatial resolution	4 m
Swath	11 km
Multispectral bands Blue Green Red Near Infrared	 450–520 nm 520–600 nm 630–690 nm 760–900 nm
Other features	Pointability

The images used in this project were acquired exclusively for this study; they were ordered according to an acquisition window of 30 days (15th December 2004 to the 15th January 2005) in order that the field measurements could be carried out while the acquisition was going on. The images of the two study areas were acquired at the same time, with similar metrological conditions; the weather was absolutely fine with zero cloud cover.

Table 5.3. IKONOS image characteristic for Rabigh area (Study area 1).

Rabigh image characteristics	
Acquisition Date/Time	17/12/2004 08:08GMT (11:08 local)
Scan Azimuth	180.00 degrees
Nominal Collection Azimuth	73.5710 degrees
Nominal Collection Elevation	73.37316 degrees
Sun Angle Azimuth	157.7686 degrees
Sun Angle Elevation	40.77079 degrees
Percent Cloud Cover	0
File Format	TIFF
Datum	WGS 1984

Table 5.4. IKONOS image characteristic for Kishran area (Study area 2).

Kishran image characteristic	
Acquisition Date/Time	17/12/2004 08:08GMT (11:08 local)
Scan Azimuth	179.98 degrees
Nominal Collection Azimuth	6.2633 degree
Nominal Collection Elevation	٨٢,٨١٧٤٨degrees
Sun Angle Azimuth	158:3827 degree
Sun Angle Elevation	43:49671
Percent Cloud Cover	0
File Format	TIFF
Datum	WGS 1984

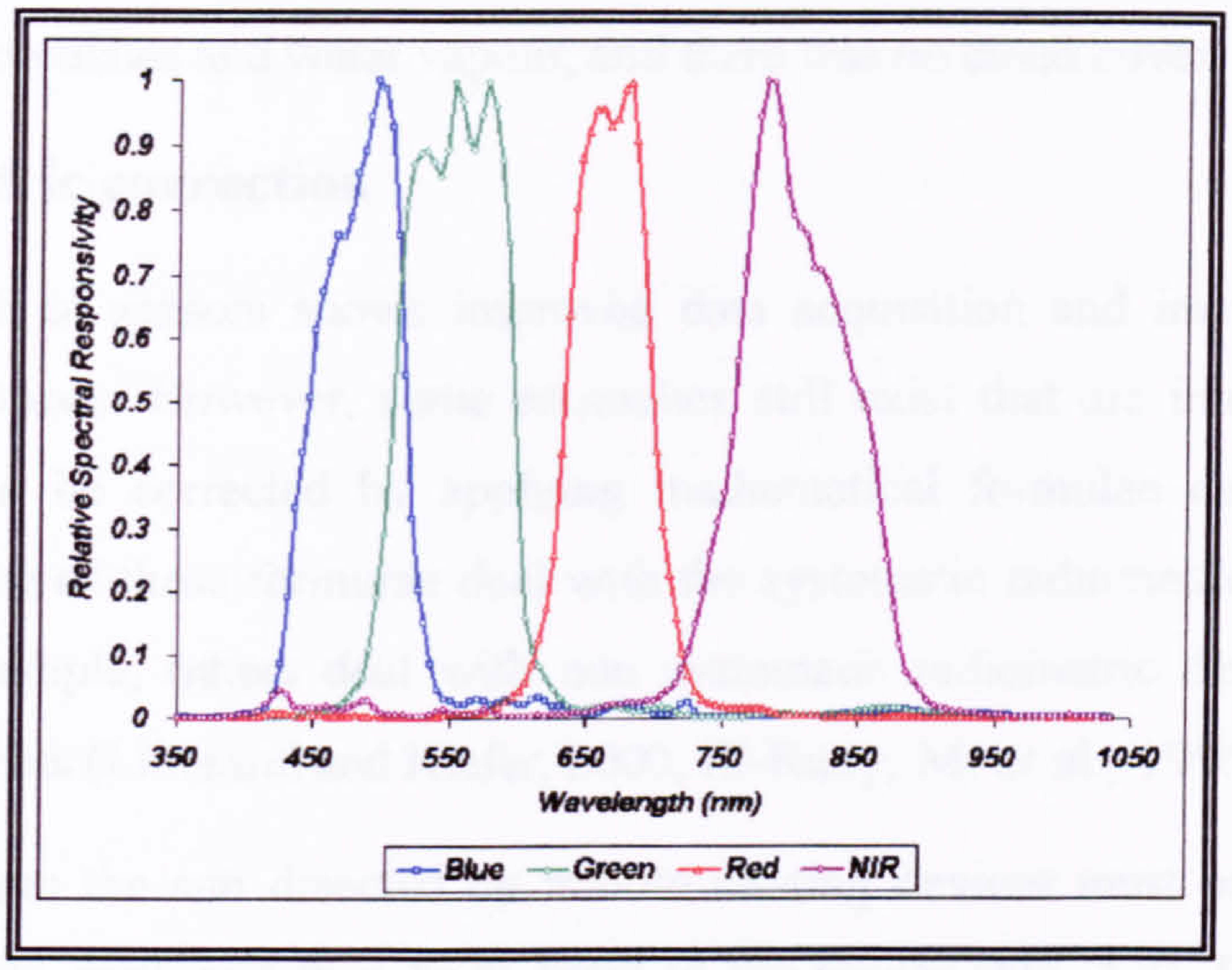

Figure 5.1. IKONOS relative spectral response.

5.3 Data acquisition

The selection of satellite images was according to the study requirement. As noted previously, the detection of coral reefs requires a spatial resolution of ٤ metres or better, with a blue wavelength band for water penetration, and green and near infrared bands to allow mapping of small islands (10 m or less) within the study area. The image base underlying this research consisted of IKONOS 11-bit multispectral satellite imagery of 4 m spatial resolution in the red, green and blue bands and 1 m resolution in the panchromatic band. The imagery was acquired on December 17 2004 at 08:08 GMT (10:08 local time). It was acquired in an 11-bit raw image format, without Modulation Transfer Function MTF or geometric corrections applied. For this study it was essential that the imagery be acquired in a non georeferenced form, rather than the usual systematically georeferenced form. The reason for this was that to make the map useful for the intended navigation purpose, the locational accuracy needed to be 4 metres or better, which could not be achieved with the automatic georeferencing applied by ground stations. Moreover, using a systematically georeferenced image, then carrying out a second georeferencing with GPS, would destroy the radiometric integrity of the image. Sea water clarity was high outside of Rabigh port area and turbid inside the port area, and the surface was calm. Atmospheric conditions were optimal, with low levels of atmospheric particulates and water vapour, and there was no cloud cover.

5.4 Radiometric correction

Each generation of sensors shows improved data acquisition and image quality over previous generations. However, some anomalies still exist that are inherent to certain sensors and can be corrected by applying mathematical formulae derived from the distortions. Some of these formulae deal with the systematic radiometric errors such as striping, for example; others deal with non systematic radiometric disorders such as atmospheric effects (Lillesand and Kiefer, 2000, El-Raey, M. et al., 1995).

All radiation from the sun detected by remote sensing devices must pass through the atmosphere to the earth and then back again to the sensor (Fig. 5.2). Due to the long distance or atmospheric path between the sensor and habitats under investigation, atmospheric effects are great. These effects are caused principally by the mechanisms of propagation of EMW through the atmosphere, including the effects of the ionosphere and troposphere. These effects could become apparent in the form of absorption and/or transmission scattering, and the removal of such effects is vital, especially when the images are to be used quantitatively or to detect habitat changes.

5.4.1 Absorption and/or transmission mode:

The absorption arrangement is frequently called the transmission mode. In contrast to scattering, atmospheric absorption results in the effective loss of energy. This normally involves absorption of energy at a given wavelength. The most efficient absorbers of solar radiation in this regard are water vapour, carbon dioxide and ozone, and these gases tend to absorb electromagnetic energy in specific wavelength bands.

5.4.2 Scattering:

Atmospheric scattering is the unpredictable diffusion of radiation by particles in the atmosphere. There are three types of scattering: Rayleigh scatter, Mie scattering and non-selective scattering. Rayleigh scattering is common when radiation interacts with atmospheric molecules and other tiny particles that are much smaller in diameter than the wavelength of the interacting radiation (Lillesand and Kiefer, 2004).

As the remotely sensed data acquired specially for this project will be used as quantitative values, the data must be radiometrically corrected. The advantage of conducting these calibrations is to get finally a standardized image presenting meaningful measures of reflectance (Karpouzli, 2003).

Green et al. (2000) mentioned that an image that is already radiometrically corrected has better definition and contrast and is free from "adjacency effects", since the absorption and scattering effects are removed. Calibration of satellite images starts with conversion of the digital number (DN) to a spectral radiance, then the radiance value needs to be converted to reflectance, and finally the atmospheric effects due to absorption and scattering have to be eliminated (Green et al., 2000).

The image being acquired for this project was ordered with zero correction before even the first stage. The processing started from the first stage by converting the image digital values (DN) into physical units of in-band radiance (mW cm^{-2} $ster^{-1}$) The distance through the atmosphere between the satellite sensors and the area under study is very long, resulting in great effects of scattering and absorption of the EMW during its propagation from the sensor to the habitats under study. These atmospheric effects must be removed, especially for marine applications due to their proportionately greater contribution to at-sensor received radiance over water targets (Gordon, 1997; Gordon et al., 1997; Gordon and Zhang, 1996; Royer et al., 1997.

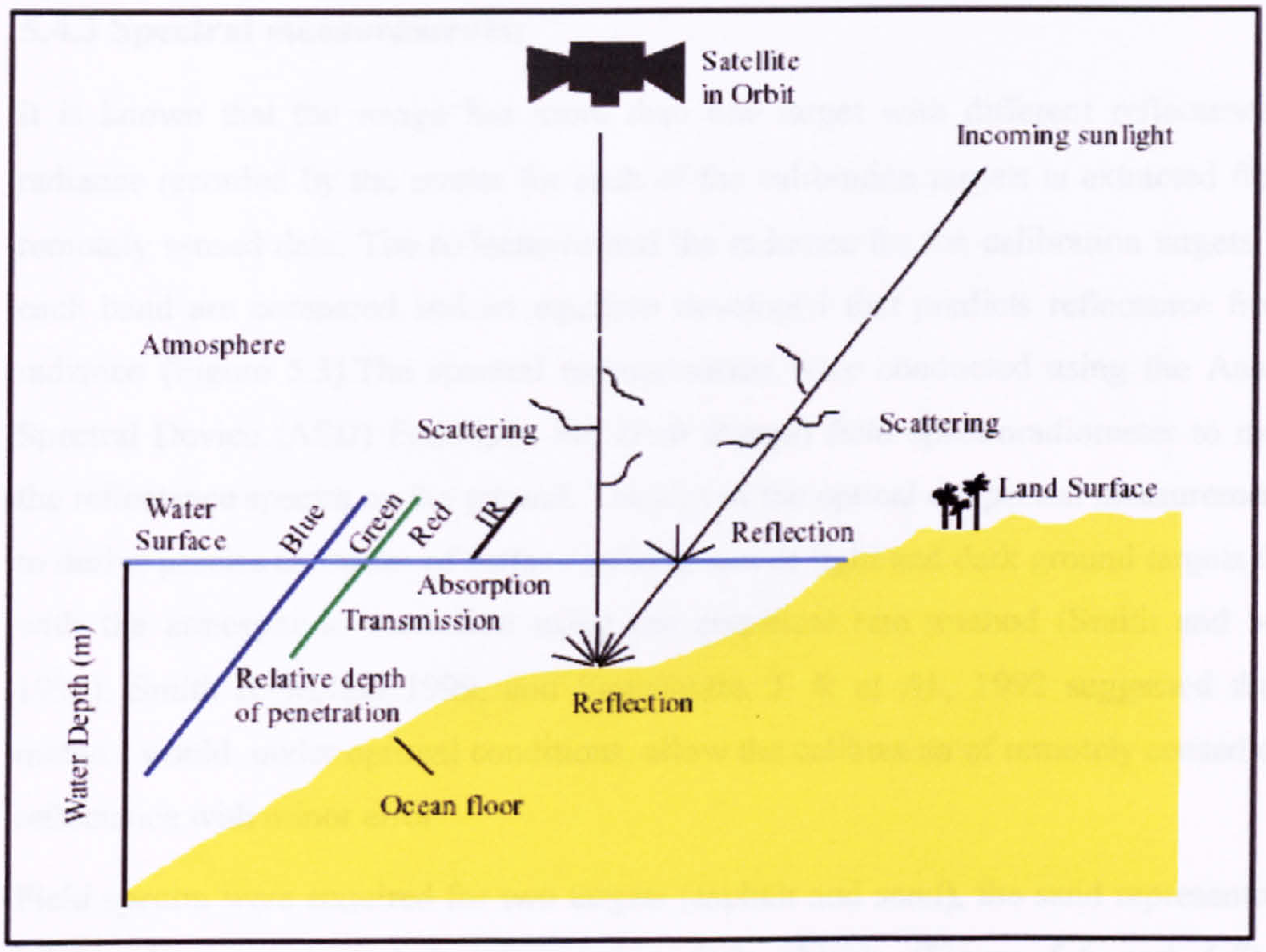

Figure 5.2. The passage of light from the sun through the atmosphere to Earth's surface and reflection from the surface up to satellite. *Source:* ***Kowalik et al., 1994.***

Perry et al. (2000) declared that the empirical line method is useful for short atmospheric distances for airborne data, due to its requirement for the identification of at least two standardized targets of contrasting reflectance, which should be large enough to be resolved. This technique has potential for the higher spatial resolution systems, such as IKONOS; however, it was difficult to calibrate spaceborne images with a pixel size of tens of metres such as Landsat TM and SPOT.

5.4.3 Spectral measurements:

It is known that the image has more than one target with different reflectances; the radiance recorded by the sensor for each of the calibration targets is extracted from the remotely sensed data. The reflectance and the radiance for the calibration targets within each band are compared and an equation developed that predicts reflectance from the radiance (Figure 5.3).The spectral measurements were conducted using the Analytical Spectral Device (ASD) FieldSpec Pro (Full Range) field spectroradiometer to measure the reflectance spectra on the ground. The aim of the optical or spectral measurement was to derive precise estimates of surface reflectances of light and dark ground targets for use with the atmospheric correction using the empirical line method (Smith and Milton, 1999). Smith & Milton 1999, and Freemantle, J. R et Al., 1992 suggested that this method would, under optimal conditions, allow the calibration of remotely sensed data to reflectance with minor error.

Field spectra were acquired for two targets (asphalt and sand), the sand representing the bright objects and asphalt representing dark objects (Figure 5.6 and 6.7). The measurements were carried out over an area of 12 x 12 metres, equivalent to a 3 x 3 pixel area, in order to negate the effects of point spread function, and to ensure a pure target pixel at the centre of the ground measurement area (Smith and Milton, 1999).

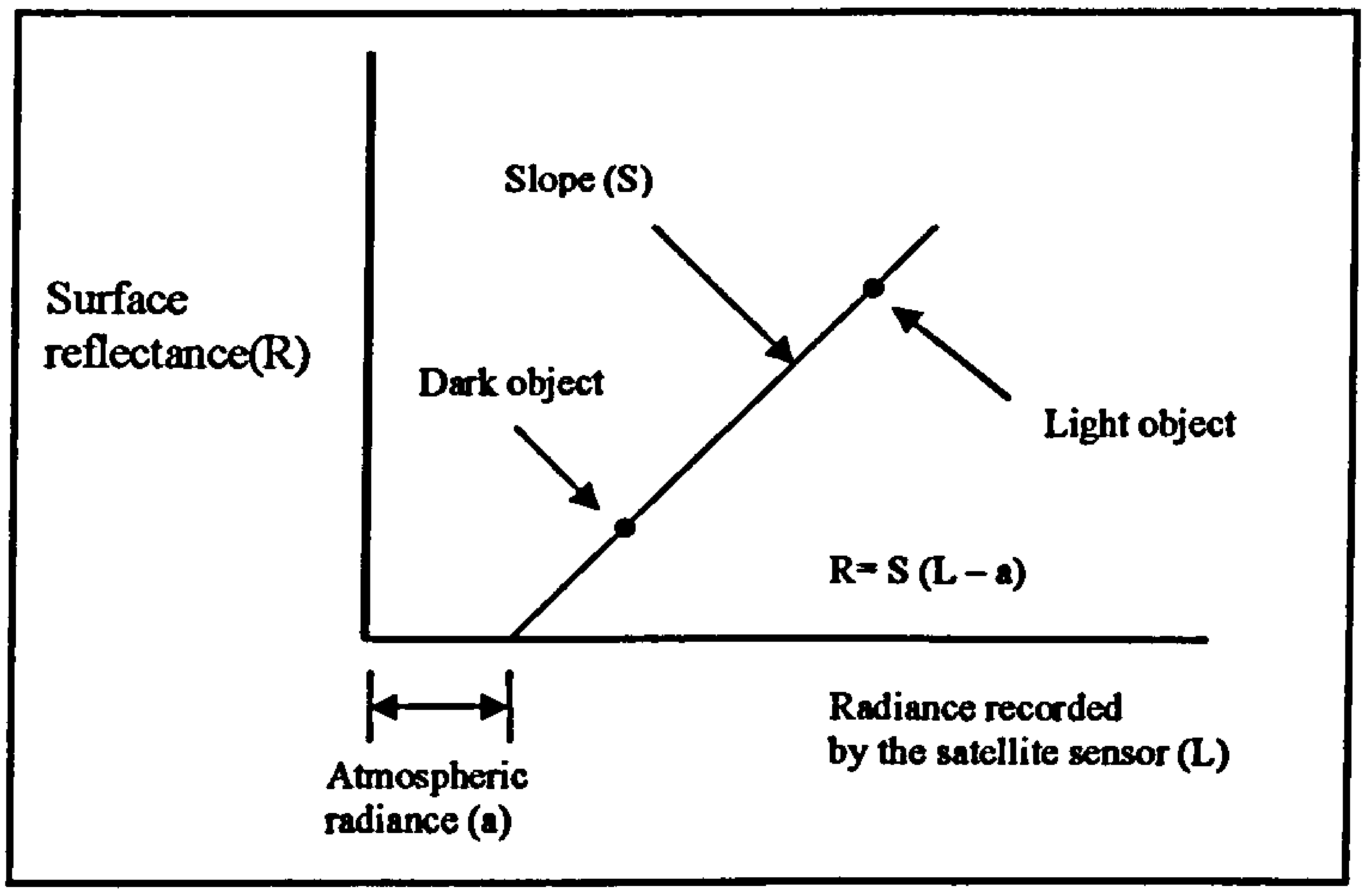

Figure 5.3. The development of a prediction equation from two calibration targets by the empirical line method. (Smith and Milton, 1998).

Figure 5.4. Practical spectral measurement of a dark object (asphalt).

Figure 5.5. Practical spectral measurement of a bright object (sand).

However, during the field collection of ground spectra, it was noticed that the dark object (asphalt) contained a light-coloured aggregate due to the old age of this object, which resulted in higher than expected reflectance values. The bright object (sand) was wet due to its location near the coast line and contained slightly darker aggregate, resulting in a lower than expected reflectance value. As a result, the spectral differences between the targets were insufficiently large to reliably establish a slope and intercept value with which to derive at-surface reflectance values from the IKONOS imagery using the empirical line method. Asphalt spectral values are given in Table 5.5 and shown in Figure 5.6, while the brightness values represented by sand are contained in Table 5.5 and Figure 5.7.

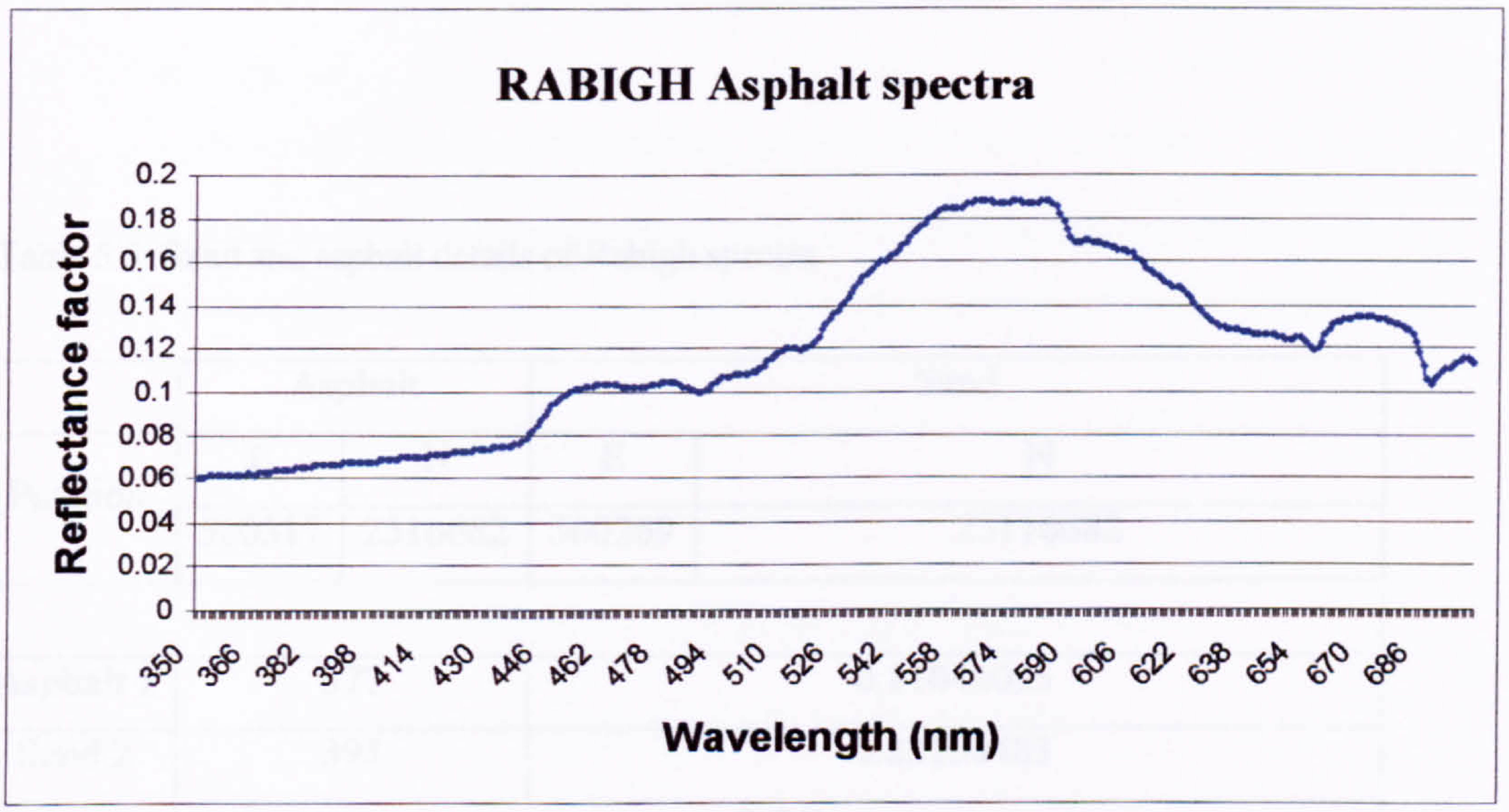

Figure 5.6. Rabigh asphalt spectra.

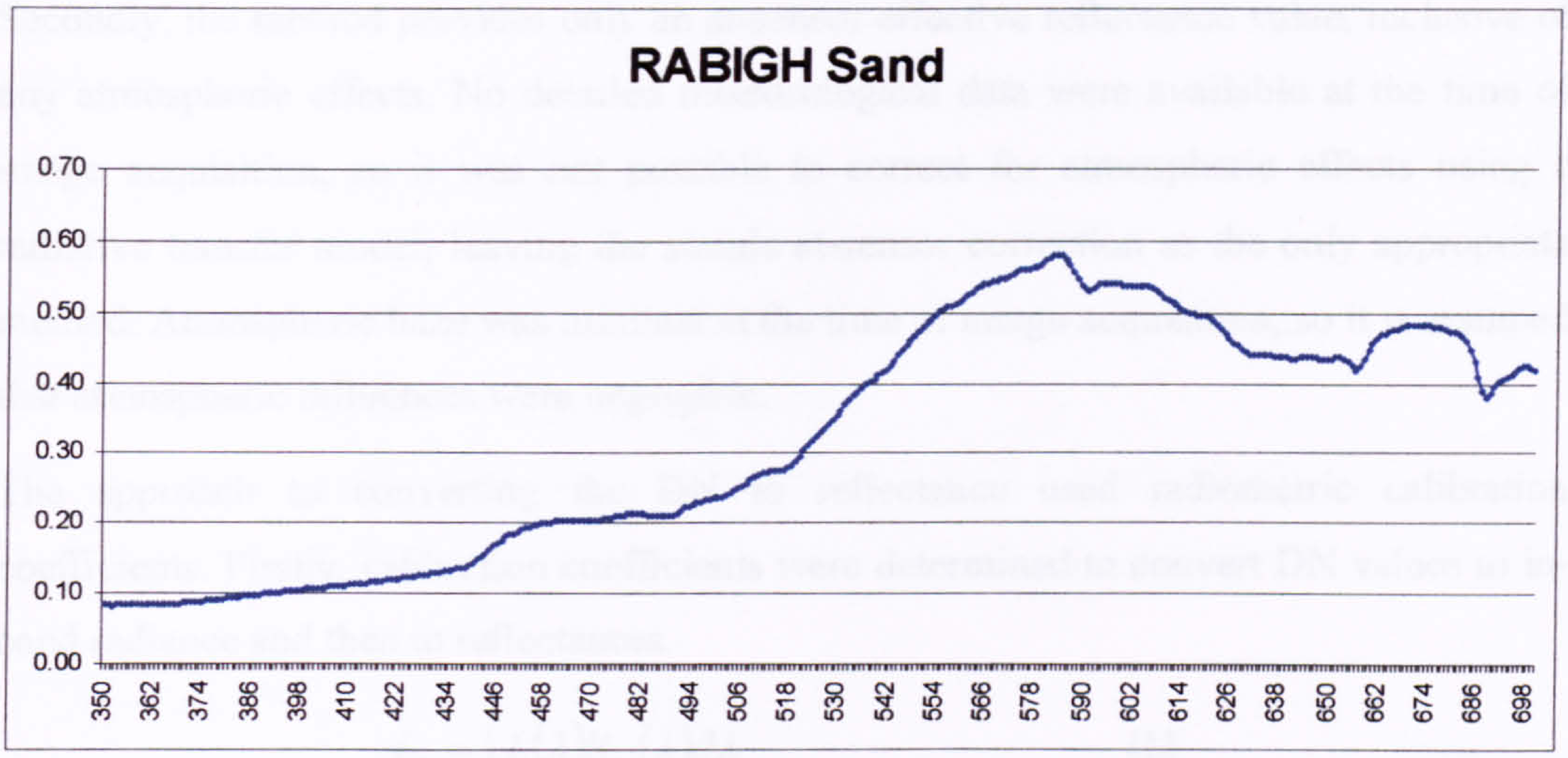

Figure 5.7. Rabigh sand spectra.

Table 5.5. Sand and asphalt details of Rabigh spectra

	Asphalt		Sand	
Position	E	N	E	N
	500317	2516682	500269	25116682
Asphalt 1	377		0.11048095	
Sand 2	393		0.23150483	
Intercept	-2.741			
Slope	0.007564			

As an alternative, the solution finally used was to convert raw DN values to at-satellite reflectances using the manufacturer's published calibration constants (Methodology of Markham and Barker, 1985, 1987), using ERDAS Imagine to carry out the process. This would not be the preferred method for two reasons. Firstly, the published calibration values are not regularly updated, so calibration drift of the sensors is not accounted for.

Secondly, the method provides only an at-sensor effective reflectance value, inclusive of any atmospheric effects. No detailed meteorological data were available at the time of image acquisition, so it was not possible to correct for atmospheric effects using a radiative transfer model, leaving the simple at-sensor correction as the only appropriate method. Atmospheric haze was minimal at the time of image acquisition, so it is assumed that atmospheric influences were negligible.

The approach to converting the DN to reflectance used radiometric calibration coefficients. Firstly, calibration coefficients were determined to convert DN values to in-band radiance and then to reflectances.

$$L_k = \int L(\lambda) R_k(\lambda) d\lambda \qquad . (1)$$

where: L_k = in-band radiance at the sensor aperture for IKONOS band k (mW/cm^2-sr)

$L_{(l)}$ = spectral radiance at the sensor aperture (mW/cm^2-sr-mm)

To convert digital values (DN) to physical units of in-band radiance (mW/cm^2-sr) equation (2) could be used and the converting model is built accordingly (Figure 5.7)

$$C_{i,j,k} = DN_{i,j,k} / C_k \qquad (2)$$

where the index i,j,k is the IKONOS image pixel *(i,j)* in spectral band *k*.

C_k is the calibration coefficient in band k $(mW/cm^2 * sr * DN)$

$C_{i,j,k}$ is in-band radiance at sensor aperture $(mW/cm^2 * sr)$

The final step of radiometric correction is the conversion of radiance to reflectance; the formula explained below is suitable to complete this process.

$$R = (\pi * L_c(\lambda)) / (E_\lambda \cos(\theta_s) * d^2) \qquad (3)$$

where:

R is the reflectance at the Top of the Atmosphere (TOA) for a given spectral calibrated radiance.

L_c Is the spectral calibrated radiance at the TOA.

E_λ Is the Solar spectral irradiance at the TOA, units $wm^{-2}\mu m^{-1}$

θ_s : The Solar zenith angle, degrees units.

d : The radius vector (ratio of mean to actual Sun-Earth distance) can be computed in the following way:

$$d = \frac{1}{(1-0.016729*\cos(0.9856(DOY-4)))} \text{ and } d = \frac{1}{d_0}.$$

With DOY : Julian day number, from 1 to 365-366.

d_0 : The Earth-Sun distance in astronomical units.

The formula could be written as:

$$R = (\pi * L_c(\lambda)) * d_0^2 / E_\lambda \cos(\theta_s) \qquad (4)$$

5.4.4 Models

Modelling processes deal with many sophisticated mathematical and statistical procedures in spatial dimensions. These processes differ from the traditional modelling processes for dealing with spatial data, often in raster format. For that reason, a special tool called ERDAS Imagine Model Maker was used to carry out the modelling procedure. ERDAS Imagine Model Maker in its original form is essentially a spatial modelling language with a graphical interface. This enables the researcher to create graphical models using a palette of easy-to-use tools. Graphical models can be run, edited, saved, or converted to script form and edited further using different programming language such as ERDAS IMAGINE SML, C and FORTRAN.

The objective of the following model is to convert the image from DN values to radiance. This conversion model depends mainly on the equations and calibration coefficients provided by the IKONOS satellite manufacturer. Table 5.4 explains the radiometric calibration coefficients and Table 5.6 shows the IKONOS spectral band characteristics.

Table 5.6 IKONOS Radiometric Calibration Coefficients for 11 bit products [mW/(cm2*sr*DN)].

Production Date	Blue	Green	Red	NIR
pre 2/22/01	633	649	840	746
post 2/22/01	728	727	949	843

Table 5.7 IKONOS Spectral Band Characteristics.

Band	**Lower 50% (nm)**	**Upper 50% (nm)**	**Bandwidth (nm)**	**Centre (nm)**
Pan	525.8	928.5	403	727.1
MS-1 (Blue)	444.7	516.0	71.3	480.3
MS-2 (Green)	506.4	595.0	88.6	550.7
MS-3 (Red)	631.9	697.7	65.8	664.8
MS-4 (VNIR)	757.3	852.7	95.4	805.0

The conversions were achieved through two main steps; firstly, conversion from raw DN to radiance, and secondly, the radiance image being converted into reflectance.

5.4.4.1 Conversion from DN values to Radiance

Figure 5.8 shows the model that was developed to convert IKONOS DN values to radiance. As shown in the aforementioned figure, the first step is to import the IKONOS image into the model. Unfortunately, ERDAS Imagine Model Maker cannot treat multi-band images with many equations at the same time. For that reason, the original IKONOS image was separated into its bands. Every band was transformed to radiance using conversion factors (intercept and slope) independently. After this step, the four radiance raster images representing the IKONOS images were produced.

The last step is to create a single multiband radiance image. To do that, the four radiance raster images were fed into the LAYER STACK process. This module – LAYER STACK – stacks the four calculated radiance bands together into memory. The final product after running the model will be the radiance image based on the original IKONOS image. The Block diagram shown in Figure 5.8 explains the conversion Model of 'Digital Number to Radiance'.

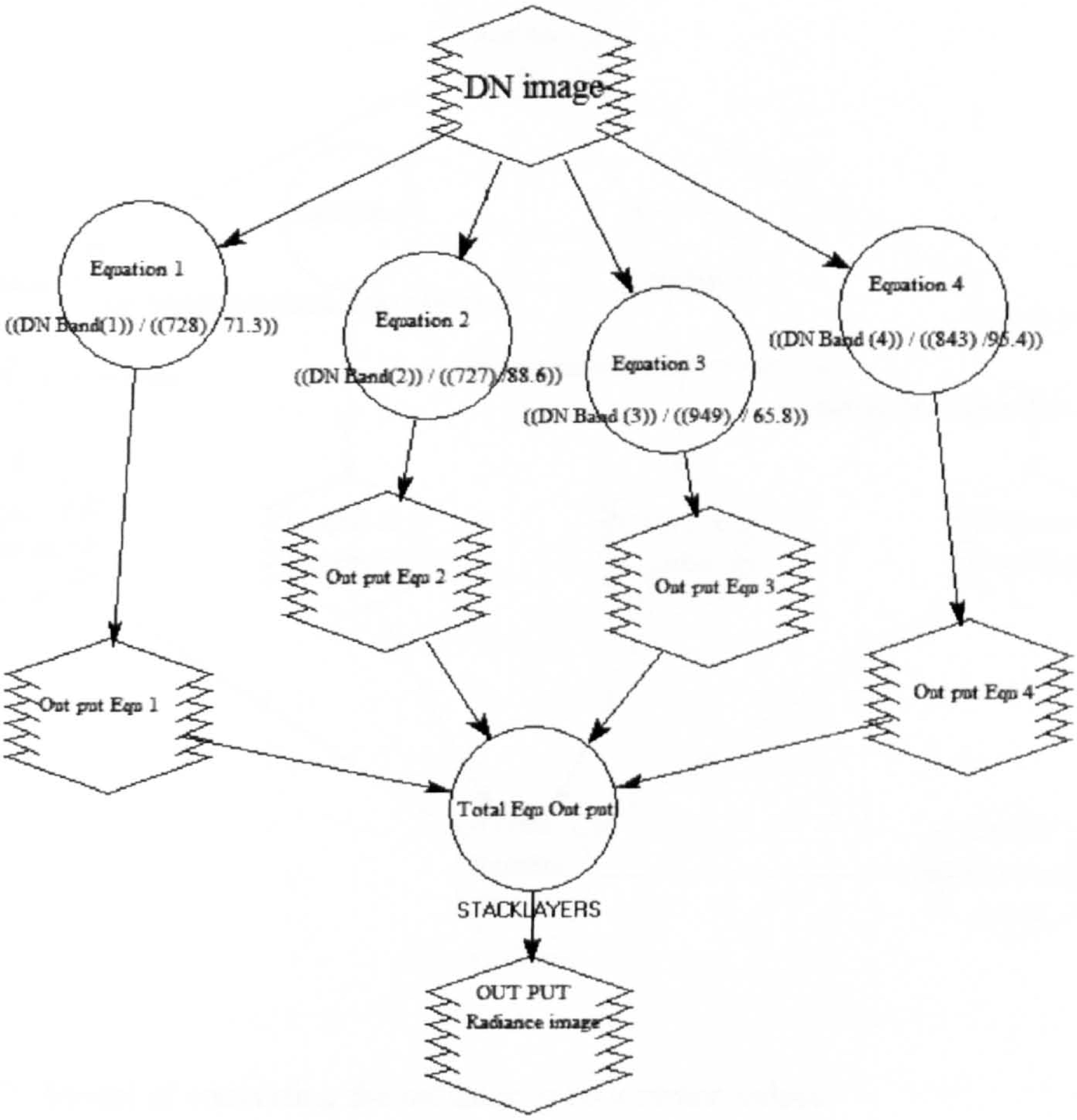

Figure 5.8 Model of converting the digital numbers to radiance values.

5.4.4.2 Conversion from Radiance to Reflectance

Conversion from radiance to reflectance follows a similar procedure to the conversion from DN to radiance presented in the previous section. The target image in this conversion is the radiance image produced previously. It was separated into four radiance images and converted using different equations, which are represented in equation 4 and 5. The results are four reflectance rasters. These four rasters are stacked using the LAYER STACK module to produce the reflectance map. The Block diagram shown in Figure 5.9 explains the conversion Model of Radiance to Reflectance.

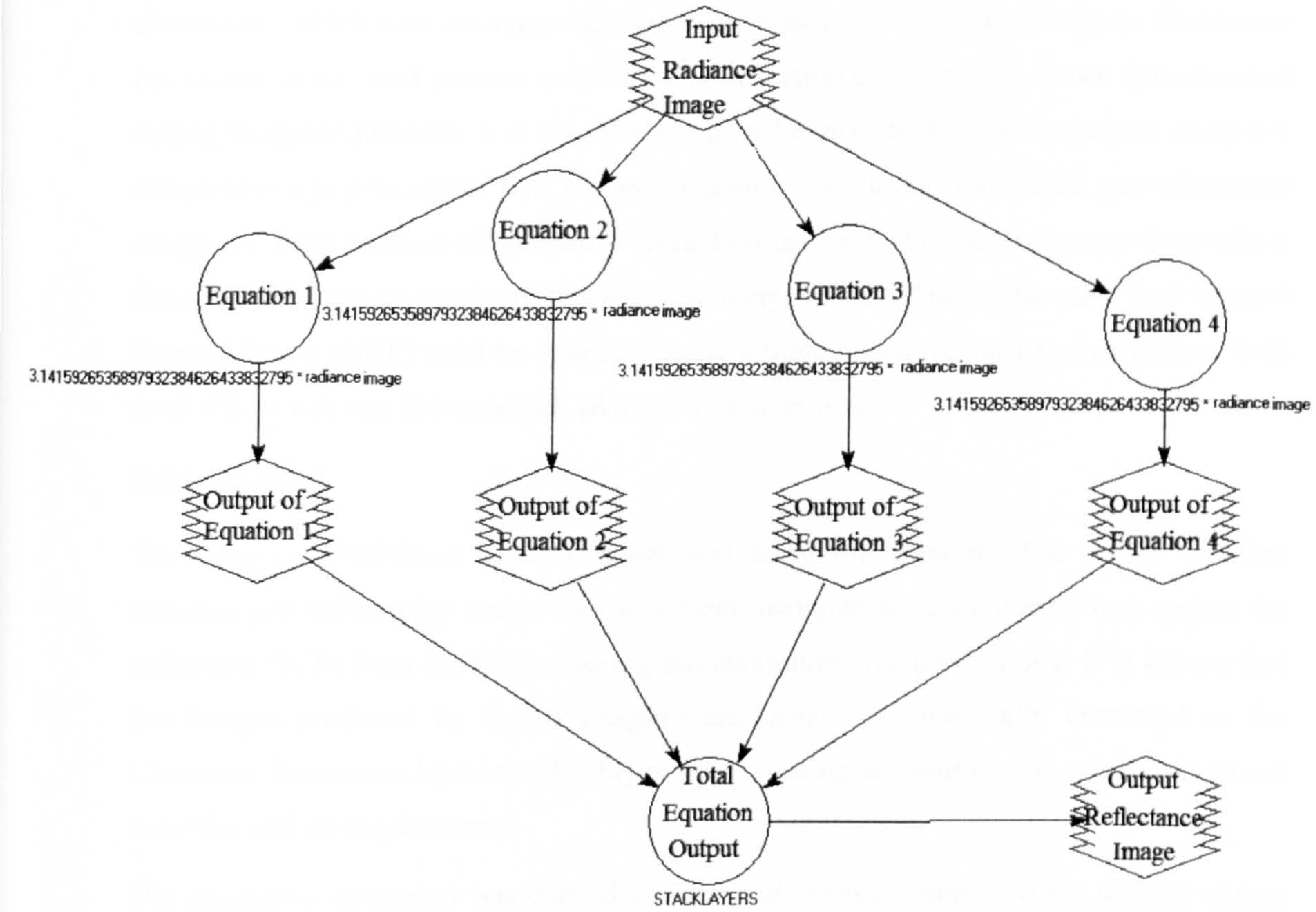

Figure 5.9. Model of converting the radiance to reflectance values.

5.5 Geometric correction

Satellite images are very important tools in various applications such as land use and land cover mapping. Remotely sensed images have to be geometrically corrected if they are to be used as maps; they are often considered as maps of the radiometric properties of the earth's surface. Since this study is focusing on hydrographic surveying to help the navigators map and identify navigational hazards, it was vital to search for accuracy starting with the positioning system, survey vessel, depth finder and other equipment used in this project.

Several factors involved in the process of image acquisition introduce geometric distortions, which then are removed by pre-processing of the digital imagery. Geometric correction is the vital process needed for rectification of geometric errors that occurred during image acquisition. It is possible to geo-reference the IKONOS imagery using the image-to-image procedure. This process is useful when there is a similar geo-referenced image. Another method of geometric correction uses a highly accurate map from which the coordinate can be obtained. If there is no image or map that can be used, then Ground Control Points (GCP) must be collected using a highly accurate positioning system, such as *d*GPS, which was the approach adopted in this project.

5.5.1 Method

The image ordered from Space Imagery was not geo-referenced. The reason was that accurate geo-referencing was to be carried out, using an accurate positioning system for collecting GCPs from the field covering the maximum area under study. It is known that the images produced by Space Imaging are usually geometrically corrected to the Universal Transverse Mercator (UTM) projection using an orbit model, which would not meet the project requirements.

The geometric correction was carried out using 30 ground control points (GCPs) within the port approach area of Rabigh (Study area 1), acquired with the Leica 500 RTK rover receiver, giving a horizontal accuracy of ± 5cm. A first order transformation of the image was carried out, using nearest neighbour resembling to preserve radiometric integrity and avoid averaging of neighbouring pixels. The GCP points consisted of jetty corners, road intersections, fixed navigational marks and other easily identified objects with stable positions (Figure 5.10). The image was transformed to a UTM projection (zone 37) with a WGS84 ellipsoid, and an overall root mean square (RMS) error of 0.4 m was obtained.

The selected GCPs were easily recognizable features that could be found within the area and the corresponding image. After collecting the GCPs from the field, the second step of the geo-reference process started by identifying these GCPs on the image using ERDAS Imagine software (version 8.5). This is done by entering the GCPs co-ordinates into the "Data preparation/ image Geometric correction". A least squares regression analysis was made for these values to find the co-ordinate transformation equation coefficients. A Root Mean Square (RMS) error was calculated for each GCP and then for all of them (see Table 5.3), where the error found for X was 0.3821 m, while Y was 0.2123 m,and the total error average for the 30 observations used for geometric correction was 0.4372 m, which is considered as acceptable. The excellent accuracy resulted from the ±5 cm delivered by the accurate positioning system.

The same procedure was carried out for the Kishran area (study area 2) using the polynomial model, with the geo-referencing performed using 14 GCPs (Table 5.4) distributed within the entire area to rectify and correct any distortion (Figure 5.11). The average RMS was 0.2409 m.

The RMS errors in Table 5.3 and 5.4 are defined as the difference or distance between the original source of GCPs and its retransformed co-ordinates. Using the polynomial model, the RMS calculated for both study areas was within the acceptable range, with these errors being less than the IKONOS pixel, and within the *d*GPS error (Karpuzli, 2003). The main goal of this project is accuracy; therefore, true and independent GCPs were used in the rectification process. The tables mentioned above explain the accuracy assessments. Generally, the accurate positioning system helped in minimizing the RMS, as the reference station of dGPS was located in the middle of the study area, which resulted in an accuracy of ±5 cm in the positioning system. One important factor that helped to achieve this accuracy in RMS was the timing of the acquisition and field measurement; the acquisition took place on the same days as the field measurements.

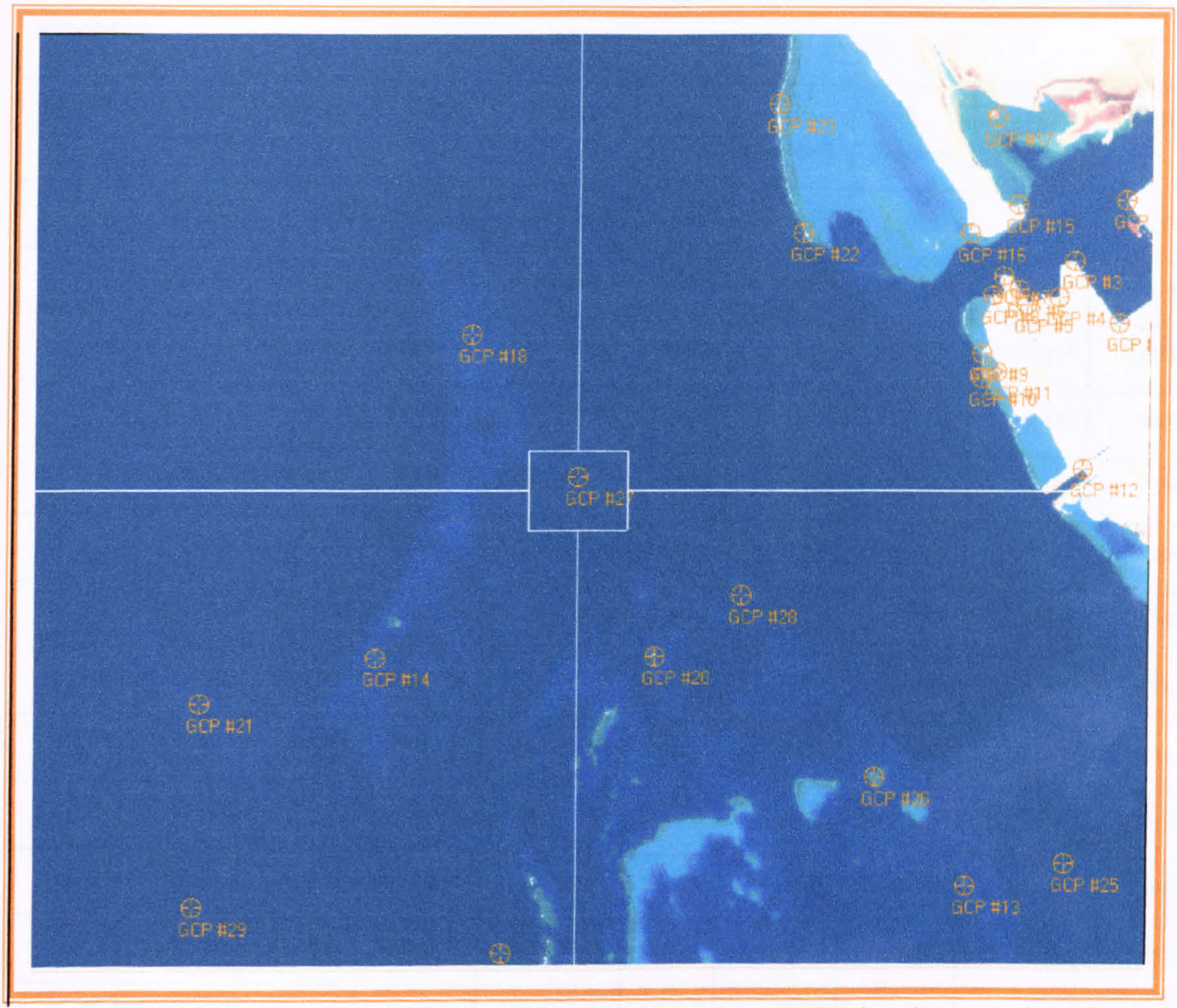

Figure 5.10. IKONOS image of Rabigh ports with selected ground control points for geo-referencing.

Table 5.8 GCPs used for geometric correction of Rabigh IKONOS image (for more details, see appendix).

GCP-ID	X input	Y input	X Ref	Y Ref	Type	X Residual	Y Residual	RMS Error	Contribution
1	3363.353	-612.327	500299.73	2515223.52	Control	0.188	-0.413	0.454	1.159
2	3344.66	-1011.12	500220.67	2513868.4	Control	-0.94	0.52	1.075	2.746
3	3239.464	-860.47	499862.87	2514376.69	Control	0.352	-0.029	0.353	0.903
4	3235.442	-850.54	499848.40	2514410.04	Control	0.146	-0.129	0.194	0.497
5	3227.524	-832.695	499819.47	2514471.93	Control	-0.382	0.266	0.466	1.190
6	3189.443	-804.542	499688.81	2514565.56	Control	-0.049	-0.091	0.104	0.264
7	3161.291	-919.539	499588.78	2514173.6	Control	0.198	0.016	0.199	0.507
8	3129.619	-926.577	499477.84	2514148.92	Control	0.043	0.037	0.057	0.146
9	3112.401	-930.599	499417.99	2514133.75	Control	0.093	-0.263	0.279	0.712
10	3077.665	-938.391	499360.02	2514124.15	Control	0.009	-0.004	0.009	0.024
11	3095.686	-933.49	499296.61	2514106.8	Control	0.173	-0.063	0.184	0.469
12	2967.618	-840.612	498916.32	2514436.04	Control	0.072	-0.337	0.345	0.881
13	2927.401	-781.417	498776.75	2514638.65	Control	-0.251	0.291	0.384	0.981
14	3292.952	-430.825	500057.02	2515840.52	Control	-0.475	-0.143	0.496	1.267
15	2883.448	-708.23	498626.16	2514886.17	Control	-0.100	0.144	0.176	0.449

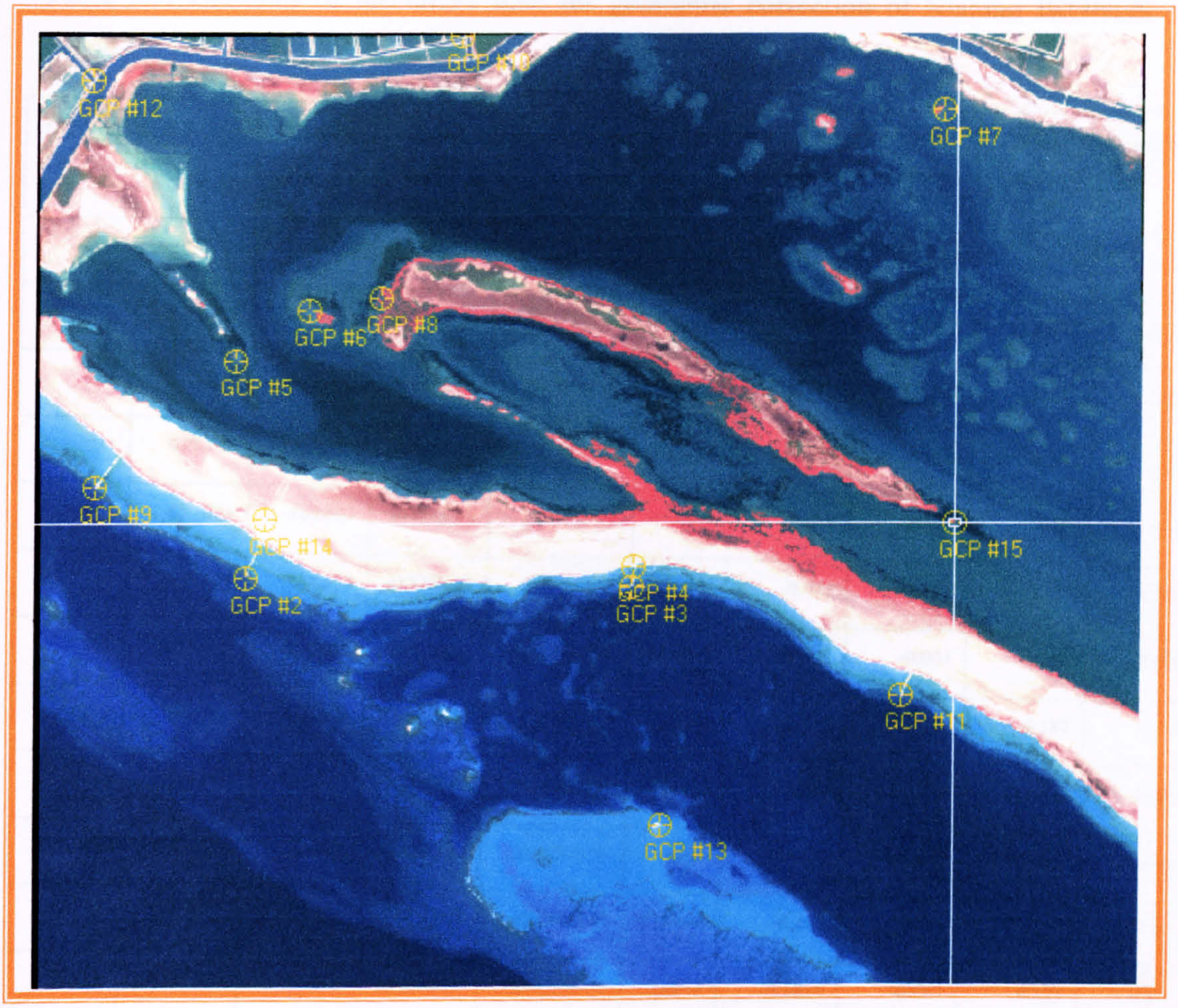

Figure 5.11. IKONOS image of Kishran area with selected ground control points for geo-referencing.

Table 5.9. Positions of the GCPs used for geometric correction of Kishran IKONOS image.

GCP-ID	X input	Y input	X Ref	Y Ref	Type	X Residual	Y Residual	RMS Error	Contribution
1	653.385	-1700.208	606641.16	2237743.145	Control	0.129	-0.28	0.308	1.28
2	1859.322	-1740.214	610616.84	2237646.46	Control	0.195	0.098	0.218	0.90
3	1863.262	-1679.295	610628.01	2237845.87	Control	-0.001	-0.113	0.113	0.47
4	625.199	-1017.379	606533.88	2239984.79	Control	-0.248	-0.075	0.260	1.08
5	850.384	-860.083	607273.57	2240507.64	Control	-0.089	-0.016	0.09	0.38
6	2829.509	-244.554	613785.25	2242582.29	Control	0.042	-0.321	0.324	1.346
7	1075.266	-820.077	608014.29	2240645.26	Control	0.000	-0.003	0.003	0.012
8	183.791	-1416.374	605088.38	2238663.47	Control	0.2647	0.174	0.317	1.314
9	1329.485	-7.835	608837.15	2243319.96	Control	0.181	0.309	0.358	1.486
10	2695.339	-2093.975	613378.35	2236509.21	Control	-0.031	0.406	0.407	1.688
11	181.271	-137.863	605054.07	2242860.47	Control	-0.165	0.071	0.1797	0.746
12	1947.514	-2492.575	610920.99	2235178.32	Control	-0.1055	-0.063	0.123	0.511
13	713.293	-1518.441	606834.40	2238342.03	Control	-0.087	-0.133	0.159	0.662
14	2863.328	-1552.442	613921.46	2238290.25	Control	-0.083	-0.05	0.097	0.4

5.6 Conclusion

This chapter explained the main procedures employed for image processing. As mentioned previously, the images acquired for this study were in raw format, with no georeference or radiometric corrections having been carried out. All processing was carried out using the accurate positioning provided by dGPS during the collection of control points within the areas under study. Spectral measurements were collected in both study areas (Rabigh and Kishran) to measure the reflectance spectra for both sand as a bright object and asphalt as a dark object using the Analytical Spectral Device (ASD) FieldSpec Pro (Full Range) field spectroradiometer. It took into consideration the size of the area under measurement; the area selected was more than 12 m by 12 m.

The target measurements were not satisfactory due to the nature of the area; the dark object (asphalt) was old so it contained a light-coloured aggregate, which resulted in higher than expected reflectance values. Also, the sand, which represented the bright objects, was wet due to its location near the coastline and contained slightly darker aggregate, resulting in lower than expected reflectance values. Thus, the manufacturer's published calibration constants were used to convert the DN values to at-satellite reflectance. This method is an alternative method for converting DN to radiance and then to reflectance, and would not be the preferred method for two reasons. Firstly, the published calibration values are not regularly updated, and secondly, the method provides only an at-sensor effective reflectance value, inclusive of any atmospheric effects. The correction of atmospheric effects using a radiative transfer model was not possible in this stage, but it is recommended that the spectral measurement (empirical line) method is used in any further calibration.

The next step of image processing was the image geo-referencing. This type of process is normally carried out if the images are to be used as maps. Geometric correction is a very important process, needed for rectification of geometric errors that occur during image acquisition. Ground Control Points (GCP) are collected using highly accurate means of positioning, such as *d*GPS. The GCP points were selected carefully using the edges of jetties, road junctions, buoys and islands edges. Generally, the accurate positioning system helped in minimizing the RMS as the dGPS reference station was located in the middle of study area, which resulted in an accuracy of ±5cm in the positioning system.

CHAPTER SIX

DATA ANALYSIS

6. DATA ANALYSIS

6.1 Introduction

The bathymetry of coastal waters such as in the Red Sea is of fundamental importance for shipping safety, due to the presence of navigational hazards. The conventional hydrographic surveying or measuring of water depth is accurate for point measurement (Li-Guang et al., 2005). On the other hand, it is characterized by a list of difficulties or disadvantages. Firstly, it is a time consuming, labour-intensive task requiring a huge budget. Secondly, the traditional survey has poor geographical coverage, particularly in coral reef areas due to the limitations of the survey vessel draught. An alternative solution was found in the remote sensing method. Since the mid 1980s, medium spatial resolution (10–30 m) optical satellite data have been used to study and monitor coral reefs (Andrefouet et al., 2001). These methods use data delivered by the Indian Remote Sensing Satellite C (IRS-C), Satellite pour l'Observation de la Terre (SPOT) 1–4 High Resolution Visible (HRV), Landsat 5 Thematic Mapper (TM), and more recently by SPOT 4–5, Landsat 7 Enhanced Thematic Mapper Plus (ETM+), and Advanced Spaceborne Thermal Emission and Reflection Radiometer (ASTER) sensors. In contrast, high spatial resolution images, i.e. those with a spatial resolution better than 10 m, such as those provided by IKONOS or Quickbird (1–4 m) (Andrefouet et al., 2003) have not been widely utilized.

This study aims to clarify the potential of high spatial resolution IKONOS data for estimating water depth.

In a review of remote sensing bathymetric applications, Lyzenga (1978) noted that the previous studies, using aerial photography, had determined that bottom reflectance patterns, even in shallow water, were modified by the attenuation of light in the overlying water column. Early studies, using multispectral methods, established that several factors control the accuracy of deriving bathymetry, including water characteristics, sea bottom type (bottom reflectance) and atmospheric conditions. Under such conditions, depth as well as the effective attenuation coefficient could be derived from multispectral imagery (Mishra and Narumalani, 2004). The theory was explained and developed by Lyzenga (1978, 1981) and then extended by Philpot (1989). Maritorena et al. (1996) confirmed the validity and problems involved with using remote sensing for the determination of water depth. Changes in water characteristics and atmospheric conditions will affect the reliability with which absolute bathymetry can be determined, and spectral data can only be used to establish depths if accompanied by contemporaneous in-situ measurements. Mapping and deriving water depth using satellite images has several limiting factors, especially those related to the variable effects of the water column on the optical reflectance properties as measured remotely and in situ (Holden and LeDrew, 2001). Although passive optical systems are limited in depth penetration and constrained by water turbidity, the use of such satellite data might be the only possible way to reliably map water depth (Stumpf and Holderied, 2003). However, the use of such satellite data is the only way to safely map coral reef areas due to the difficulty of obtaining water depth by traditional hydrographic depth measurement. In order to measure water depth in regions where coral reefs present a major hazard to navigation and their horizontal extent can be 10 m or less, the optical satellite imagery required to provide a reliable tool for mapping such reefs must have a spatial resolution of 4 m or better. Landsat and SPOT imagery offer global coverage of coral reefs, but they have limitations caused by the pixel sizes of 30 and 20 m, respectively

Aircraft can provide sufficiently high spatial resolution for coral reef mapping, but with high costs. It was not until the 1999 launch of the first commercial Very High spatial Resolution (VHR) satellite, IKONOS-2, that digital satellite imagery of adequate spatial resolution became available to the civilian market. The 1999 IKONOS-2 launch was followed in 2001 by QuickBird 2 and in 2003 by Orbview 3, all of which are capable of providing multispectral imagery with spatial resolution of 4 m or finer. These satellites provide multispectral data with three visible bands (blue, green and red) and one near infrared band (NIR). Stumpf et al. (2003) stated that the information about bathymetry related to globally extensive coral reefs is fragmented and incomplete due to difficulties of obtaining echo sounding data for oceanic regions. They challenged that the development of new strategies to enhance depth estimation techniques could be possible with high spatial resolution imagery such as IKONOS and Quick Bird.

The objective of this research is to develop a method for the production of accurate bathymetry maps of shallow water areas in the Red Sea using high spatial resolution multispectral IKONOS satellite imagery and field measurements. Two study sites were utilized for this research, representing the extremes of water conditions encountered in the region. The first site, representative of turbid water conditions, was the Rabigh port manoeuvring area. The second site at Shab Tanta was representative of clear water conditions within coral reef areas. Simple linear regression was applied to relate field measured water depths to pixel brightness values in the blue band of IKONOS multispectral imagery that had been corrected to at-satellite reflectance using published calibration coefficients. The regression relationship at the clear water site was highly accurate (r^2 = 97%) for water depths in the range of 2 to 18 m. Some deterioration in the regression fit for turbid regions was noted, due to variability in image reflectance, but an r^2 fit of 81.9% was achieved, which meant that the linear equation was transferable between the sites. Finally, a comparison between actual depth measured by hydrographic echo sounder during the field measurement and the estimated depth derived from satellite images was made to establish the margins of error in the estimates. A mean of error of 2.65% (SD = 3.3 m, Median = 1.7) overall, with an accuracy of 97.35% was found. This result demonstrates that, for this region, depth estimations of sufficient accuracy for bathymetric mapping can be derived from IKONOS imagery without the need to collect in-situ atmospheric measurements or field spectroscopy for correction to at-surface reflectance values.

6.2 Modifying the single-band algorithm, using simple linear regression to predict water depth of the Rabigh area

Since we have the actual values of depth measurement taken from the Rabigh area and the values of reflectance (band 1) from the preceding steps, the depths in unknown areas can be predicted. Note that data was collected from both turbid and clear water. A simple linear regression technique has been employed. The model can be expressed in the following form:

$$D_i = \beta_0 + \beta_1 R_i \qquad (1)$$

where:

D_i is the value of the actual depth in the *i*th observation (response variable);

R_i is the value of the reflectance in the *i*th observation (predictor variable);

β_0 is the R intercept of the regression line. In our study β_0, by itself, has no meaning since the study does not cover reflectance at zero;

β_1 is the slope, i.e. the change rate of reflectance; and

i=1… n where n is the number of observations.

We need to estimate the coefficients of regression in model (1) using the available data. By using *Minitab*, we could easily derive the model.

$$\hat{D} = 77.2 - 598R \qquad (2)$$

Table 6.1. Regression analysis equation of Rabigh water.

Predictor	**Coef.**	**SE Coef.**	**T**	**P**
Constant	77.1945	0.9159	84.28	0.000
Ref-1	-598.459	8.707	-68.74	0.000

S = 0.657095 R^2 = 96.8% R^2(adj) = 96.7%

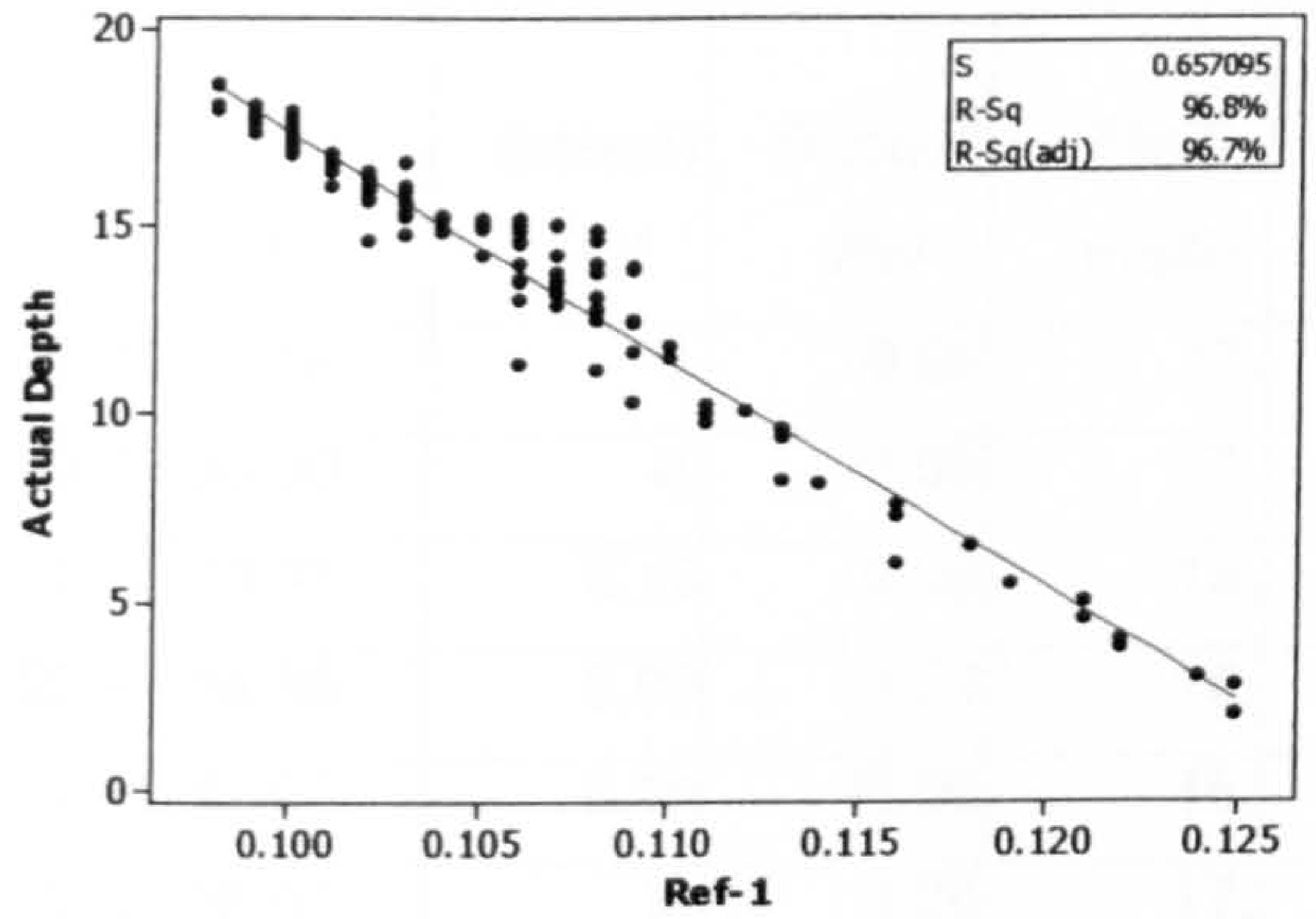

Figure 6.1(a). Regression model for all of the Rabigh area, both clear and turbid water.

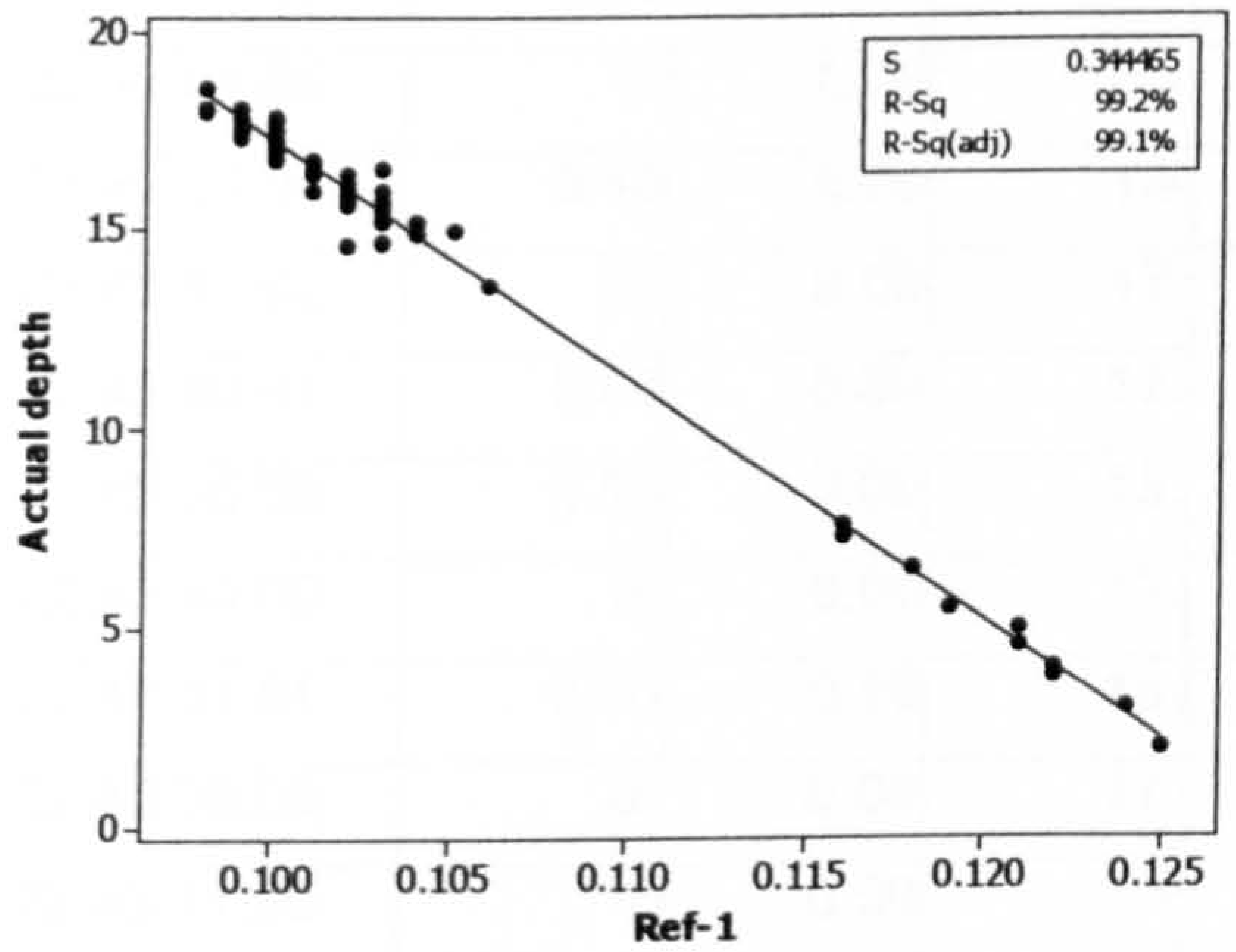

Figure 6.1(b). Regression model of the Rabigh area for clear water (the gap shown in the centre is for Port data (Turbid water), see Figure 6.1(a)).

Table 6.2. Rabigh reflectance, field depths and estimated depths of selected locations for clear waters, followed by estimated depths given by the Al-Llith algorithm.

Long	Lat	Babnd1 Ref	Babnd2 Ref	Field depth	Estimated depths	Estimated depth using Al-lith algorithm
38 55 45.22	22 42 37.94	0.	0.09	17.	17.	16.7
38 55 46.72	22 42 36.00	0.	0.09	17.	17.	16.4
38 55 46.99	22 42 33.95	0.10	0.09	15.	1	15.4
38 55 47.90	22 44 08.95	0.09	0.09	18.	17.	17.2
38 55 48.84	22 42 32.88	0.10	0.09	15.	16.	15.7
38 55 50.22	22 42 36.03	0.	0.09	17.	17.	16.7
38 55 51.04	22 44 08.65	0.	0.09	17.	17.	16.9
38 55 51.80	22 42 34.02	0.10	0.09	1	15.	15.2
38 55 51.97	22 42 54.00	0.10	0.09	15.	16.	15.7
38 55 52.97	22 43 01.05	0.	0.09	16.	1	16.4
38 55 53.03	22 42 50.94	0.10	0.09	14.	14.	14.4
38 55 53.04	22 43 57.02	0.	0.09	17.	17.	16.7
38 55 53.74	22 43 40.01	0.09	0.09	17.	17.	17.2
38 55 54.98	22 42 55.08	0.10	0.09	15.	15.	14.7
38 55 54.98	22 43 49.00	0.	0.09	17.	17.	16.7
38 55 55.98	22 42 51.61	0.10	0.09	15.	15.	14.7
38 55 56.06	22 43 38.56	0.	0.09	17.	17.	16.9
38 55 56.08	22 43 41.00	0.	0.09	1	1	16.4
38 55 56.09	22 43 57.13	0.	0.09	17.	17.	16.9

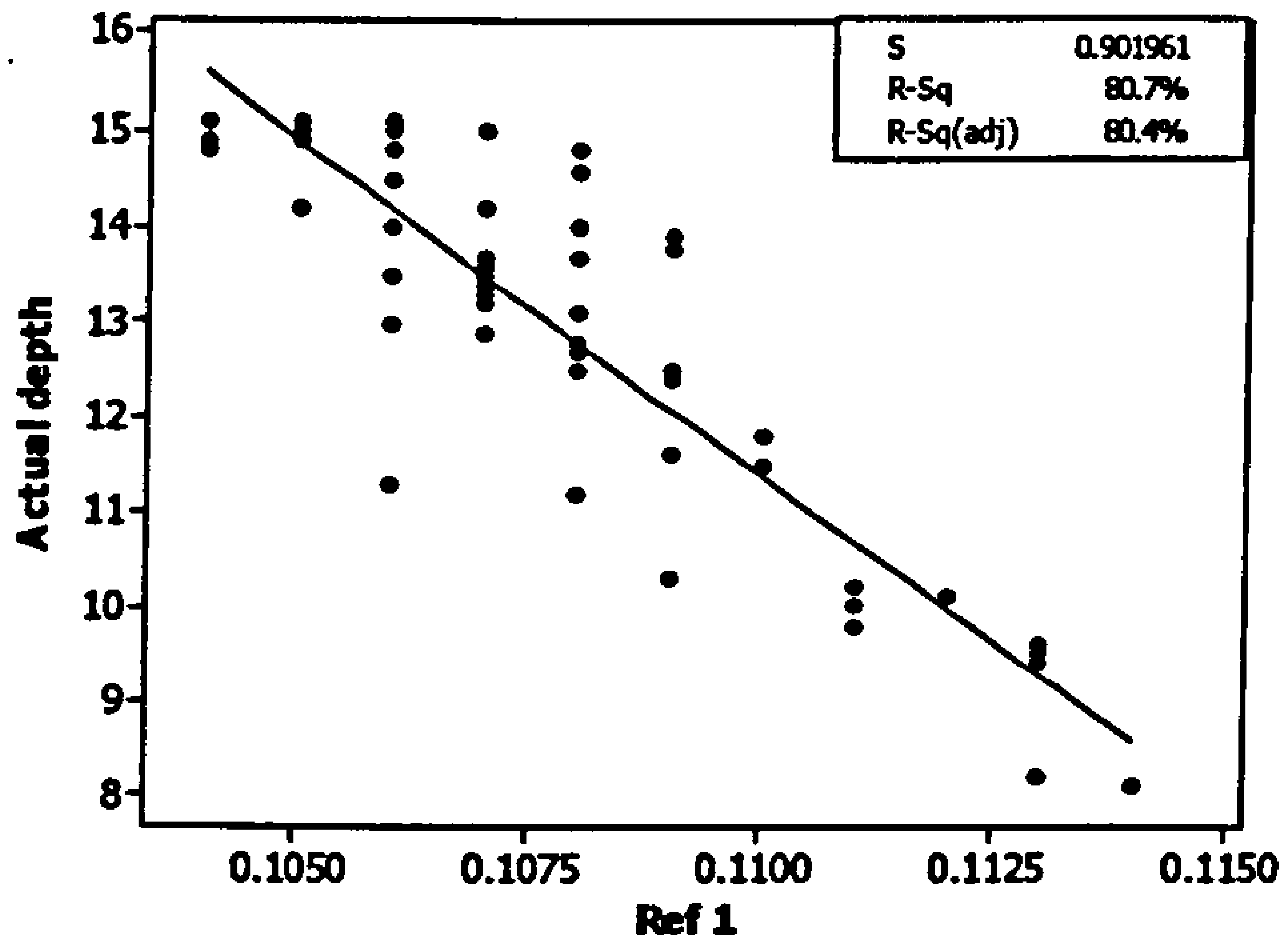

Figure 6.1(c). Regression model of the Rabigh area turbid water

Table 6.3. Rabigh reflectance, field depths and estimated depths of selected locations for turbid waters, followed by estimated depths adopted by the Al-Llith algorithm.

Long	Lat	Babnd1 Ref	Babnd2 Ref	Field depth	Estimated depth	Estimated depth b Al-lith model
38 59 33.29	22 44 07.18	0.10	0.10	13.	13.	12.7
38 59 34.03	22 44 05.94	0.10	0.11	12.	12.	12.2
38 59 36.00	22 44 11.00	0.10	0.10	14.	14.	14.2
38 59 38.95	22 44 51.03	0.10	0.1	14.	13.	12.7
38 59 38.99	22 44 50.43	0.1	0.11	11.	11.	10.95
38 59 39.00	22 44 46.00	0.10	0.10	14.	14.	14.2
38 59 39.01	22 44 10.93	0.10	0.10	14.	15.	14.7
38 59 39.25	22 44 50.01	0.10	0.11	1	13.	12.9
38 59 39.95	22 44 48.99	0.10	0.10	12.	12.	11.95
38 59 40.02	22 44 10.99	0.10	0.10	15.	13.	13.4
38 59 40.03	22 44 10.99	0.10	0.10	1	13.	13.4
38 59 40.03	22 44 10.02	0.10	0.10	15.	13.	12.5
38 59 41.09	22 44 11.33	0.10	0.10	15.	14.	13.7
38 59 41.11	22 44 07.99	0.10	0.11	1	13.	12.7
38 59 46.59	22 44 49.15	0.10	0.	14.	1	14.2
38 59 58.90	22 44 09.01	0.10	0.10	14.	13.	12.9
38 59 59.02	22 44 08.97	0.10	0.11	14.	12.	12.2
38 59 59.12	22 44 10.00	0.10	0.11	14.	14.	13.9

6.3 Prediction of new depths

The aim of this step is to predict new depths using available data (actual depth measured by echo sounder and estimated depth predicted by the actual depth versus pixel reflectance). This can be done by conducting a new linear regression analysis of actual depth versus estimated depth (equation 3).

$$\hat{D}_{new} = B_0 + B_1\hat{D} \qquad (3)$$

$$\hat{D}_{new} = 0.\text{١٤٥} + 0.99\text{٥}\ \hat{D}$$

Table 6.4. Regression analysis of actual depth versus estimated depth of Rabigh water.

Predictor	Coef.	SE Coef.	T	P
Constant	0.1454	0.1712	0.85	0.39
Ref-1	0.99515	0.01164	85.52	0.00

Table 6.5. Analysis of variance of the Rabigh area, clear and turbid water.

Source	DF	SS	MS	F	P
Regression	1	2066.47	2066.47	7818.19	0.000
Residual	158	41.76	0.26		
Total	15	2108.23			

S = 0.514116 R-Sq = 98.0% R-Sq (adj) = 98.0%

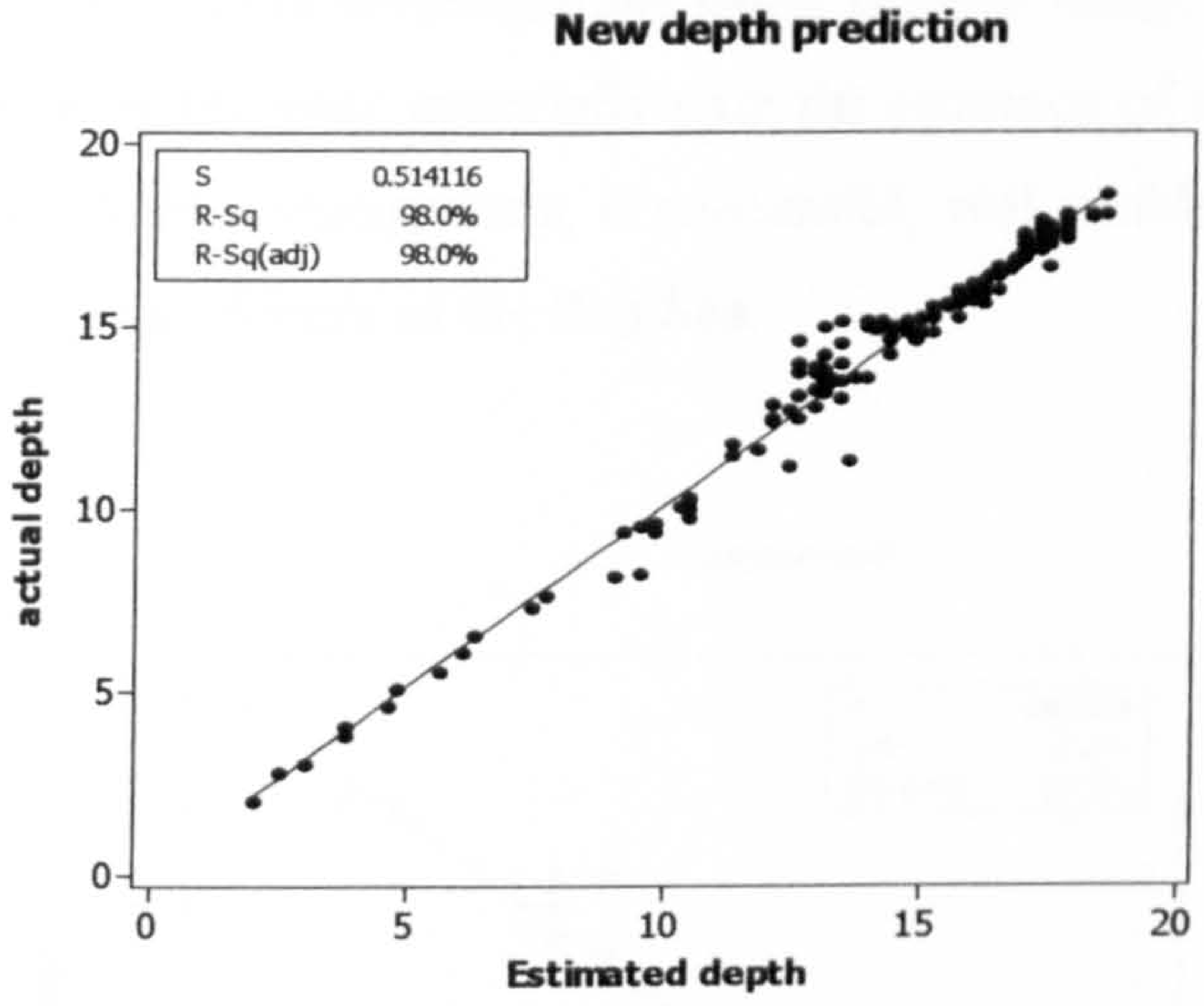

Figure 6.2. New depth prediction using actual depth against estimated depth.

6.4 Using the Rabigh algorithm model to predict Kishran depths

One of the valuable conclusions found during the analyses in this project is the possibility of using one algorithm model to predict water depth for different locations (Alzahrani et al., 2007). The algorithm model of 160 observations in Rabigh (first study area) can be used to build a new model for the Kishran image (second study area 400 km from Rabigh), using the ERDAS Imagine Model Builder module. The output image of this model has been investigated and compared with the output image created using the Kishran observation model. The predicted depths were nearly the same; the overall difference in r2 was just 1.5%. Figure 6.3 shows the regression model for the Kishran area using actual depth versus the reflectance's (band 1) taken from Kishran observations only. The regression relationship was accurate (r2 = 95.3%). When the model derived from the Rabigh observations was applied to the Kishran imagery, the regression fit versus actual depth showed r2 = 96.8%, as shown in Figure 6.4, which is more accurate than the model derived by Kishran algorithm, the reason is that the number of observations in Rabigh are more than the observations in the case of Kishran. However, when we take the estimated depth of Kishran produced by the Rabigh model as the predictor variable and the reflectance of Kishran image band 1 as the response variable, r-squared was extremely high (r2 = 99.1%). This leads us to think deeply about carrying out more investigations using another image of the same area, but in a different season of the year, especially with the presence of water vapour and humidity. The results of these investigations, if successful, will enable us to use this technology for the entire coastal waters of the Rea Sea.

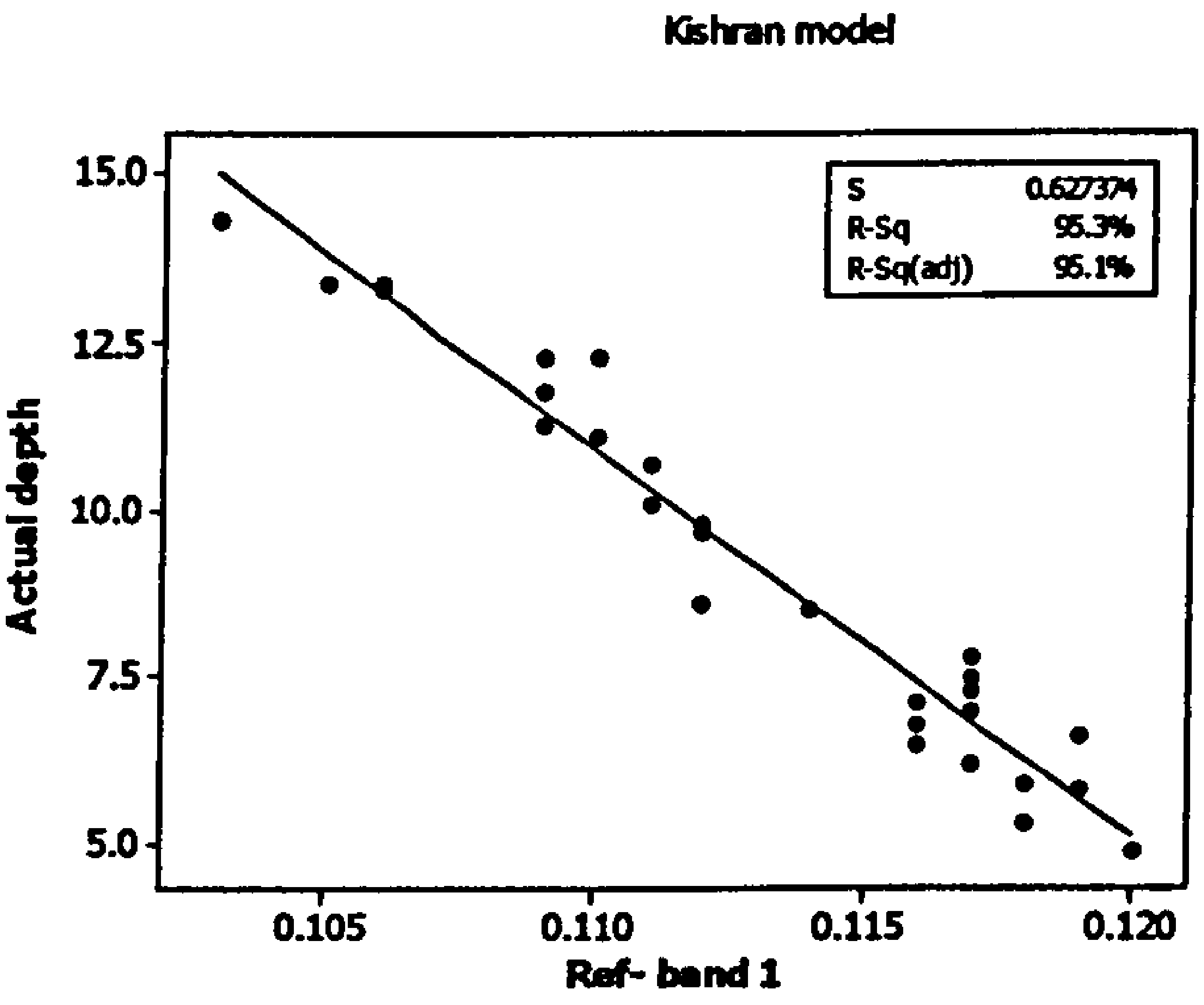

Figure 6.3. Kishran regression model created using actual depth versus band 1 reflectance.

S = 0.627374 R-Sq = 95.3% R-Sq(adj) = 95.1%

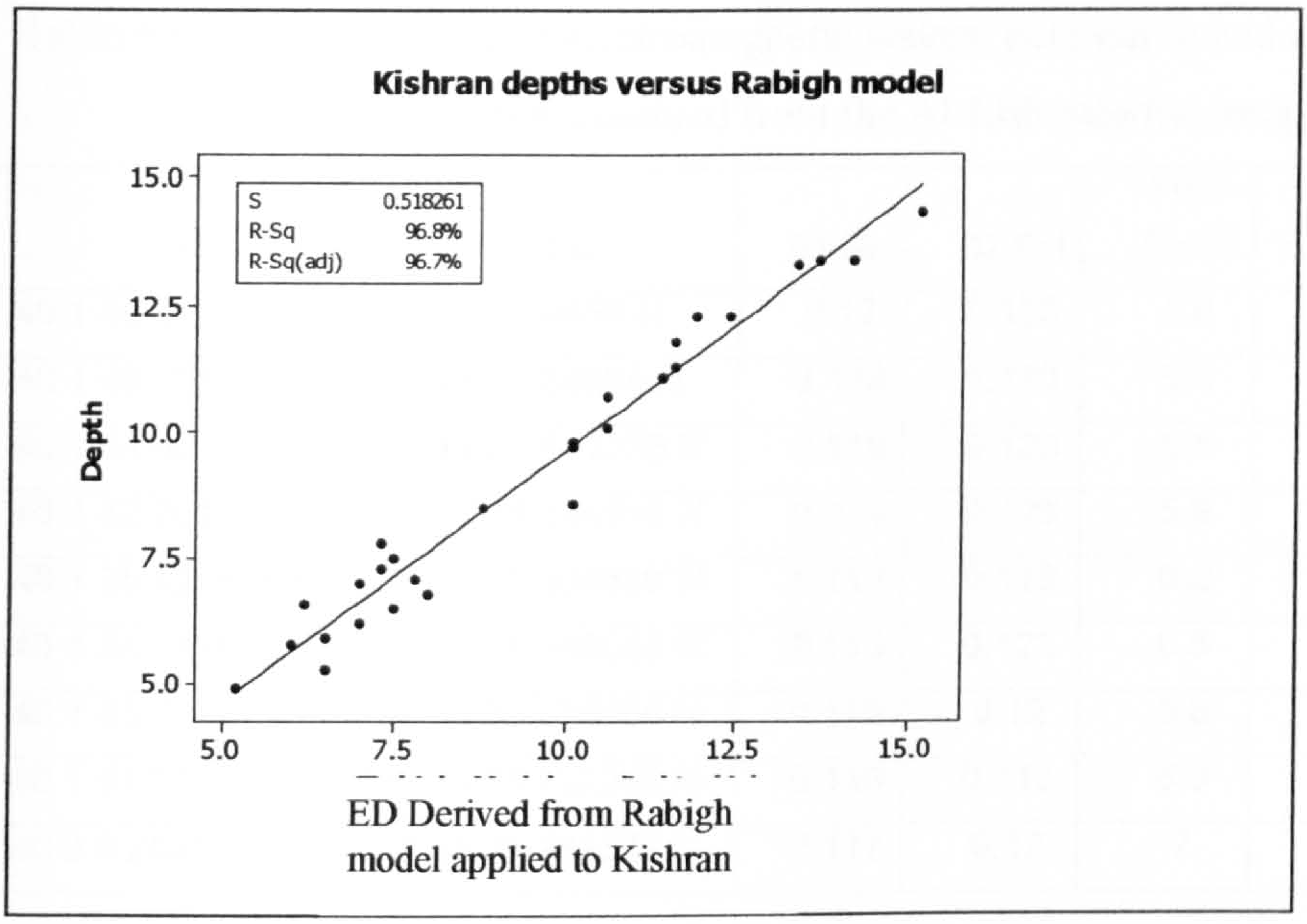

Figure 6.4. Rabigh model applied to Kishran area.

S = 0.518261 R-Sq = 96.8% R-Sq (adj) = 96.7%

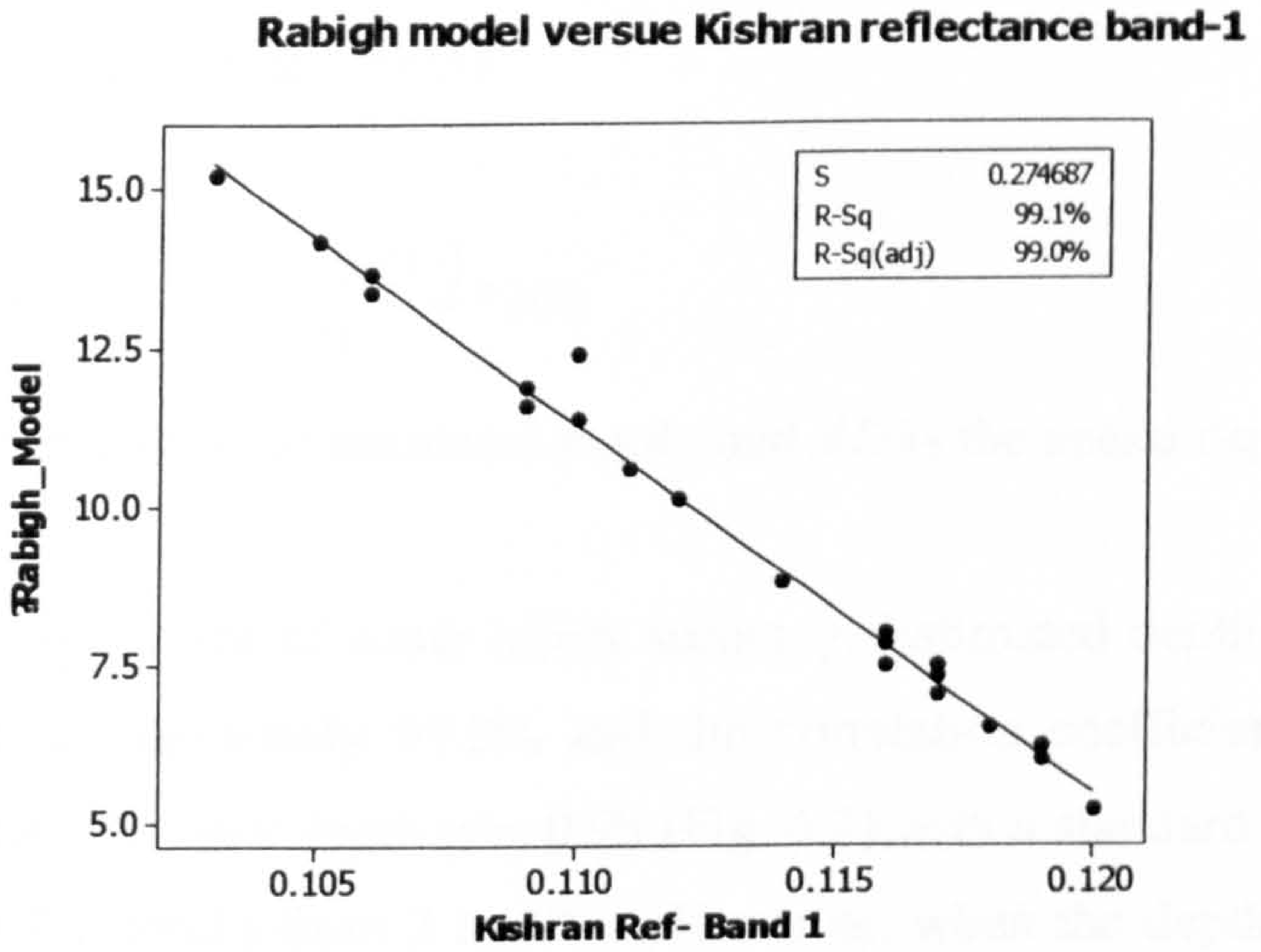

Figure 6.5. Rabigh model versus Kishran reflectance band 1.

Table 6.6. The reflectance of electromagnetic waves, field depth and estimated depths of some locations derived from the Al-Lith satellite images.

Long	Lat	B1-Ref	B2-Ref	Field Depth	E- depth	E-depths using Rabigh algorithm
40 1 45.68746 E	20 13 45.9456 N	0.12	0.129	4.9	4.9	5.2
40 1 40.205578 E	20 13 26.30964 N	0.118	0.133	5.3	6.1	6.5
40 1 44.437736 E	20 13 21.621838 N	0.119	0.123	5.8	5.6	6
40 1 42.781584 E	20 13 45.244916 N	0.118	0.128	5.9	6.1	6.5
40 1 35.526884 E	20 13 31.304856 N	0.117	0.119	6.2	6.6	7
40 1 34.747806 E	20 13 34.146054 N	0.116	0.123	6.5	7.1	7.5
40 1 43.73945 E	20 13 22.738166 N	0.119	0.12	6.6	5.9	6.2
40 1 51.70547 E	20 13 15.722098 N	0.116	0.113	6.8	7.6	8
40 3 9.206536 E	20 13 21.741532 N	0.117	0.12	7	6.7	7

6.5 Accuracy Assessment

The accuracy assessment has been calculated using the in situ depth data (a total of 160 points) and the estimated depth predicted from the actual depth and pixel reflectance by regression models. The following algorithm has been used to evaluate the bathymetric accuracy (Louchard et al., 2003):

$$ER = \frac{(ED - AD)}{AD} * 100$$

ER is the error, *ED* is the estimated depth, and *AD* is the actual depth.

Both clarity and depth of water affect accuracy. Estimated depth in clear water had an accuracy of approximately 97.3% and the correlation coefficient between the actual depth and the estimated depth was 0.98 (Fig. 6.2) with a standard error of 2.65%. These values were for depths from 2 to 18 m. However, when the depth was more than 18 m the standard error increases due to the absorption of electromagnetic waves by the water, which is expected. Although the models created and the methodologies of field measurements were extremely accurate, there were still minor errors in depth as mentioned above (2.65%). These errors need to be overcome, since navigation requires a high degree of accuracy. To do this, a safety factor, which should be more than the maximum error recorded, must be added or subtracted from depths estimated by the bathymetry models. This will give us a safe range within which the correct depth will fall (details of safety factor calculation are found in Section 6.7).

6.6 Results

This project was carried out in two parts, within a short time period. The field measurements, which included spectral measurement, dGPS and bathymetric measurements of the two study areas, comprised the first part. The bathymetry and dGPS equipment were interfaced to a laptop computer in order to save each depth against its location (Fig 4.11).

In the second part, the image processing, analysing and model building were carried out according to the research requirements. The first study area consisted of two different environments, one of them being the main port used by cargo and oil container ships that caused water turbidity, and the other with very clear water over coral reef areas located out of the port (about 5 miles). The total number of depth observations taken in this area was 160, 104 in clear water and 56 observations in turbid water. Three different models were derived. The first model was for the entire area, including both clear and turbid water ($r^2 = 97\%$, Fig 6.1a). The clear water model was more accurate ($r^2 = 99.2\%$, Fig. 6.1b). The third model was for the turbid water, which gave lower accuracy ($r^2 = 80.7\%$, Fig. 6.1c), as expected. However, the effect of turbid water on the first model was very minor due to the small number of observations compared with clear water. The procedures applied to Rabigh were repeated for the second study area (Kishran, Fig. 6.3) and a high R-squared value was achieved ($r^2 = 95.3\%$). Transferability testing established that models created for the first study area could be used to predict water depth in the second study area with only a minor decrease in the accuracy, giving squared values ranging from 95.3% to 99.1% (Figs. 6.3, 6.4 and 6.5).

6.7 Navigational safety factor (prediction interval):

Since we have predicted the estimated depth based on actual depth and pixel reflectance, it is then essential to extract a new safety depth by adding or subtracting ε , where ε is a small value called the safety factor. To find the prediction interval, equation (4) has been employed (Alzahrani 2006)

$$\hat{D}_{new} \pm t(1-\alpha/2; n-2)s\{\hat{D}_{new}\} \qquad (4)$$

where:

$\hat{D}_{new}$ is the new depth to be predicted; and

α is the confidence level.

$s\{\hat{D}_{new}\}$ is the standard deviation of $\hat{D}$ and is given by the following formula:

$$s^2\{\hat{D}_{new}\} = MSE\left[\frac{1}{n} + \frac{(R_d - \bar{R})^2}{\sum_{i=1}^{n}(R_i - \bar{R})^2}\right] \qquad \text{(Neter J. et al., 1996)}$$

MSE is the mean square error, R_d is the desired reflectance point, e.g. R = 102.

$\bar{R}$ Is the average reflectance.

Example 1: Consider a navigator has estimated depths for a certain area and needs to navigate with more safety and security of depth under the ship's keel. To predict the new depth at an estimated depth point of 17 m with 95% as the confidence level, equation (4) is applied with $MSE = 0.26$ (see Table 3) to get a prediction interval.

$$16.0087 \leq 17 \leq 18.1173$$

With a confidence prediction of 0.95, the navigator predicts that the maximum depth would not exceed 18.1173 m and the minimum would not be less than 16.0087 m. The safety factor would be ± 1 m.

As a navigator is responsible for the safety of the crew and the ship, the minimum predicted value should be taken into consideration. If the navigator had a list of estimated depths, such as the depths shown on Figure 6.3, another approach would be to use the maximum error as the safety factor; so if the ED of 9.5 m is taken, the interval would be:

$$8.5413 \leq 9.5 \leq 10.6574$$

So the safe depth for navigation will be 8.5 m.

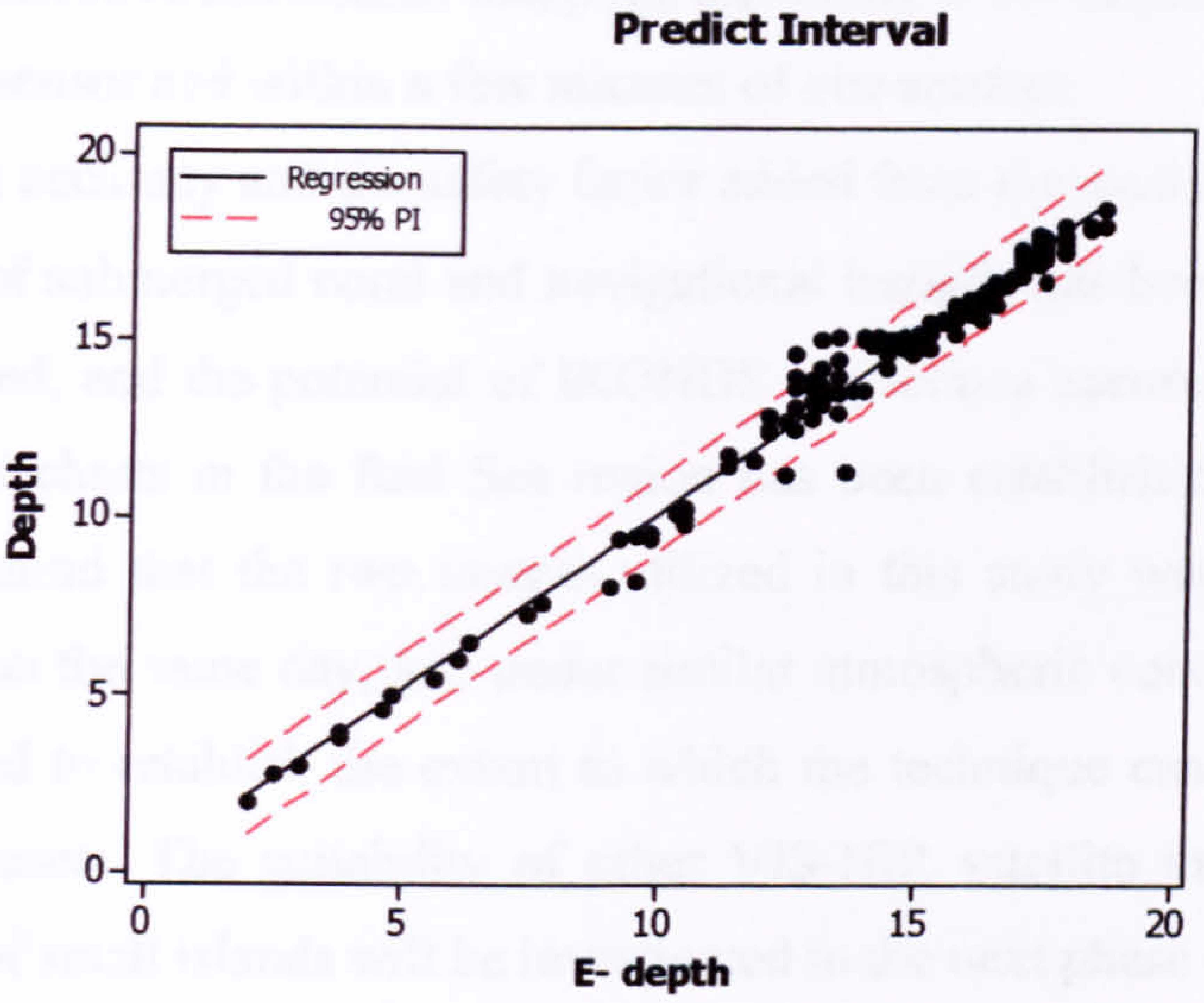

Figure 6.6. Predicted interval for the Rabigh area, clear and turbid water.

6.8 Discussion & conclusions

Due to high accuracy of the methodology used in field measurements, their data were very useful throughout the satellite image processing and also in building the different models.

Error analysis revealed a significantly higher uncertainty in the red band than in the blue band due to the increasing light attenuation. The green band also displayed noticeable errors as the depth increased and when turbid water was included with clear water the r^2 was found to be 67%, which is not an encouraging result and is not going to support the research aim of nautical chart updating.

The regression relationship was not valid for depths greater than 18 m for the blue band due to light diffusion as the depth increased, causing the absorption of electromagnetic energy. This study presented encouraging results, which should enable the creation bathymetry maps of shallow coastal areas that were previously marked only as hazardous areas on bathymetric maps generated using traditional methods. Furthermore, initial transferability investigations using an observation model from one location to predict water depths from imagery of another location offers the potential for more rapid and cost-effective sea bottom mapping, especially if the acquisition of the imagery is by the same sensor and within a few minutes of one another.

With high accuracy and the safety factor added from the model shown in Figure 6.6, the problem of submerged coral and navigational hazards has been solved for the two sites investigated, and the potential of IKONOS to produce accurate, high spatial resolution navigation charts in the Red Sea region has been established. It should, however, be borne in mind that the two images utilized in this study were from the same sensor, acquired on the same day, and under similar atmospheric conditions. Further work will be required to establish the extent to which the technique can be applied to multi-date image datasets. The suitability of other VIS-NIR satellite image sources for reliable mapping of small islands will be investigated in the next phase of this project.

CHAPTER SEVEN

APPLYING THE FIELD MEASUREMENTS TO IMAGES ACQUIRED UNDER THE MOST UNFAVORABLE CONDITIONS

(JULY 2006)

7. APPLYING THE FIELD MEASUREMENTS TO IMAGES ACQUIRED UNDER THE MOST UNFAVORABLE CONDITIONS (JULY 2006)

7.1 Introduction

It is known that the magnitude of the energy of the signal being sent through the atmosphere varies depending upon the atmospheric conditions; the worst atmospheric conditions being during the summer season (June, July and August; see Table 7.1).

In Chapter Six, the data analyses and regressions carried out were for images acquired in good environmental conditions, where there was low humidity, temperature and low water vapour. These parameters play a part in the excellent results achieved; however, new images were acquired in the summer of 2006 when there was maximum humidity, temperature and water vapour as explained in Table 7.1, and these images have been applied and processed according to the same procedures used in Chapter Six and the results then compared with the field measurements taken in 2004. In this chapter, simple linear regression is performed for field depths versus electromagnetic reflectance of the new IKONOS images dated June 2006, without consideration of bottom types, which normally contain combinations of coral reefs, sea grass, sands and sometimes mud. The approach was according to the aim of this study, which concentrates on the relationship between the water depth and the reflectance of electromagnetic waves and then the building of suitable models for the estimation of water depths.

The question here is what accuracy and reliability can be obtained from the new images acquired in the worst atmospheric conditions, as explained in Table 7.1.

The accuracy of the image-derived water depth will be estimated by conducting simple linear regression for the in situ data measured by the shipboard hydrographic echo sounder versus pixel brightness values in the blue band of the IKONOS multispectral imagery that had been corrected to at-sensor reflectance using published calibration coefficients.

Table 7.1. The average of some atmospheric conditions that affect EMW.

Month	Temp mean average	Temp maximum average	Humidity Maximum average	mean_vapour_pressure
Jan	26	34	76.4	16.3
Feb	26.4	34.9	65.8	13
Mar	27.9	37.5	78.2	16.7
Apr	30.1	41.1	75.6	18.5
May	32.1	43	81	24.6
June	33.3	42.3	80	26
Jul	33.4	42.3	80	28.3
Aug	32.9	45.3	81	33
Sep	32.7	41.3	76.5	28.4
Oct	31.1	40.9	82.2	25.8
Nov	29.1	42.3	80.1	23.2
Dec	26.7	35.9	79	21.8

7.2 Data

The data acquired for this stage cover the same study areas, but at different times. The Rabigh area, which contains the Rabigh port and the approach area, is located 150 km north of Jeddah; the second study area is Kishran, containing Sheb Aljefen and Sharifa Island, and located 200 km south of Jeddah and 30 km south of the town of Al-Lith. The acquisition date and time for the Rabigh image was the 19th June 2006 at 08:06 GMT, while the Kishran image was acquired on 17th May 2006 at 08:04 GMT. The time of acquisition was selected for the worst atmospheric condition throughout the year. The image for Rabigh was taken in cloud free conditions, while Kishran had 20% coverage, with cloud being one of the causes of the low accuracy found, but not the main cause. Figures 7.1 and 7.2 show the new image for the areas under study.

Figure 7.1. Study area image acquired on 19th June 2006.

Figure 7.2. Study area 2 (Kishran area). Image acquired on 17th May 2006.

7.3 Prediction of water depth using simple linear regression

The aim in this chapter is to assess the accuracy of data achieved from the images acquired in difficult atmosphere conditions. Thus, the images were ordered to meet our aims in this chapter, namely, those acquired during June 2006. However, from the processing and analysis points of view, simple linear regression was carried out for the actual field depth versus reflectance values (band 1), with the output result of this process leading to predictions of the depths for unknown areas using the following model:

$D_i = \beta_0 + \beta_1 R_i$ (See Chapter 6 equation 1)

Using *Minitab,* the regression coefficients can be estimated in model (1) by using the available data, and then the estimated model can be easily derived.

$\hat{D} = 77.2 - 598R$ (See Chapter 6 equation 2)

Predictor	Coef.	SE Coef.	T	P
Constant	22.7697	0.4710	48.34	0.000
Ref-1	-47.427	3.051	-15.54	0.000

S = 1.55639 R-Sq = 73.8% R-Sq (adj) = 73.4%

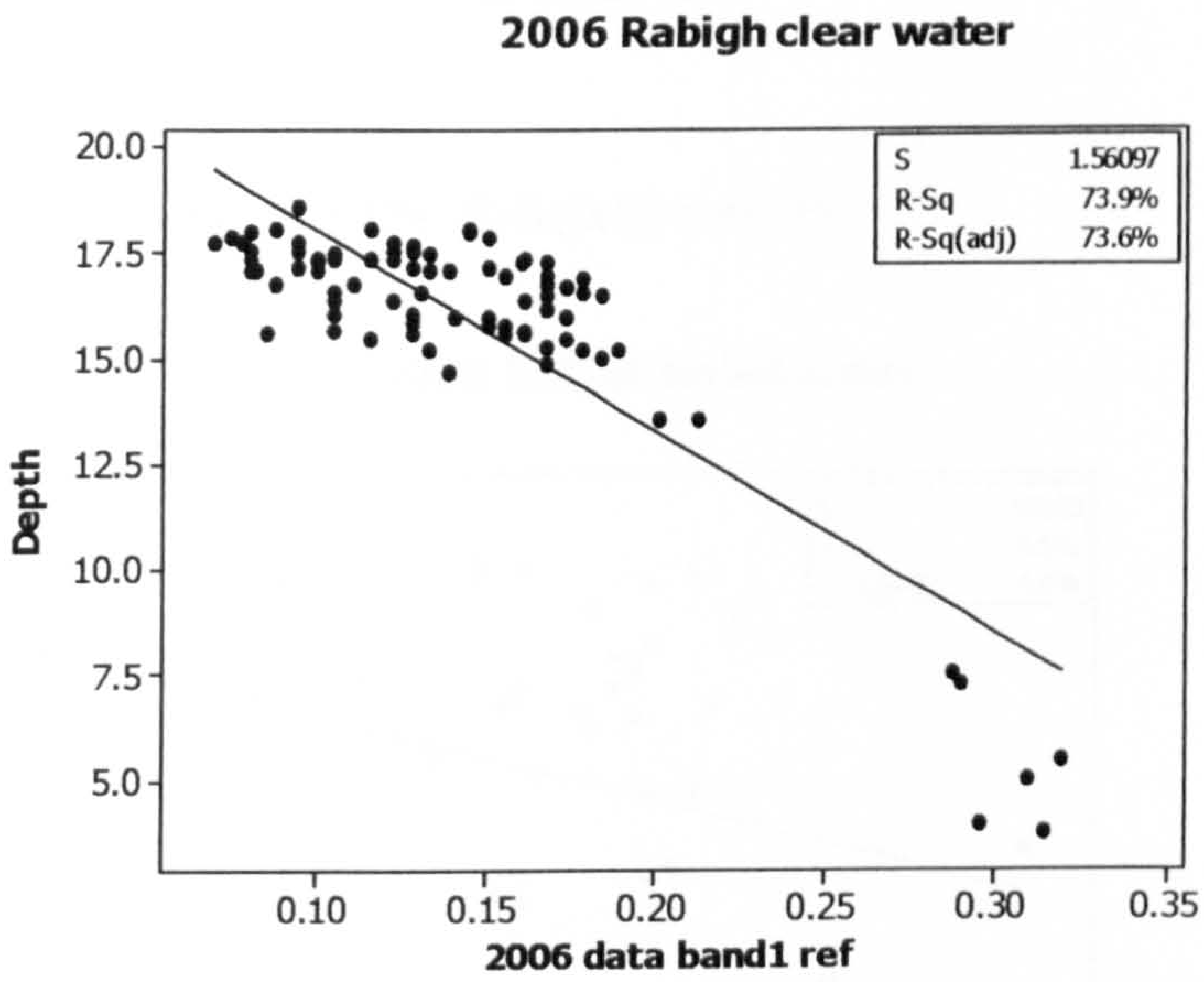

Figure 7.3. Rabigh 2006. Clear water regressions.

Depth = 22.77 - 47.54 2006 data band1 ref

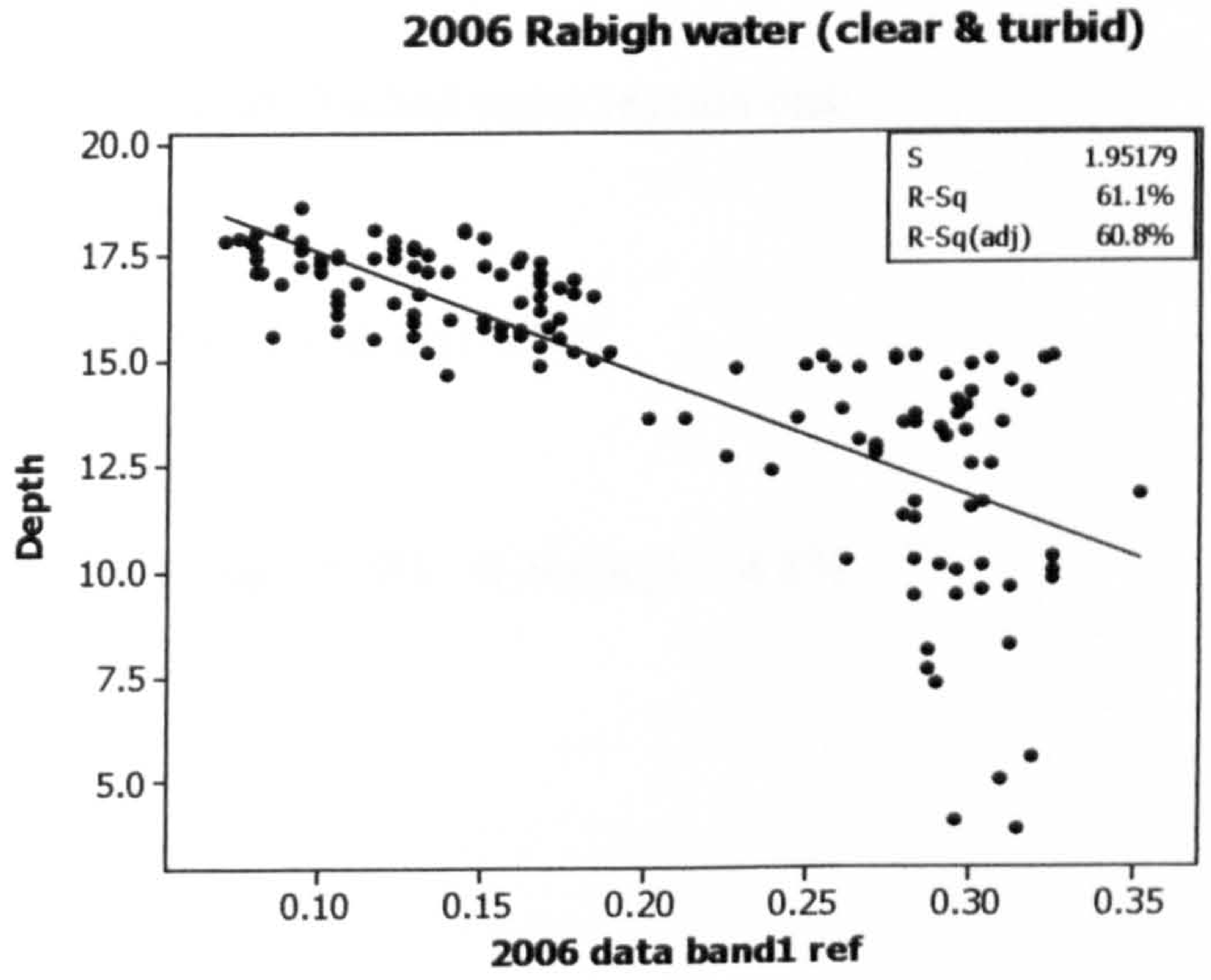

Figure 7.4. Rabigh 2006. Clear and turbid water regressions.

Depth = 20.45 - 28.95 2006 data band1 ref

S = 1.95179 R-Sq = 61.1% R-Sq(adj) = 60.8%

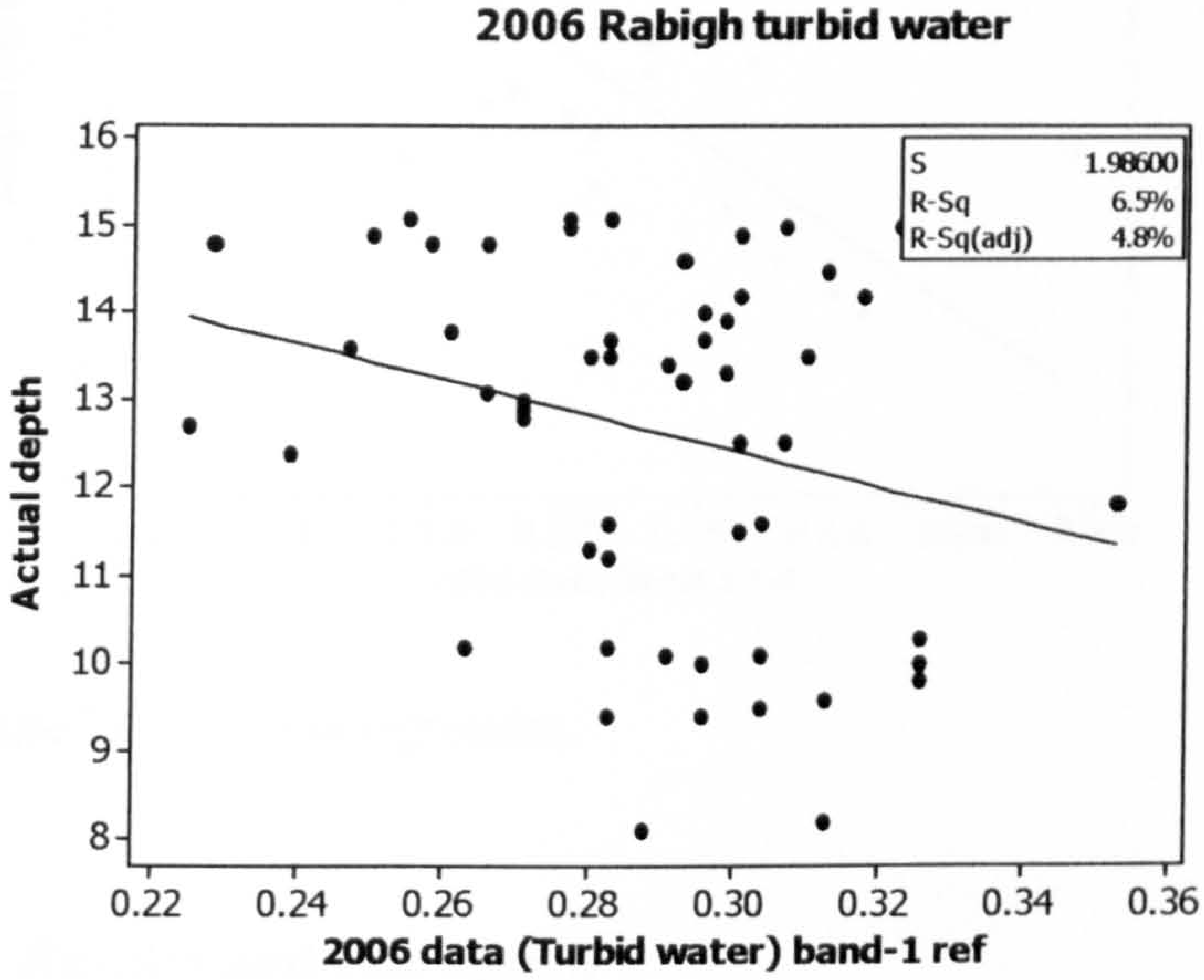

Figure 7.5. Rabigh. Turbid water regressions.

Depth = 18.53 - 20.40 refl-2006

S = 1.98600 R-Sq = 6.5% R-Sq(adj) = 4.8%

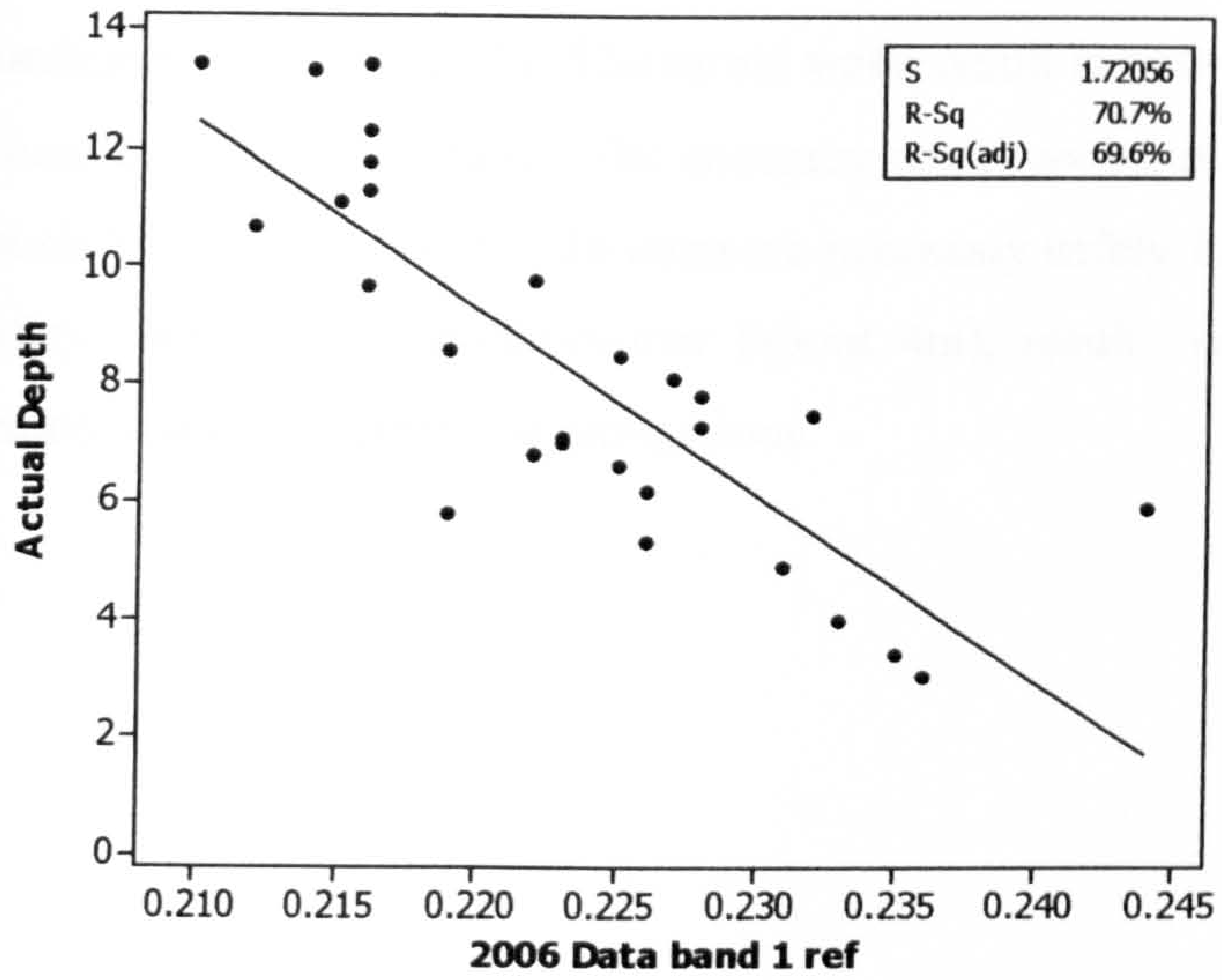

Figure 7.6. Kishran regression.

7.4 Results and conclusion

In this chapter, the data processed was acquired at a time selected when the weather was not good for image acquisition. During the summer period in the Red Sea, the temperature usually reaches its maximum, as does the humidity and water vapour, and these conditions cause errors. However, the selection of this time was decided and planned after getting the excellent results described in Chapter Six, in order to investigate how much information can be obtain during periods of difficult weather; moreover, to investigate the possibility of using this image in deriving bathymetry information.

However, the results achieved using the new images was different from the results we presented in Chapter Six, although the same methodology was carried out, simple linear regression was applied for electromagnetic reflectance versus field depths. In clear water sites, the regression relationship was not as highly accurate as the regressions for the December 2004 images; the r^2 was found to be 73.8%, which is not bad but it is not accepted as an accurate methodology, the main goal of this project. The turbid water investigation gave the worst result due to the water turbidity and the shocking weather conditions, with $r^2 = 6.5\%$. The turbid water result is not to be trusted in the normal case, when the weather is stable. The accuracy could poor but charts could be generated with much longer safety factor. To compare necessary safety factor for good weather 1m with safety factor of difficult weather (about 4m), results would be safe charts, but with unnecessary restrictions on navigations.

CHAPTER EIGHT

APPLICATION OF STUDY RESULTS FOR NAVIGATIONAL PURPOSES USING GIS TECHNIQUES

8. APPLICATION OF STUDY RESULTS FOR NAVIGATIONAL PURPOSES USING GIS TECHNIQUES

8.1 Introduction

Nowadays, Geographic Information Systems (GIS) technology has become a very important tool; it can be used for scientific investigations, resource management and development planning (Aronof, 1989). This chapter will explain how GIS can be the main tool for converting the raster image to a navigational map, which then can be very useful for navigational purposes (Alzahrani 2007). In addition, GIS might allow emergency planners to easily calculate emergency response times in the event of a natural disaster. GIS has powerful analytical functions, which enable the user to get answers to many questions about phenomena tied to specific locations on the earth (Konecny, 2003; Burrough, 1986; El-Hattab, 2007; Alzahrani 2007). This ability makes GIS the most suitable technique to tackle a wide range of applications. A GIS can also convert existing digital information, which may not yet be in map form, into forms that can then be recognized and used (El Raey, M. et al., 2005). For example, digital satellite images can be analysed to produce a map-like layer of digital information of bathymetry in the same way as census or hydrologic tabular data can be converted to map-like form, serving as layers of thematic information in a GIS.

The previous chapters explained the different processing and models used to discover a suitable method for deriving water bathymetry from space. To achieve the main goal of this project, the methodologies followed were the fieldwork, which was carried out during the acquisition of the satellite images (see Chapter 4), the combination of the field measurements and satellite images, and the required processing. Finally, there was the data analysis, in which suitable models were used to convert the raster image from reflectance values to estimated depths, using regression equations.

The results achieved were quite accurate and acceptable for navigational purposes, especially in good atmospheric conditions. However, these results were presented in raster format and can only be used with specialist software, which is useful for highly skilled decision makers but are not like a map or chart to be used by a navigator. New navigational maps needed to be extracted from these bathymetric images (raster format), and these new maps had to contain the necessary information that is normally available on navigational charts, such as depths, contour lines (labelled with depth figures), compasses, scales, etc. In order to produce these maps, geographic information systems (GIS) techniques are required. The procedures and techniques will now be described in detail.

8.2 Integration of remote sensing and GIS

The integration of remote sensing (RS) and geographic information systems (GIS) in marine environmental applications has become increasingly common in recent years. Remotely sensed images are a cost-effective source for environmental GIS applications and, conversely, GIS capabilities are being used to improve image analysis and information extraction procedures and to allow their analysis in conjunction with other data (Sharma S.K. and Anjaneyulu D., 1993; Hinton, J.C., 1996; Welsh, R. et., al., 1992; IDRISI, 2001; ESRI, 2004). At the simplest level, both remote sensing and GIS analysis can be conceived as consisting of three stages: measurement and sampling, the fitting of models or application of techniques to achieve some objective; and finally, validation of the results achieved (Vieira and Mather, 2004).

Digitally storing the produced information in a database and relating it to its accurate coordinates is the basis of GIS. Thus, it is possible to evaluate the spatial interaction of the data with each other and access geographical information such as coordinates, area and length. All feature and location information of each element of data can be evaluated at the same time, so visual interpretations and analysis can be made. When necessary, it is possible to produce intelligent digital maps, which allow modelling to be carried out.

8.3 GIS Techniques

GIS has a wide variety of processing techniques; one of those techniques that this study depends on is spatial analysis. Spatial analysis provides a rich set of tools to perform cell-based (raster) analysis. The three main types of GIS data are raster, vector, and Triangulated Irregular Network TIN; the raster data structure provides the most comprehensive modelling environment for spatial analysis.

Cell-based systems divide the world into discrete uniform units called cells, based on a grid structure; every cell represents a certain specified portion of the earth, such as a square kilometre, hectare, square metre, or even pixel in an image. Each cell is given a value to correspond to the feature or characteristic located at that cell, such as depth value. In a cell-based system, geographic location is not defined as an attribute, but it is inherent in the storage structure, which is known as the location perspective.

The location perspective allows Spatial Analyst model in GIS to store continuous data (for our study, the depth values) more effectively. In continuous data, each location has a quantity, magnitude, or intensity assigned to it and the values are meaningful relative to one another. In spatial analysis, reclassifying data simply means replacing input cell values with new output cell values. There are many reasons why the data needs to be reclassified. Some of the most common reasons are: firstly, to replace values based on new information; secondly, to group certain values together; and finally to set specific values to NoData or to set NoData cells to a value. There are several approaches to reclassifying data: by individual values, by ranges, by intervals or area, or through an alternative value. One of the important functions that can be used effectively in this study is interpolation. The interpolation technique predicts values for cells in a raster from a limited number of sample data points. It can be used to predict unknown values for any geographic point's data: depth, elevation, chemical concentrations, and so on. In other words, visiting every location in a study area to measure the value of a phenomenon (depth in our case) is usually difficult or expensive. Instead, strategically dispersed sample input point locations can be selected and predicted values can be assigned to all other locations. Input points can be either randomly or regularly spaced points containing concentrated measurements. The assumption that makes interpolation a viable option is that spatially distributed objects are spatially correlated (things that are close together tend to have similar characteristics) (McCoy & Johnston, 2001., Hongxing Liu, Zhiyuan Zhao, and Kenneth C. Jezeh, 2004).

The available interpolation methods are: inverse distance weight, spline, and Kriging. These all make certain assumptions about how to determine the best estimated values. Based on the phenomena the values represent and on how the sample points are distributed, different interpolators will produce better estimates relative to the actual values. No matter which interpolator is selected, however, the more input points and the greater their distribution, the more reliable will be the result (Weibel, R. & Heller M. 1990., Weibel, R. & Heller M. 1991., Nasser El-shimy, 1999).

In this study the number of points used was very high as the input was the raster image representing the extracted depths for both study areas (Rabigh and Kishran).

The Inverse Distance Weight method is interpolation method which use the linearity weighted combination for the input point to calculate the cell values. It is suitable for those parameters that decrease regularly as distance from the source increases, such as air pollution distribution from point sources (like chimneys and stacks). On the other hand, the second method "Spline" describes naturally distributed phenomena such as rain water distribution over a large area (ESRI 2005). It has two types regularized and tension type.

The Inverse Distance Weighted (IDW) and Spline methods are referred to as deterministic interpolation methods; because they are directly based on the surrounding measured values or on specified mathematical formulae that determine the smoothness of the resulting surface. A second family of interpolation methods consists of geo-statistical methods (such as Kriging), which are based on statistical models that include autocorrelation (the statistical relationship among the measured points). Because of this, not only do geo-statistical techniques have the capability of producing a prediction surface, but they can also provide some measure of the certainty or accuracy of the predictions.

Kriging assumes that the distance or direction between sample points reflects a spatial correlation that can be used to explain variation in the surface. Kriging fits a mathematical function to a specified number of points, or all points within a specified radius, to determine the output value for each location. Kriging is a multi step process; it includes exploratory statistical analysis of the data, variogram modelling, creating the surface, and (optionally) exploring a variance surface. Kriging is most appropriate when it is known that there is a spatially correlated distance or directional bias in the data. The Kriging method is the most suitable method for data extraction in this project due to the type of data used (depth measurement) and the accuracy result needed.

8.4 Data Processing

The software packages used to process the data were ArcView and ArcGIS with their different extensions, such as Spatial Analyst, Image Analyst and 3D Analyst, and ERDAS Imagine.

The first step was to prepare the outputs from the models in a format suitable for the GIS software without loosing any information, such as pixel values (which represent depths) or projection. This step was achieved using ERDAS Imagine software and it required two procedures:

i. Smoothing process.

ii. Converting process.

The smoothing process was used to eliminate noise from data obtained from the modelling process. A suitable smoothing filter and window size are critical choices, because any error in smoothing could cause the loss of data or conversion to unreal values.

A low pass filter of window size 7 by 7 was used in both the Rabigh and Kishran areas. The images before and after the smoothing process are shown in Figures 8.1 and 8.2, where it can be seen that the visual contrast is enhanced.

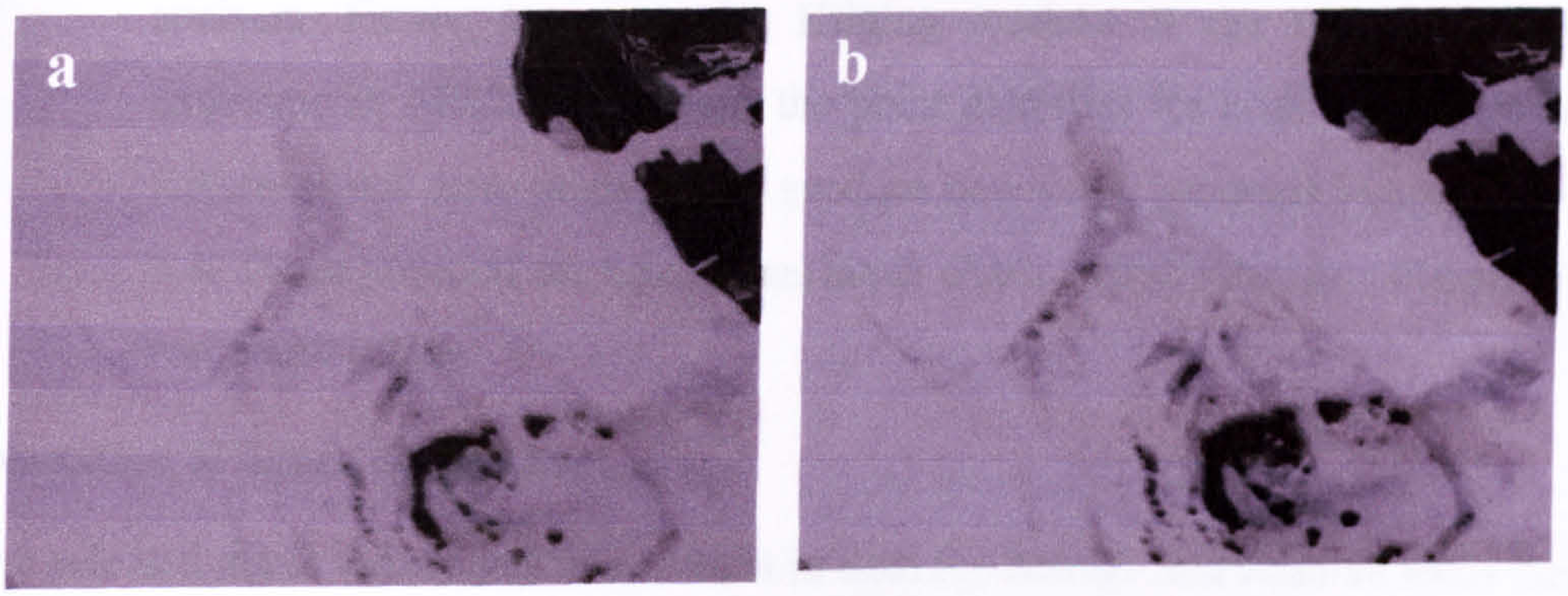

Figure 8.1. Rabigh image (a) before and (b) after smoothing process.

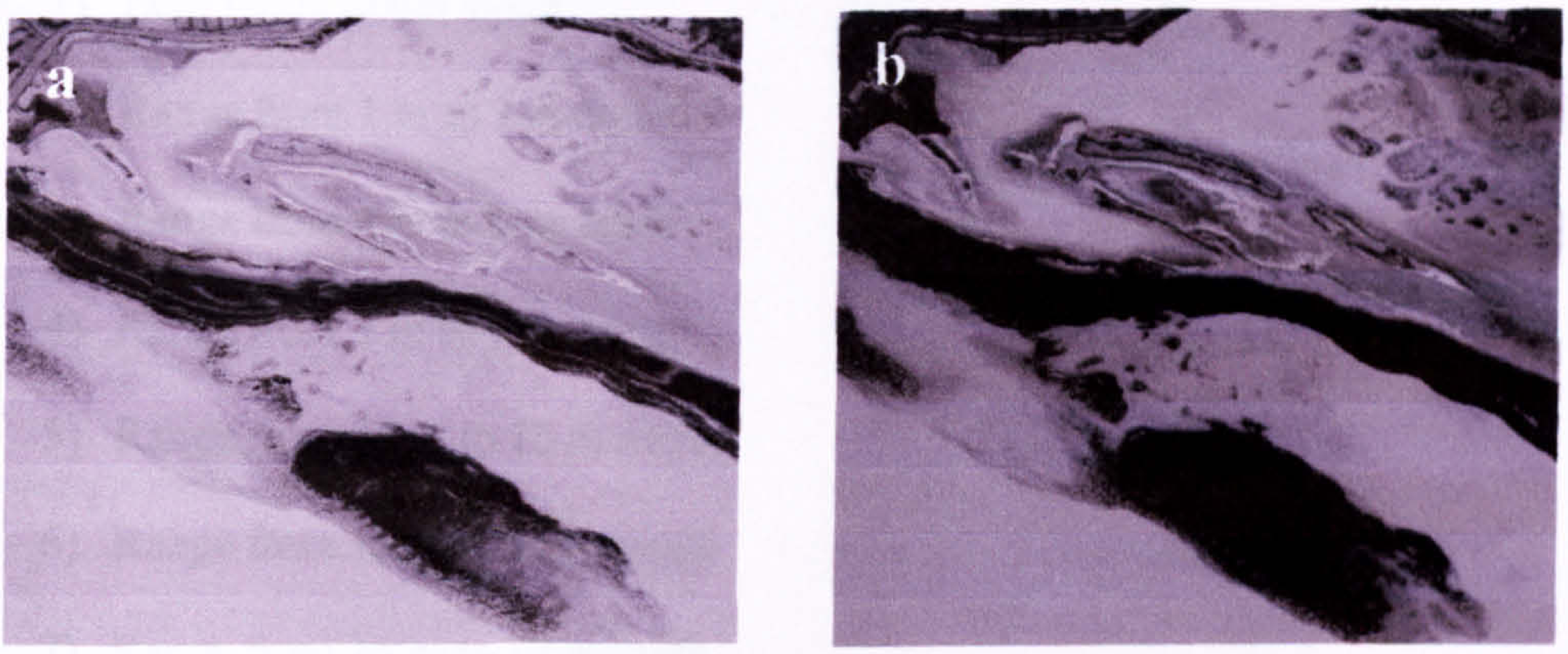

Figure 8.2. Kishran image (a) before and (b) after smoothing process.

The second step converted the smoothed images for both areas into LAN format suitable for import by GIS.

The ArcView software prepared the input to the GIS. The processing procedure consisted of several steps:

i. Importing the previously created LAN images into the GIS environment.
ii. Converting the LAN image into GRID format, then into a GIS Shape file.
iii. The depth shape file is then sliced into a number of shape files, each of them representing a specific depth value or range using the "Query Builder" extension in the ArcView software, see Figure 8.3 and 8.4

iv. After converting both layers into depth points, they were subjected to spatial analysis. Firstly, by using the Kriging module in the Spatial Analysis extension in ARCGIS software, the point data files for both the Rabigh and Kishran areas were processed to produce new raster products Figure 8.7 and 8.8. Those products are continuous depth charts, categorized according to the real depth values.

Explanation of figure 8.3 and 8.4

The selected depth values and ranges used in both the Rabigh and Kishran areas were as follows:

1) Zero metre depth value
2) Range from 1 m to 3 m depth
3) Range from 4 m to 6 m depth
4) Range from 7 m to 9 m depth
5) Range from 10 m to 12 m depth
6) Range from 13 m to 15 m depth
7) Range from 16 m to 17 mdepth
8) Depth values grater than 18 m (as the model does not succeed in predicting or extracting depths of more than 18 m).

The next two figures represent those eight different depth ranges extracted in both the Rabigh area (Figure 8.3) and the Kishran area (Figure 8.4).

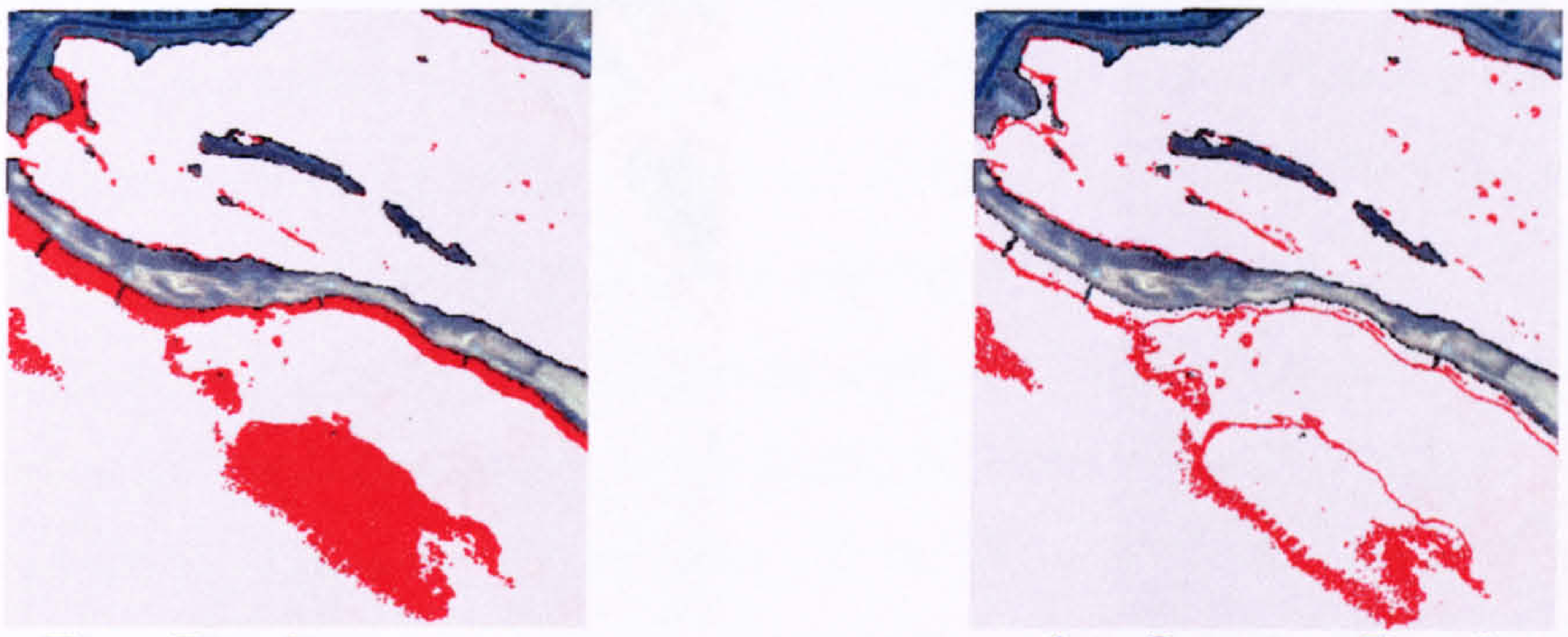

Zero Depth **1 to 3 meters Depth**

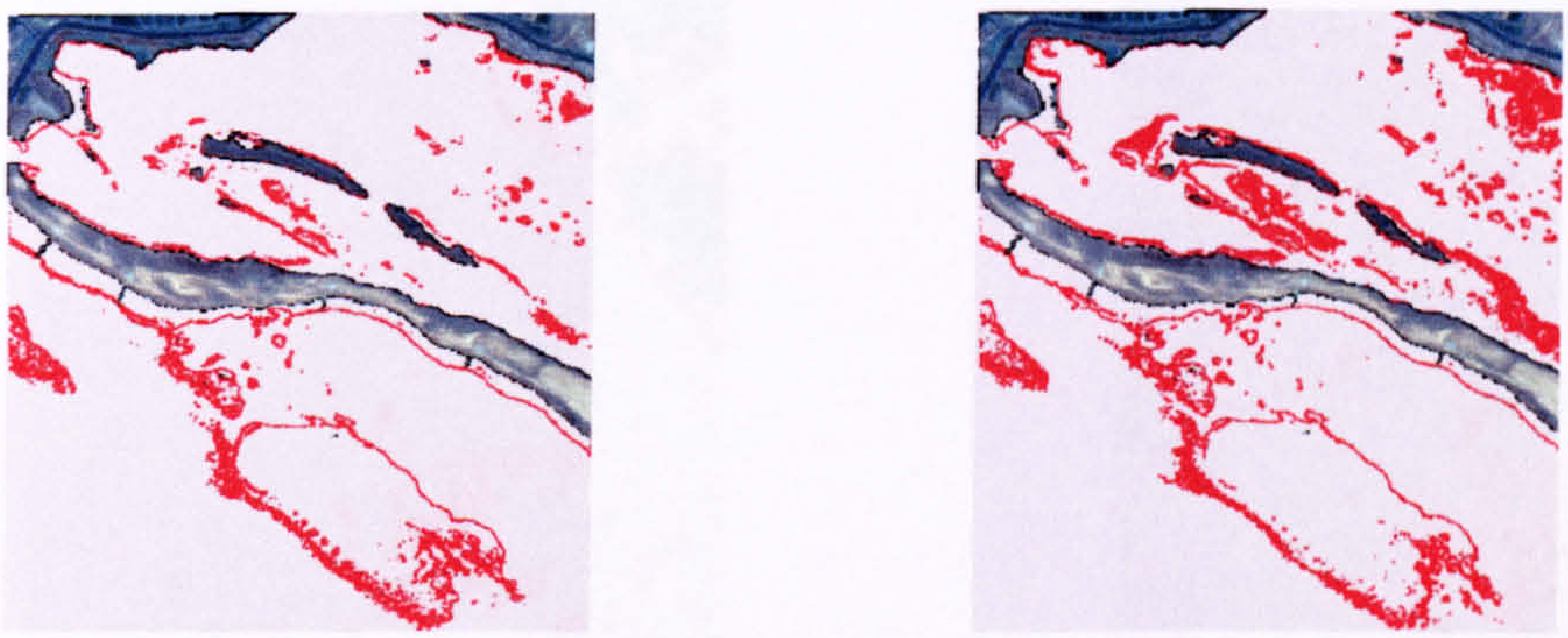

4 to 6 meters Depth **7 to 9 meters Depth**

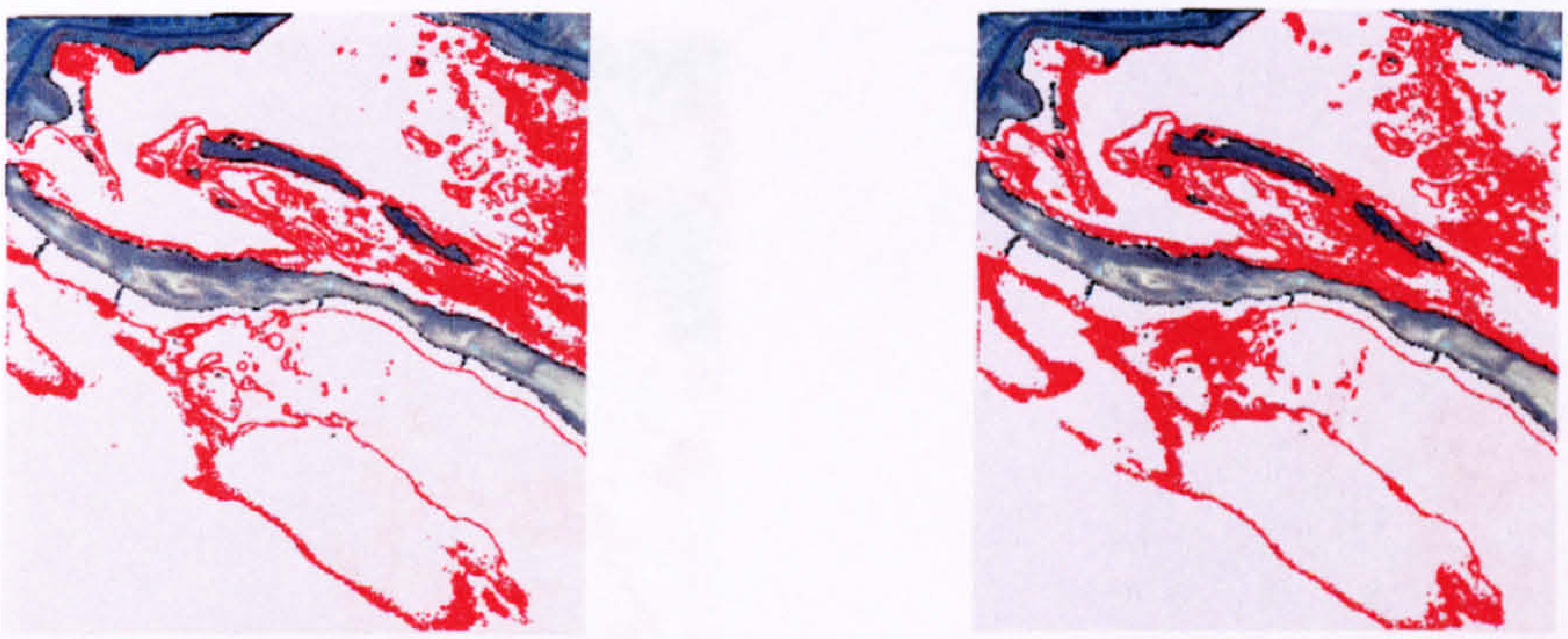

10 to 12 meters Depth **13 to 15 meters Depth**

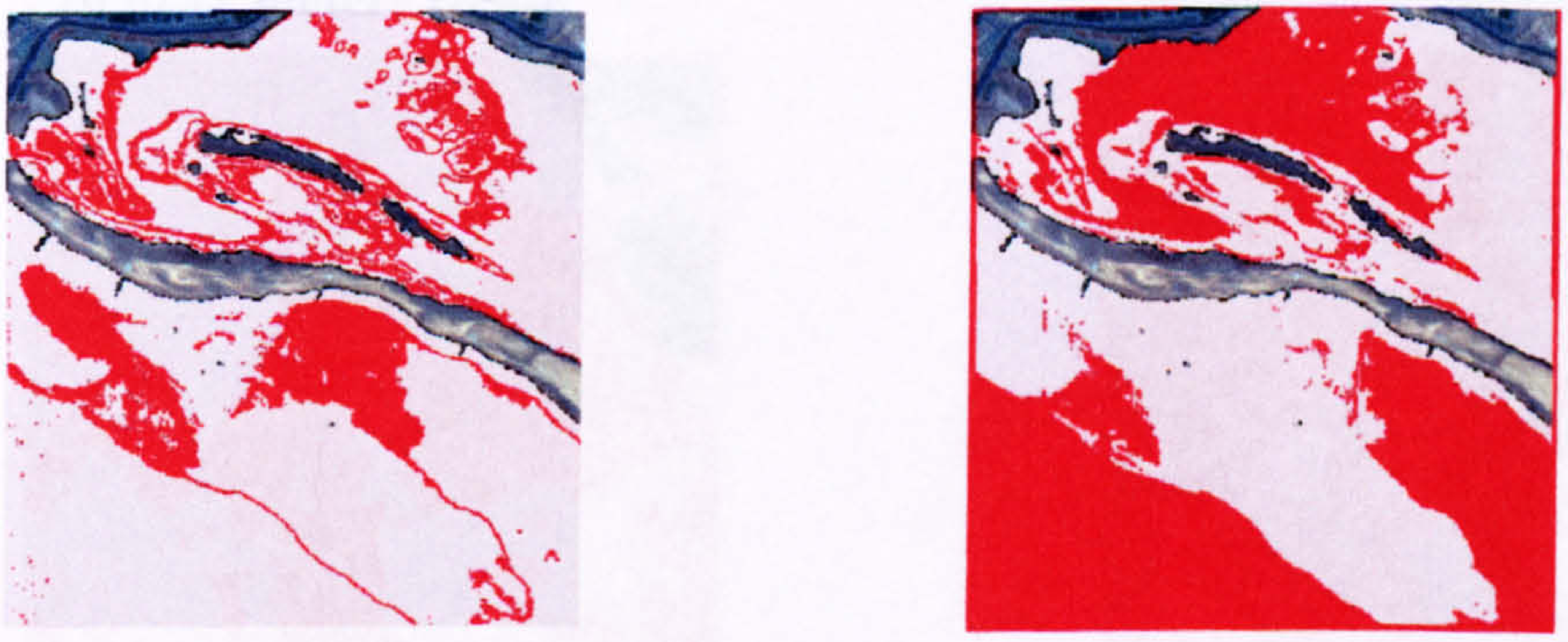

16 to 18 meters Depth **Depth greater than 18**

Figure 8-3: The eight different depth ranges extracted for Kishran area.

Zero Depth

1 to 3 meters Depth

4 to 6 meters Depth

7 to 9 meters Depth

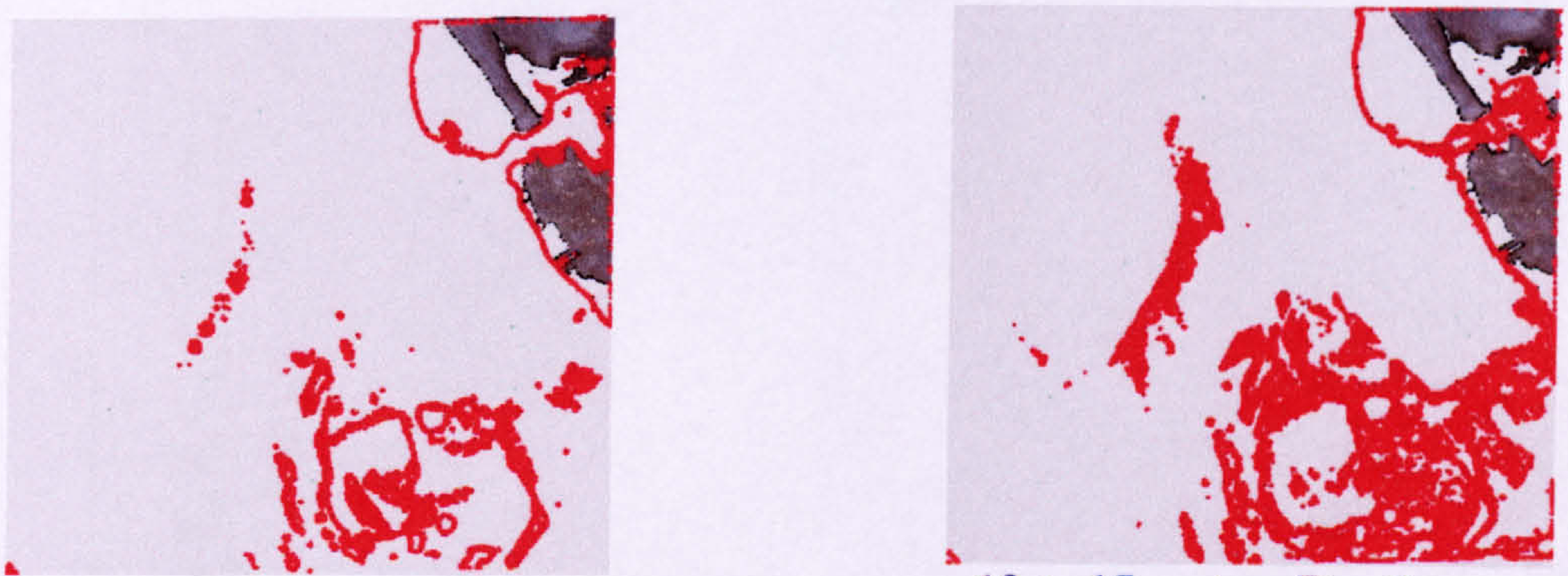

10 to 12 meters Depth

13 to 15 meters Depth

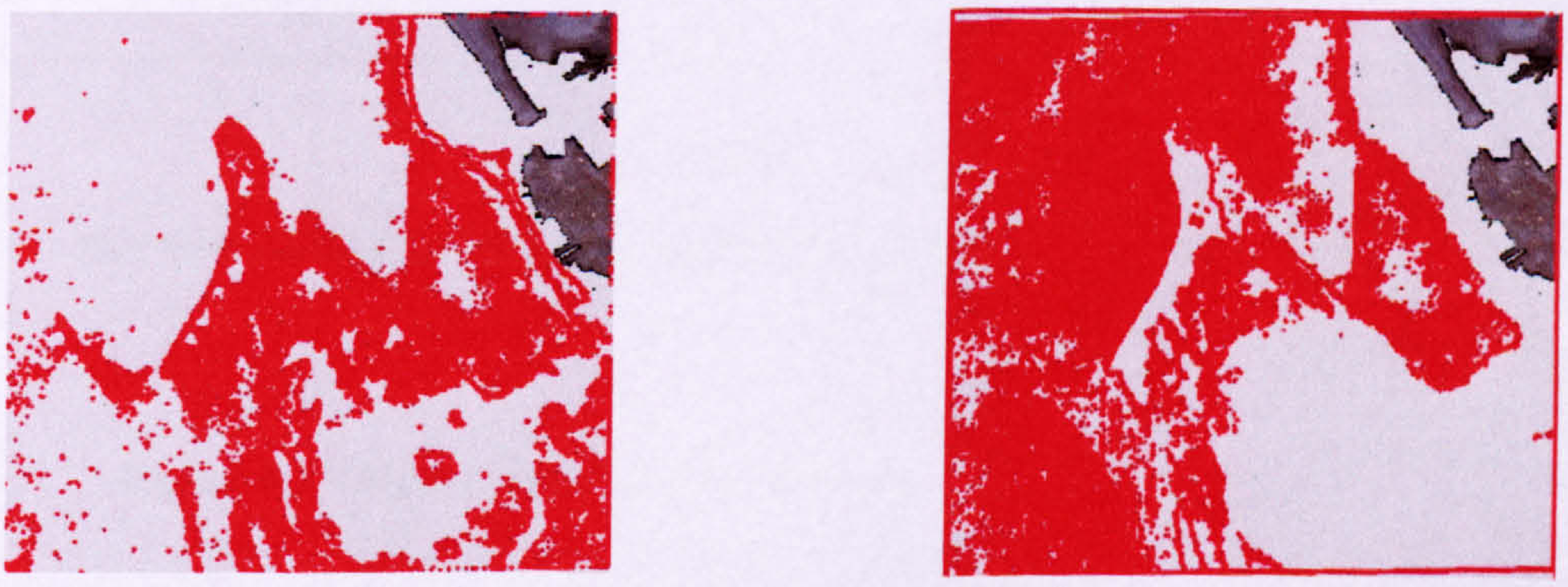

16 to 18 meters Depth

Depth greater than 18 meters

Figure 8-4: The eight different depth ranges extracted for Rabigh area.

The following steps convert all eight polygon layers extracted for each area into point format; the number of points created in the Rabigh area is 15,936, while in the Kishran area the number of extracted points is 10,463, Figure 8.5 represents the depth points layer for Rabigh, while Figure 8.6 represents the depth points layer for the Kishran area. In those two figures, produced using ARCGIS software, the land was masked using the mask module. For each point, the depth value was assigned, but for points indicating depths of greater than 18 m, 30 and 60 (as an assumed depths for interpolation purposes). The final step is to merge all point layers into one GIS point layer, see Figures 8.7 and 8.8.

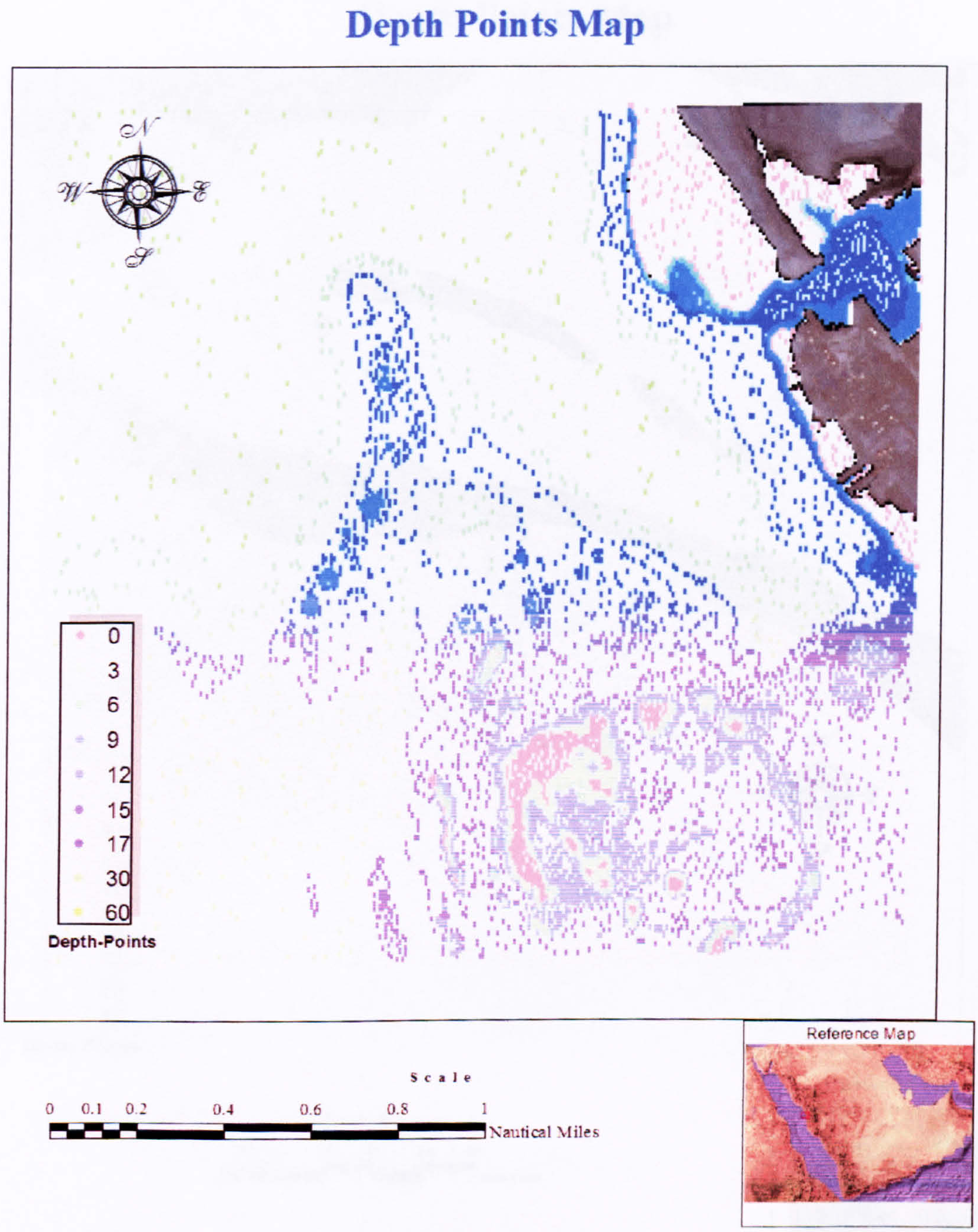

Figure 8.5. Depth points layer for Rabigh.

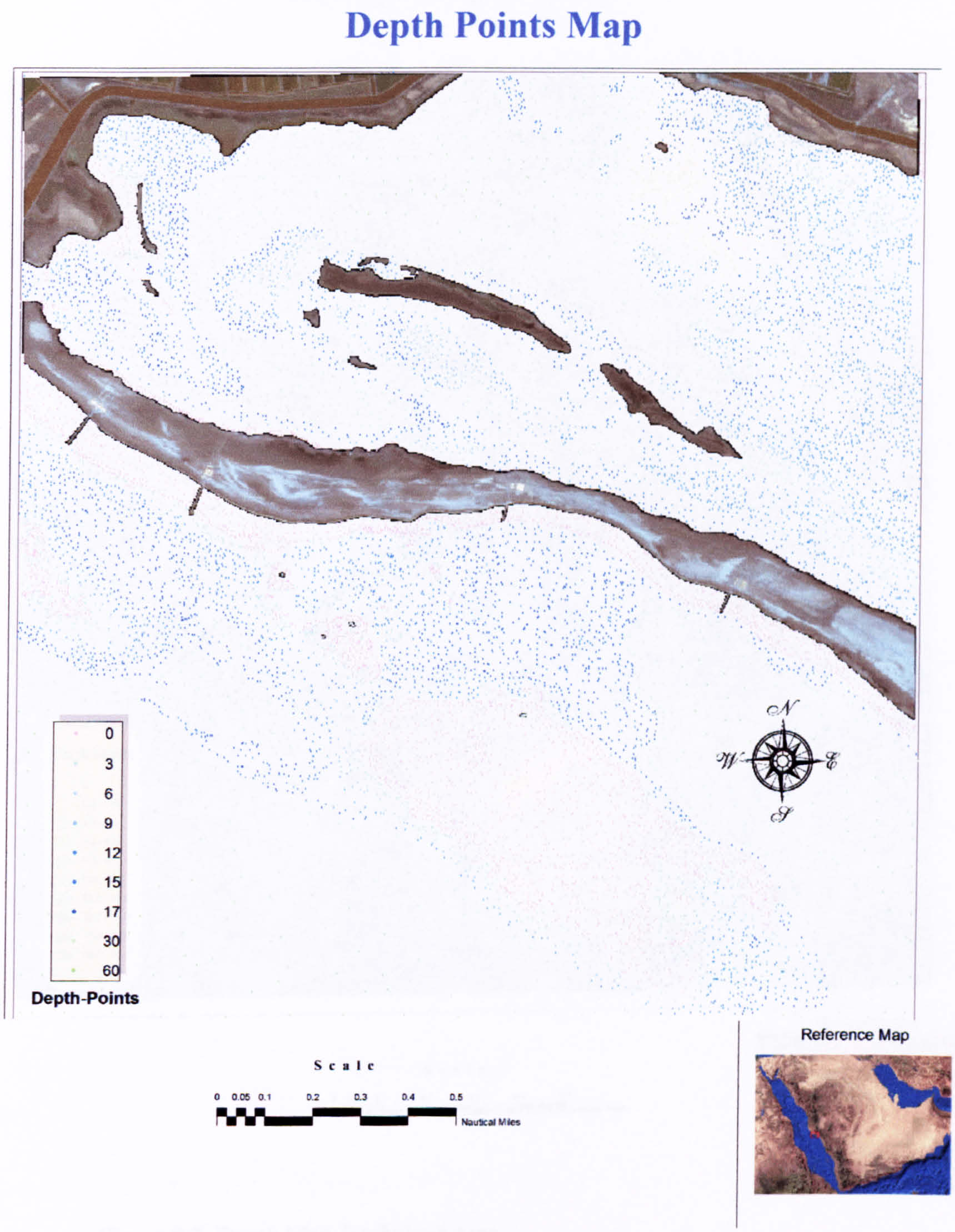

Figure 8.6. Depth points layer for Kishran area

Rabigh Depth Chart

Figure 8.7. Depth Map for Rabigh area.

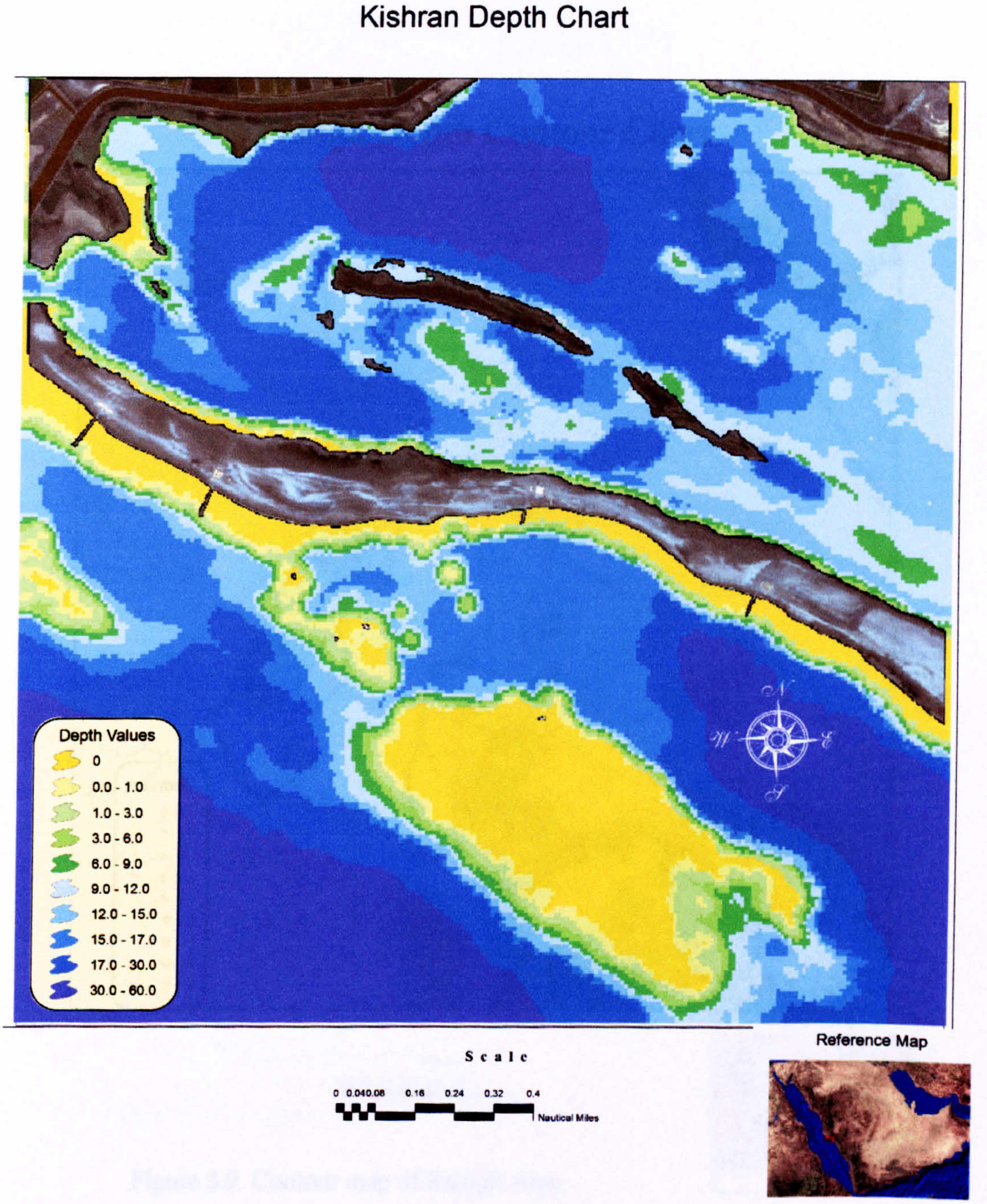

Figure 8.8. Depth Map layer for Kishran area.

For navigation purposes, the extracted depth maps for both areas were converted into contour maps, see Figure 8.9 and 8.10

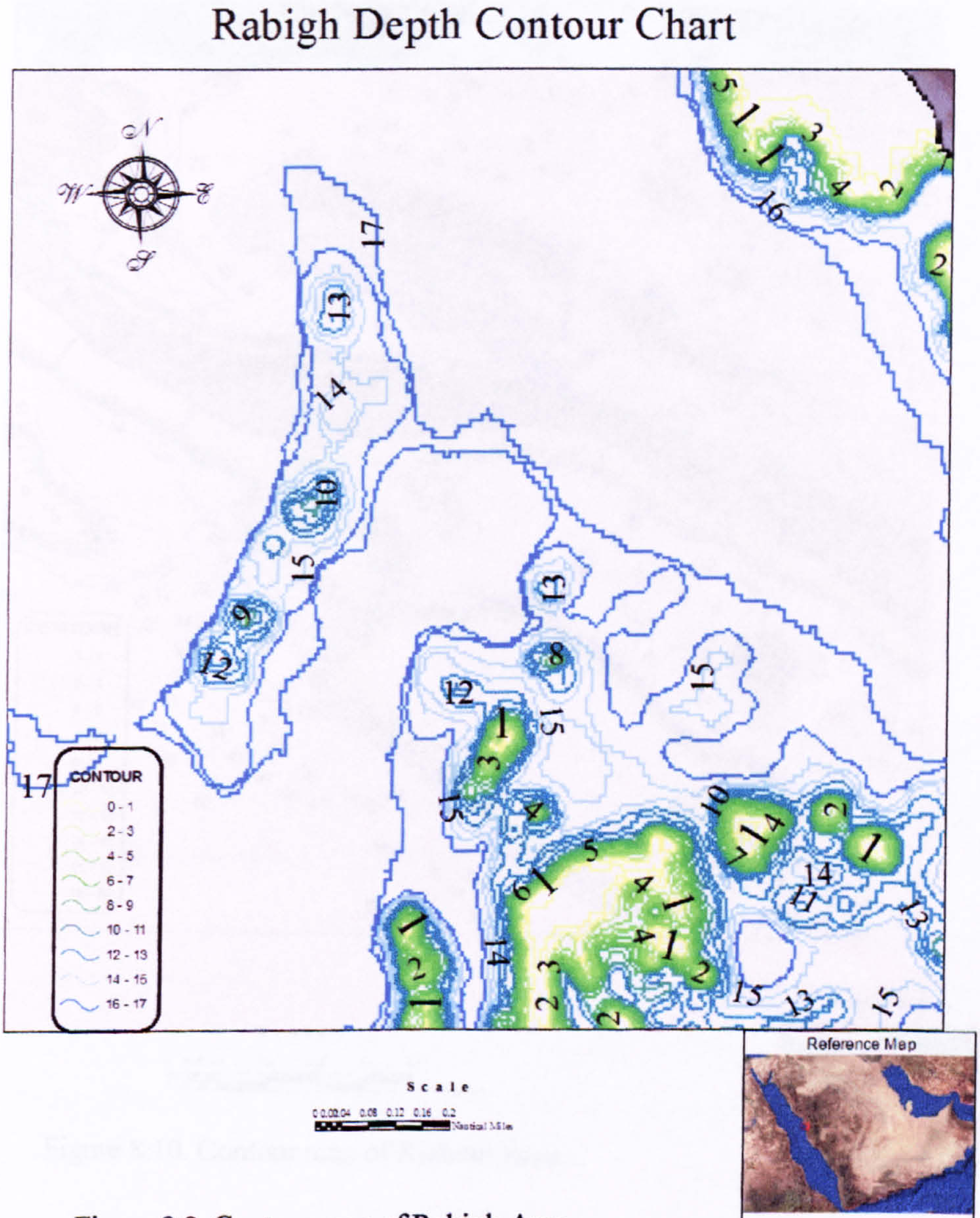

Figure 8.9. Contour map of Rabigh Area.

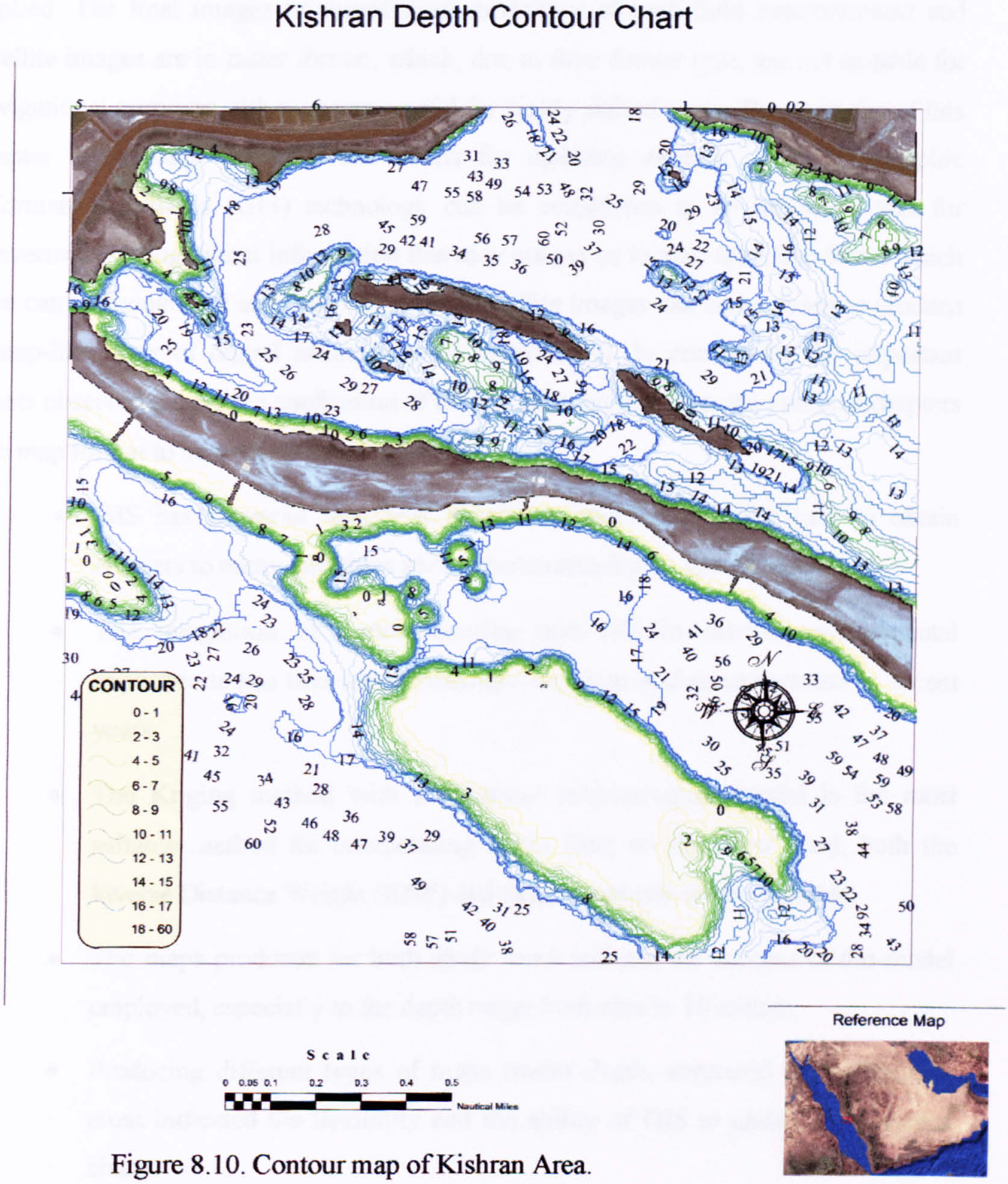

Figure 8.10. Contour map of Kishran Area.

8.5 Conclusions:

This chapter explained how the results extracted from the previous chapters were applied. The final images produced from modelling of both field measurements and satellite images are in raster format, which, due to their format type, are not suitable for navigational purposes, although very useful for highly skilled users. The main aim of this chapter is to make use of these results for updating nautical charts. Geographic Information Systems (GIS) technology can be considered as an important tool for converting existing digital information that may not yet be in map form into forms which then can be recognized and used (i.e. digital satellite images can be analysed to produce a map-like layer of digital information of bathymetry). In conclusion, the important points observed during the application of the results achieved from the previous chapters into map format to be used by shipping were:

- GIS has powerful analytical functions, which enable the user to obtain answers to many questions about phenomena tied to specific locations.
- The integration of remote sensing and GIS in marine environmental applications has become increasingly common and recommended in recent years.
- The Kriging method with a spherical semivariogram model is the most suitable method for interpolating depth data; on the other hand, both the Inverse Distance Weight (IDW) and Spline methods are not suitable.
- The maps produced for both study areas indicate the success of the model employed, especially in the depth range from zero to 18 metres.
- Producing different types of maps (raster depth, contours) for both study areas indicated the flexibility and the ability of GIS to update navigational charts.

CHAPTER NINE

CONCLUSIONS AND RECOMMENDATIONS

9. CONCLUSIONS AND RECOMMENDATIONS

9.1 Introduction

The methodology of this study was focused and based on the aims and research questions, which were mentioned in Chapter One of this thesis. The main aim of this research is to demonstrate the suitability of VHR multispectral satellite imagery for the creation of bathymetric maps appropriate to conditions in the Red Sea coastal areas; thus IKONOS satellite images were selected for the project. Very accurate field measurements where conducted to measure the real depths, using a dual frequency echo sounder and *d*GPS.

The previous chapters contain conclusions for the different processes carried out; a summary and final conclusion will be presented in this chapter for the whole thesis.

The study was performed on two areas (Rabigh and Kishran), 400 km apart and containing most of the marine environments of the Red Sea. The selection of these areas as case studies was due to several factors. Firstly, they contain all habitats related to our study, such as coral reefs, shallow waters, deep waters, vegetation, islands, clear and turbid waters. Secondly, all facilities needed for surveying, such as survey vessels and their crew, were available there. Thirdly, the two areas are located near to the Saudi national geodetic network, which was used for establishing a new reference station for *d*GPS. Finally, the socio economic importance of these areas is high.

Briefly, the main methods of study followed were:

- Field work
- Image processing
- Data analyses
- Application of study results for navigational purposes using GIS techniques

9.2 Thesis summary

9.2.1 Data acquisition and field measurements.

The images were acquired specially for this study after the selection of the study areas. IKONOS images were selected according to the needs of the study; the request to purchase these images was made with some conditional requirements, namely, they should be 4 metre multi-spectral (4 bands), no geo-referencing applied and full 11-bit radiance imaging, the viewing angle must be 72-90°, and finally they should be on a single date and not a mosaic, as an important issue in this acquisition was that field measurements were to be carried out during the acquisition of the imagery.

The field measurements (position and depth) were made according to highly accurate methodologies. The field measurements took place in the two study areas during the acquisition of the satellite images. This work was done in three main stages. Firstly, for the horizontal coordinates, new reference stations were established referenced to known stations located away from the study areas using dGPS. The known stations were equipped with radios to send the corrections to the GPS rover on board the survey vessel. The positioning error was found to be ±5 cm, which is less than the pixel size of 4 m x 4 m.

Secondly, for the vertical coordinates that represent the depth measurements, the survey boat used was 12 m in length, with a 500 hp engine and a 0.5m draught, equipped with a HT100 portable digital echo sounder with a resolution of 0.01 m. The dGPS and echo sounder were interfaced to the laptop computer to record the depth readings and the positions. Calibration of the echo sounder was carried out before starting the real survey using the bar check technique. 50 m was the distance between the survey lines, with a scale of 1:5,000 according to International Hydrographic Organization IHO procedures. Tide prediction was taken into consideration to correct the depth measured by the echo sounder. The depth measurement was not the only work done in this study. The coastline and port jetties were mapped using dGPS, to be used for image georeferencing.

Finally, spectral measurements were performed using the Analytical Spectral Device (ASD), to measure the reflectance spectra on the ground for dark and bright objects. The main goal of these measurements was the radiometric correction of the images.

9.2.2 Image processing

As mentioned previously, the images were requested and acquired specially for this study, ordered as raw format, with no geometric or radiometric corrections, so that the corrections and calibration could be applied according to the collected field data. All processes were made using *d*GPS for the control points in order to georeference the images. Spectral measurements were collected from the areas under study for both dark and bright targets using Analytical Spectral Device (ASD) FieldSpec Pro (Full Range). Asphalt represented dark objects while sand represented bright objects; the areas tested or measured were more than 12 m by 12 m in size.

In this study, the spectral measurements were not satisfactory due to the old age of the asphalt, which contained a light-coloured aggregate resulting in higher than expected reflectance values; the sand, which represents the bright objects, was wet due to its location near the coastline and contained slightly darker aggregate, making the resulting measurements lower than expected. The alternative solution or method uses the manufacturer's published calibration constants to convert the DN values to at-satellite reflectance; this method is used to convert the DN to radiance and then to reflectance, but would not be the preferred solution for two reasons. Firstly, the published calibration values are not regularly updated, and secondly, the method provides only an at-sensor effective reflectance value, inclusive of any atmospheric effects. The correction of atmospheric effects using a radiative transfer model was not possible in this stage, but it is recommended that the spectral measurement (empirical line method) is used in any further calibration.

The next stage of image processing was the geo-referencing; the geometric corrections are needed for rectification of geometric errors that occur during image acquisition, and usually this type of process is required when the images are to be used as maps. Ground Control Points (GCP) were collected using highly accurate means of positioning, such as *d*GPS. The GCP points were selected carefully using the edges of jetties, road junctions, buoys and island edges. The accurate positioning system helped in minimizing the root mean square (RMS) as the *d*GPS reference station was located in the middle of the study area, which resulted in an accuracy of ±5cm in the positioning system.

9.2.3 Water depth prediction

The first study area (Rabigh) consisted of two different environments, one of them the port, which represents the turbid water resulting from cargo and container ships during entrance and departure, the other environment with very clear water over coral reef areas located out of the port. Different models were derived. The first model covered the entire area of Rabigh (Study area 1), which included both clear and turbid water, and the accuracy achieved was $r^2 = 97\%$. The clear water model was more accurate ($r^2 = 99.2\%$). Finally, the turbid water gave lower accuracy ($r^2 = 80.7\%$), as expected. The first model, which includes both clear and turbid water, shows minor effects of turbid water due to the small number of observations compared with clear water. The same procedures were applied for the second study area (Kishran, and a high R-squared value of $r^2 = 95.3\%$was achieved). Transferability testing established that models created for the first study area could be used to predict water depth in the second study area with high accuracy.

The data extracted from field measurements were very useful for building different models for the satellite processing and this accuracy was achieved due to the very accurate methods used in the fieldwork.

Higher errors were noticed in the red band than in the blue band due to the increasing light attenuation. The green band also displayed noticeable errors as the depth increased and when turbid water was included with clear water the r^2 was found to be 67%, which is not an encouraging result and is not going to support the research aim of nautical chart updating.

In the case of depths greater than 18 m, the regression relationship was not valid due to light diffusion as the depth increased, causing the absorption of electromagnetic energy. However, the results achieved were still very useful, and could help in deriving bathymetry maps of shallow coastal areas that were previously marked only as hazardous areas on bathymetric maps generated using traditional methods. Furthermore, initial transferability investigations using an observation model from one location to predict water depths from imagery of another location offers the potential for more rapid and cost-effective sea bottom mapping, especially if the acquisition of the imagery is by the same sensor and within a few minutes of one another.

With high accuracy and the safety factor added from the model presented in this study, the problem of submerged coral and navigational hazards has been solved for the two sites investigated, and the potential of IKONOS to produce accurate, high spatial resolution navigation charts in the Red Sea region has been established. Further work will be required to establish the extent to which the technique can be applied to multi-date image datasets. The suitability of other VIS-NIR satellite image sources for reliable mapping of small islands will be investigated in the next phase of this project.

9.2.4. Applying the field measurements to images acquired under the most unfavourable conditions (July 2006)

The first acquisition was during December 2004. The weather in this period was quite good compared with other months such as in the summer season, and the result achieved from these images was very good and useful for updating nautical charts. The reason for performing this process was to investigate how much information can be obtained from satellite imagery acquired during unfavourable conditions. During the summer period in the Red Sea, the temperature, humidity and water vapour usually reach their maximum values; these conditions affect the electro magnetic waves and cause errors. However, the selection of this time was decided and planned after obtaining the excellent results described in Chapter Six, which were acquired in good weather as mentioned, to investigate the possibility of using this image in deriving bathymetry information.

However, the results achieved using the new images was different from the results we presented in Chapter Six, although the same methodology was carried out, with simple linear regression being applied for electromagnetic reflectance versus field depths. In clear water sites, the regression relationship was not as accurate as the regressions for the December 2004 images; the r^2 was found to be 73.8%, which is not accepted as an accurate methodology. The turbid water investigation gave the worst result, due to the water turbidity but also the difficult weather conditions, with $r^2 = 6.5\%$. The turbid water result is not to be trusted in the normal case, when the weather is stable.

9.2.5 Application of study results for navigational purposes using GIS techniques.

This is the last stage of this project, its main purpose being to use the excellent results from the previous chapters. The final images produced from modelling of both field measurements and satellite images are in raster format, which, due to their format type, are not suitable for navigational purposes, although very useful for highly skilled users. The main aim of this stage is to make use of these results for updating nautical charts. Geographic Information Systems (GIS) technology can be considered as an important tool for converting existing digital information that may not yet be in map form into forms that can be recognized and used (i.e. digital satellite images can be analysed to produce a map-like layer of digital information of bathymetry). The important points observed during the application of the results achieved from the previous chapters into map format to be used by shipping and presented earlier in chapter 8 were:

- GIS has powerful analytical functions, which enable the user to obtain answers to many questions about phenomena tied to specific locations.
- The integration of remote sensing and GIS in marine environmental applications has become increasingly common and recommended in recent years.

- The Kriging method with a spherical semivariogram model is the most suitable method for interpolating depth data; on the other hand, both the Inverse Distance Weight (IDW) and Spline methods are not suitable.
- The maps produced for both study areas indicate the success of the model employed, especially in the depth range from zero to 18 metres.
- Producing different types of maps (raster depth, contours) for both study areas indicated the flexibility and the ability of GIS to update navigational charts.

9.3 Recommendations

After discussing both the results and conclusions of the chapters in this thesis, some recommendations are produced that will enable the updating of bathymetric charts for coastal waters and guide the future work to improve the methodology.

9.3.1 Recommendations for application of the results of this thesis

- The study was focused on the coastal waters, which are important for local shipping and the patrolling vessels of the Border Guard. The author recommends that the Border Guard establish a training centre to train their staff to deal with new technology such as image processing and the creation of their own charts.
- It is advised that the procedure adopted in this thesis be used for updating and creating new navigational charts.
- Create new navigational charts with more details for the areas near the coast containing notifications of all hazards that threat the local shipping, and safe passages marked with navigational aids.

9.3.2 Recommendations for further work

- State the new sensors that could offer better resolution for updating the nautical charts.
- It is necessary to continue processing and analysing different sensor's images to investigate and select the most suitable ones for bathymetry and marine environment studies.
- This study has two acquisition times, which produced different results, so the author recommends 12-months of satellite image acquisition be processed with the same methodology to investigate what is the most suitable time for acquisition.
- It is recommended that space technology be used for observing and monitoring the earth's features, especially for studying the marine environment and costal areas.
- Evaluate applicability of this method to the Arabian Gulf coastal waters and other worldwide locations such as northern Australian.
- This thesis attempted to establish accuracy at the greatest depth possible, but further work could explore improved accuracy for shallower depths using other spectral bands such as Red and Green

REFERENCES

REFERENCES

Abdulrahman S. M. (1995). Estimating wind field offshore Jeddah based on land weather measurements. KAU, Marine science, V.6,PP 15-24

Al-Shammari R. (1996). Real-Time construction of plant poisioning by 'ON-THE_FLY' GPS. MSc thesis, Notingham University

Alzahrani A. S. (2002). Updating nautical charts using Landsat5- TM data " Farasan Bank " Red Sea ,Saudi Arabia, PhD thesis submitted to Arab Academy for science and technology and marine transport, Alexandria, Egypt.

Alzahrani A., Birmingham R. and Williams M. (2006). Shallow water bathymetry derived from VHR satellite (IKONOS) remote sensing in the Red Sea (Saudi Arabia) MELAHA international conference (AIN) Alexandria Egypt

Alzahrani A. and Birmingham R. (2007). VHR (IKONOS) Satellite images and deriving shallow water depth, Saudi innovation conference 2007, Newcastle University

Alzahrani A. and Birmingham R. (2007). Application of data analysis results of image processing and field measurements for navigational purposes using GIS techniques, Saudi innovation conference 2007, Newcastle University

Alzahrani A. and Birmingham R. (2007). "The reliability of using satellite imagerydata to derive coastal water bathymetry for navigational purposes" geomatics2007 international conference, Canadian Institute of Geomatics, Toronto Canada.

Alzahrani A. and Birmingham R. (2007). "Investigation of using satellite imagery model of one site to predict water depths of other sites in the Red Sea" Paper accepted to be presented in the Scientific Committee of the Third National GIS Symposium in Dammam, Saudi Arabia,

Andre-fouet, S., Muller-Karger, F., Hochberg, E., Hu, C. & Carder, K. (2001). Change detection in shallow coral reef environments using Landsat 7 ETM+ data. Remote Sensing of Environment, 79, 150–162.

Andre–fouet, S., Kramer, P., Torres-Pulliza, D., Joyce, K. E., Hochberg, E. J., Garza-Perez, R., Mumby, P. J., Riegl, B., Yamano, H., White, W. H., Zubia, M., Brock, J. C., Phinn, S. R., Naseer, A., Hatcher, B. G. & Muller-Karger, F. E. (2003). Multi-site evaluation of IKONOS data for classification of tropical coral reef environments. Remote Sensing of Environment, 88, 128–143.

Appleyard, S. F., Linford, R. S. & Yarwood, P.J. (1980). Marine electronic navigation. London & New York: Routledge & Kegan Pan.

Bantan, R. (1999). Geology and sedimentary environments of Farasan bank (Saudi Arable) Southern Red Sea: A combined remote sensing and field study. Ph.D Thesis, University of London.

Behairy, A. K. A., Sheppard, C. R. C. & El-Sayed, M. K. (1992). A review of the geology of coral reefs in the Red Sea. UNEP Regional Seas Reports and Studies No. 152, 1–36.

PERSGA (1998). Red Sea and Gulf of Aden.

Blank, H. R., Johnson, P. R., Getting, M. E. & Simmons, G. C. (1986). Geologic map of the Jizan Quadrangle Sheet. Kingdom of Saudi Arabia, Ministry of Petroleum, Directorate General of Mineral Resources, 16F, 25p.

Bonatti, E., Clocchiatti, R. Colantoni, P., Gelmini, R. & Marinelli, G. (1983). Zabargad (St. John's) Island: An uplifted fragment of sub-Red Sea lithosphere. Journal of the Geological Society of London, vol. 140, 677–690.

Borre, G. S. A. K. (1997) Linear Algebra, Geodesy and GPS, United States, Whellsley-Cambridge Press.

Brock, J. C., Sallenger, A. H., Krabill, W. B., Swift, R. N., & Wright, C. W. (2001). Recognition of fiducial surfaces in lidar surveys of coastal topography. Photogrammetric Engineering and Remote Sensing, 67(11), 1245–1258.

Brock, J. C., Wright, C. W., Clayton, T. D. & Nayegandhi, A. (2004). LIDAR optical rugosity of coral reefs in Biscayne National Park, Florida. Coral Reefs, 23(1), 48–60.

Brock, J. C., Wright, C. W., Sallenger, A. H., Krabill, W. B., & Swift, R. N. (2002). Basis and methods of NASA Airborne Topographic Mapper lidar surveys for coastal studies. Journal of Coastal Research, 18(1), 1–13.

Burrough, (1986), Principals of Geographic Information System for Land Resources Assessment, Mckferlin Press.

Capolsini, P., Andre'foue"t, S., Rion, C., & Payri, C. (2003). A comparison of Landsat ETM+, SPOT HRV, IKONOS, ASTER, and airborne MASTER data for coral reef habitat mapping in South Pacific Islands. Canadian Journal of Remote Sensing, 29, 1 – 14.

Celik, R. (1996). Integration of DGPS and Conventional Systems in Offshore Surveying, PhD thesis, University of Newcastle Upon Tyne, Newcastle, UK.

Chen, G. (1998) GPS Kinematic Positioning for the Airbome Laser Altimetry at Long Valley, California. Department of Earth, Atmospheric, and planetary. Cambridge, Massachusetts Institute of Technology.

Clarke, C. D., Mumby, P. J, Chisholm, J. R. M., Jaubert, J. & Andre-fouet, S. (2000). Spectral discrimination of coral mortality states following a severe bleaching event. International Journal of Remote Sensing, 21, no. 11, 2321–2327.

Coleman, R. G. (1993). Geologic Evolution of the Red Sea. Oxford: Oxford University Press, 186 p.

Condit, C. D. & Chavez, P. S. (1979). Basic concept of computerized digital processing for geology. United States Geological Survey Bulletin, 1462 p.

Dullo, W. C. & Montaggioni, L. (1998). Modem Red Sea coral reef: a review of their morphologies and zonation. In Sedimentation and tectonics in Rift Basin: Red Sea-Gulf of Aden. (Eds. Purser, B. H. & Bosence, D W. J.). Chapman & Hall, pp. 583–594.

IDRISI 32: Guide to GIS and Image Processing, Volume 1, May 2001, J. Ronald Eastman, Release 2

Edwards, F. J., and Head, S. M., (1987). Red Sea, (Key Environments) HRH the Duke of Edinburgh

El-Hattab M. M. 2007. The Role of Remote Sensing and GIS Techniques in Monitoring and Management Coastal Environmental Disasters.. 2nd Symposium of Management of Marine Disasters, Organized by Border Guard, Ministry of Interior, Kingdom of Saudi Arabia.

El-Raey, M.; S.M., Nasr; M.M. El-Hattab and O.E.,Frihy (1995). Change detection of Rosetta promontory over the last forty years. International Journal of Remote Sensing, Vol. 16, No. 5, pp. 825-834

El Raey, M.; Frihy, O.; S.M. Nasr; El-Hattab, M.; Y. Fouda; A. Shalaby and W. Ahmed, 2005. Remote Sensing Linked GIS For Integrated Management of the Coastal Zone Of Abu Qir Bay, Egypt. Submitted in International Conference “Development and Tourism in Coastal Areas”, Sharm El-Sheikh, Egypt, 9-12 March 2005. Work is supported by Commission of European Communities Contract ICA3-CT-2002-10006 (SMART project).

El-Raey, M. 1988, Remote sensing of environment, Symposium of Environmental Science (UNARC), Alexandria, Egypt, pp. 1-19.

El-Raey M., S. Nasr, and M. El-Hattab, 2000. Assessment of Land Cover Changes along the Northwestern Coastal Zone, Egypt, Second International Conference on Earth Observation and Environmental Information (EOEI), 11-14 Nov. 2000, Cairo, Egypt.

Nasr, S., El-Raey, M., El-Shenawy, M., Okbah, M., Absulsoeud, A., El-Hattab, M., Abdel Khalik, M. 2004. Assessment of Water Quality of Abu-Qir Bay along the Mediterranean Coast of Egypt. Submitted to EARSEL Symposium at Dubrovnik, May 2004.

El-Rabbany, A. (2002). Introduction to GPS: the Global Positioning System. Boston: Artech House.

El-Rabbany, A. (2006). Introduction to GPS: the Global Positioning System. Boston: Artech House.

El Sayed, A. (1985). World and Red Sea, Historical and strategic study.

El-shimy N. (1999), Digital Terrain Modeling, The University of Calgary, Canada, PP 8-9)

ESRI, 2004: "Using ArcView GIS, The Geographic Information System for Everyone", Environmental System Research Institute (ESRI), New York.

ESRI., 2005, Environmental Studies and Research Institute (ESRI), www.esri.com

Farrand, W. H., Singer, R. B., and Merenyi, E., 1994, Retrieval of apparent surface reflectance from AVIRIS data - a comparison of empirical line, radiative-transfer and spectral mixture methods. Remote Sensing of Environment, 47, 311-321.

Ferrier, G., 1995, Evaluation of apparent surface reflectance estimation methodologies.International. Journal of Remote Sensing, 16, 2291-2297.

Ferrier, G., andWadge, G., 1996, The application of imaging spectrometry data to mapping alteration zones associated with gold mineralisation in southern Spain. International. Journal of Remote Sensing, 17, 331-350.

Freemantle, J. R., Pu, R., andMiller, J. R., 1992, Calibration of imaging spectrometer data to reflectance using pseudo-invariant features. Proceedings of the 15th Canadian Symposium on Remote Sensing (Toronto: Canadian Remote Sensing Society & Canadian Aeronautics and Space Institute), pp. 452-455.

Gladstone, W., Tawfiq, N., Nasr, D., Andersen, I., Cheung, C., Drammeh, H., Krupp, F. & Lintner, S. (1999). Sustainable use of renewable resources and conservation of renewable resources in the Red Sea and Gulf of Aden: issues, needs and strategic action – patterns and processes in extreme tropical environments. Ocean and Coastal Management, 42, 8, 671–697.

Gordon, H. R. & Mccluney, W. R. (1975). Estimation of the depth of sunlight penetration in the sea for remote sensing. Applied Optics, vol. 14, 2, 413–417.

Gordon, H. R. & Zhang, T. M. (1996). How well can radiance reflected from the ocean atmosphere system be predicted from measurements at the sea surface? Applied Optics, 35, 6527–6543.

Gordon, H. R. (1997). Atmospheric correction of ocean color imagery in the earth observing system era. Journal of Geophysical Research-Atmospheres, 102, 17081–17106.

Gordon, H. R., Zhang, T. M., He, F. & Ding, K. Y. (1997). Effects of stratospheric aerosols and thin cirrus clouds on the atmospheric correction of ocean color imagery: Simulations. Applied Optics, 36, 682–697.

Green, E. P., Mumby, P. J., Edwards, A. J. & Clark, C. D. (1996). A review of remote sensing for the assessment and management of tropical coastal resources. Coastal Management, 24, 1–40.

Green, E.P.,Mumby, P.J., Edwards, A.J., Clark, C.D., 2000. Remote sensing handbook for tropical coastal management. UNESCO, Paris, 316 p.

Hochberg, E. & Atkinson, M. (2000). Spectral discrimination of coral reef benthic communities. Coral Reefs, 19, 164–171.

Hochberg, E. J., & Atkinson, M. J. (2003). Capabilities of remote sensors to classify coral, algae, and sand as pure and mixed spectra. Remote Sensing of Environment, 85, 174–189.

Holden, H. & LeDrew, E. (1999). Hyperspectral identification of coral reef features. International Journal of Remote Sensing, 20, 2545–2563.

Holden, H. & LeDrew, E. (2001). Effects of water column on hyperspectral Reflectance of submerged coral reef features. Bulletin of Marine Science, 69, 685–699.

Holden, H. & LeDrew, E. (2002). Measuring and modeling water column effects on hyperspectral reflectance in a coral reef environment. Remote Sensing of Environment, 81, 300–308.

Hongxing Liu, Zhiyuan Zhao, and Kenneth C. Jezeh: Correction of Positional Errors and Geometric Distortions in Topographic Maps and DEMs Using a Rigorous SAR Simulation Technique. PE& RS, September 2004).

IHO: 1987, "Standards for Hydrographic Survey" Special Publication No. 44, 3rd edition.

JUPP, D. L. B. 1988. Background and extensions to depth of penetration (DOP) mapping in shallow coastal waters, p. IV.2.1– IV.2.19. In Proceedings of the International Symposium on Remote Sensing of the Coastal Zone, Gold Coast, Queensland. KIMES, D. S., J. A. SMITH, AND K. J. RANSON. 1980. Vegetation reflectance measurements as a function of solar zenith angle.Phot. Eng. Remote Sens. 46: 1563–1573.

Karpouzle, E. (2003). High resolution remote sensing of marine reef habitats: towards an integration of satellite and sonar imaging techniques. PhD. Thesis, Herriot Watt University.

King, M. (2003). Track Kinematic GPS Processing Tutorial. University of Newcastle Upon Tyne, Department of Geomatic.

Konecny, Gottfried (2003): Geoinformation, Remote Sensing, Photogrammetry and Geographic Information Systems. Taylor &Francis. 11 New Fetter Lane, London EC4P 4EE, UK.

Kowalik, W. S., Dean, B. P. & Harris, P. M. (1994). Acquisition, processing and interpretation of satellite images. (Eds Harris, P. M. & Kowalik, W. S.). The American Association of Petroleum Geologists (AAPG). Methods in exploration series, No. 11, 1–28.

Krakiwsky, E. (1986). An overview of deformations, measurement technologiesm and mathematical modelling analyses. Deformation measures Workshop-Modern Methodology in precise Engineering and deformation survey-II (Ed.Y. Bock), 7–33.

Leick, A. (2004). GPS Satellite Surveying, 3rd Edition. John Wily & Sons, Inc, ISBN 0-471-05930-7.

Neter J., Kutner M. H., Wassemman, W. and Nachtsheim C. J. (1996). Applied linear statistical models. Mc Graw – Hill/ Irwin; 4th edition.

Li-Guang Leua, Heng-Wen Changb (2005). Remotely sensing in detecting the water depths and bed load of shallow waters and their changes. Ocean Engineering, 32, 1174–1198.

Lillesand, T. M. & Kiefer, R. W. (2000). Remote sensing and image interpretation. 3rd (Edition), John Wiley & Sons, Inc., 734 p.

Lillesand, R.W. Kiefer and J. W. Chipman (2004). Remote sensing and image interpretation. 5th (Edition), Jhon Wiley & Sone, Inc., 752 p.

Lubin, D., Li, W., Dustan, P., Mazel, C., & Stamnes, K. (2001). Spectral signatures of coral reefs: features from space. Remote Sensing of Environment, 75, 127–137.

Lyzenga, D. (1978). Passive remote sensing techniques for mapping water depth and bottom features. Applied Optics, 17, 379–383.

Lyzenga, D. R. (1981). Remote sensing of bottom reflectance and water attenuation parameters in shallow water using aircraft and Landsat data. International Journal of Remote Sensing, vol. 2, No. 1, pp. 71–82.

Liceaga M. A. – correa and J.I. Euan – Avila (2002). Assessment of coral reef bathymetric mapping using visible Landsat Thematic Mapper data. International journal of remote sensing, 2002, vol. 23, no. 1, 3–14

Magnavox Advanced Product and Systems Company, Magnavox report R-6245, 2829 Maricope Street, Torrance, California 90503, 1–10.

Maritorena, S. (1996). Remote sensing of the water attenuation in coral reefs: a case study in French Polynesia. International Journal of Remote Sensing, 17, 155–166.

Markham, B. L. & Barker, J. L. (1985). Spectral characterization of the Landsat Thematic Mapper sensors. International Journal of Remote Sensing, 6(5), 697–716.

Markham, B. L., & Barker, J. L. (1987). Radiometric properties of U.S. processed Landsat MSS data. Remote Sensing of Environment, 22, 39–71.

McClay, K. R., Nichols, G. J., Khalil, S. M., Darwish, M. & Bosworth, W. (1998). Extensional tectonics and sedimentation, eastern Gulf of Suez, Egypt. In Sedimentation and tectonics in Rift Basin: Red Sea-Gulf of Aden (Eds. Purser, B. H. and Bosence, D. W. J.), Chapman & Hall, pp. 223–238.

McCoy J.and Kevin Johnston (2001). Using ArcGIS Spatial Analyst (Paperpack) published by ESRI Press, 240p

MEPA (Meteorology and Environment Protection Administration). (1984). Climatic record, Jizan. 1974–1984. Jeddah.

MEPA (Meteorology and Environment Protection Administration. (2005). Climatic record of the Red Sea.

Mishra D & Narumalani, S. (2004). Bathymetric mapping using IKONOS multispectral data. GIScience and Remote Sensing, 41, 301–321.

MISRA, P. & ENGE, P. (2001) Global Positioning System, Signals, Measurements, and Performance, Ganga-Jamuna Press .

Morcos, S. A. (1970). Physical and chemical oceanography of the Red Sea. In Oceanography and Marine Biology, vol. 8, (Ed. M. Barnes), London: George Allen and Unwin Ltd., pp. 73–202.

Mumby, (2001). Beta and habitat diversity in marine systems: a new approach to measurement, scaling and interpretation. Oecologia (2001) 128:274–280

Mumby, P. J. & Edwards, A. J. (2002). Mapping marine environments with IKONOS imagery: Enhanced spatial resolution can deliver greater thematic accuracy. Remote Sensing of Environment, 82, 248–257.

Mumby. P. J.; Green. E. P.; Edwards. A. J. & Clark C. D. (1997) Coral reef habitat mapping: how much detail can remote sensing provide? Marine Biology (1997) 130: 193±202

Mumby. P. J.;Green. E. P.;Clark. C. D. & Edwards A. J. (1998). Digital analysis of multispectral airborne imagery of coral reefs. Coral Reefs (1998) 17 : 59-69

Myers, M. R., Hardy, J. T., Mazel, C. H., & Dustan, P. (1999). Optical spectra and pigmentation of Caribbean reef corals and macroalgae. Coral Reefs, 18, 179–186.

Naval Oceanography Command, (1982). Climatic study of the Red Sea South and Gulf of Aden. Asheville, N. C., 133p.

Palandro, D., Andre'foue¨t, S., Dustan, P. & Muller-Karger, F. E. (2003). Change detection in coral reef communities using IKONOS satellite sensor imagery and historic aerial photographs. International Journal of Remote Sensing, 24(4), 873–878.

Parkinson, B., J, Spilker (1996). Global Positioning System: Theory and Applications. vols.1 and 2, American Institute of Aeronautics, 370 L'Enfant Promenade, SW, Washington, DC, 1996 .

Purkis, S. J., Kenter, J. A. M., Oikonomou, E. K., & Robinson, I. S. (2002). High-resolution ground verification, cluster analysis and optical model of reef substrate coverage on Landsat TM imagery (Red Sea, Egypt). International Journal of Remote Sensing, 23, 1677– 1698.

Purser, B. H. and Hötzl, H. (1988). The sedimentary evolution of the Red Sea rift: A comparison of the northwest (Egyptian) and northeast (Saudi Arabia) margins. Tectonophysics, vol. 153, 193–208.

Robinson, M. K. (1979). Atlas of N. Atlantic Ocean - Indian Ocean Monthly Mean Temperatures and Mean Salinities of the surface layer. United States Naval Oceanographic Office, Reference Publication 18.

Roelfsma, C., Phinn, S., & Dennisson, C. W. (2002). Spatial distribution of benthic microalgae on coral reefs determined by remote sensing. Coral Reefs, 21, 264–274.

Sharma S.K. and Anjaneyulu D.(1993). "Integration of remote sensing and GIS in water resource management". Int. J. Rem. Sens. 14(17): 3209-3220.

Siddall, M., Smeed, D. A., Hemleben, C., Rohling, E. J., Schmelzer, I. & Peltier, W. R. (2004). Understanding the Red Sea response to sea level. Earth and Planetary Science Letters, 225 (3-4), 421–434

Smith, G. M. & Milton, E. J. (1999). The use of the empirical line method to calibrate remotely sensed data to reflectance. International Journal of Remote Sensing, 20, 2653–2662.

Stumpf, R. P. K, Holderied, K. & Sinclair, M. (2003). Determination of water depth with high–resolution satellite imagery over variable bottom types. Limnol. Oceanogr., 48, 547–556.

Stumpf,R.P., Holderied, K. & Sinclair, M. (2003). Determination of water depth with high–resolution satellite imagery over variable bottom types. Limnology and Oceanography, vol. 48, 547–556.

Thome, K. (2001). Absolute radiometric calibration of Landsat 7 ETM+ using the reflectance–based method. Remote Sensing of Environment, 78, 27–38.

Vieira C. A. O., Mather P. M. and Aplin P. (2004). Assessing the positional and thematic accuracy of remotely sensed data. ISPRS Conference 2004 International Society for Photogrammetry and Remote Sensing - paper No. 979

Weibel, R. and Heller, M. (1990). A framework for digital terrain modelling, 4th InternationalSymposium on Spatial Data Handling, Zurich, pp.219-229.

Weibel, R. and Heller, M. (1991). Digital Terrain Modelling. in: Maguire, D. J., Goodchild, M. F., and Rhind, D. W. (eds.) Geographical Information Systems: Principles and Applications, pp.269-297.